

NONLINEAR CABLE DYNAMICS

by

HYUNKYOUNG SHIN

B.S. in Naval Architecture and Marine Engineering
Seoul National University (1979)
M.S. in Naval Architecture and Marine Engineering
Seoul National University (1981)
Ocean Engineer, Massachusetts Institute of Technology
(1985)

SUBMITTED TO THE DEPARTMENT OF OCEAN
ENGINEERING IN PARTIAL FULFILLMENT OF THE
REQUIREMENTS FOR THE DEGREE OF
DOCTOR OF PHILOSOPHY

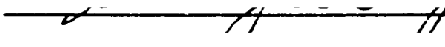
at the

MASSACHUSETTS INSTITUTE OF TECHNOLOGY

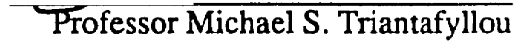
June 1987

Copyright (c) 1987 Massachusetts Institute of Technology

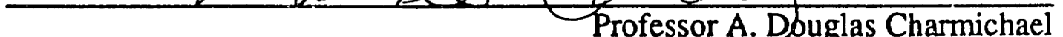
Signature of Author


Department of Ocean Engineering
June 12, 1987

Certified by


Professor Michael S. Triantafyllou
Thesis Supervisor

Accepted by


Professor A. Douglas Charnichael
Chairman, Departmental Graduate Committee
Department of Ocean Engineering

MASSACHUSETTS INSTITUTE
OF TECHNOLOGY

JAN 06 1988

LIBRARIES

NONLINEAR CABLE DYNAMICS

by

HYUNKYOUNG SHIN

B.S. in Naval Architecture and Marine Engineering
Seoul National University (1979)

M.S. in Naval Architecture and Marine Engineering
Seoul National University (1981)

Ocean Engineer, Massachusetts Institute of Technology
(1985)

SUBMITTED TO THE DEPARTMENT OF OCEAN
ENGINEERING IN PARTIAL FULFILLMENT OF THE
REQUIREMENTS FOR THE DEGREE OF

DOCTOR OF PHILOSOPHY

at the

MASSACHUSETTS INSTITUTE OF TECHNOLOGY

June 1987

Copyright (c) 1987 Massachusetts Institute of Technology

Signature of Author _____

Department of Ocean Engineering
June 12, 1987

Certified by _____

Professor Michael S. Triantafyllou
Thesis Supervisor

Accepted by _____

Professor A. Douglas Chermichael
Chairman, Departmental Graduate Committee
Department of Ocean Engineering

MASSACHUSETTS INSTITUTE
OF TECHNOLOGY

JAN 06 1988

LIBRARIES

NONLINEAR CABLE DYNAMICS

by

HYUNKYOUNG SHIN

Submitted to the Department of Ocean Engineering on June 12, 1987 in partial fulfillment of the requirements for the degree of Doctor of Philosophy.

Abstract

Three topics in nonlinear cable dynamics are studied in detail, because of their importance in offshore applications. The first topic is the motion of a cable in water when buoys are attached along its length. The second topic is the effect of the geometric nonlinearity on the dynamic behaviour of the cable, in the presence of fluid drag. The third topic is the effect of zero total tension due to large dynamic tension amplification. Particular attention is paid to the third topic, because of its importance on towing in rough seas, and on the dynamic response of mooring cables in extreme storms.

The nonlinear equations are first simplified to allow the development of efficient numerical schemes, and then comparisons are made with existing experimental data. A spectral method based on Chebyshev polynomials is used, employing the collocation method spatially and Newmark's method for time integration. The agreement with experimental data is found to be good overall, while the most important parameters affecting the dynamic cable response are identified.

Thesis Supervisor: Professor Michael S. Triantafyllou
Title: Associate Professor of Ocean Engineering

Dedication

To my Wife 'Soonyoung' and my Children 'Soomyoung' and 'Jaemyoung'.

To my Family in Seoul - Mother and my late Father and Brothers and Sister.

Acknowledgments

I would like to express my deep appreciation to Professor Michael S. Triantafyllou, my thesis supervisor, who first excited my interest in cable structures. I would also like to thank my thesis committee members, Professor Jerome H. Milgram and Professor Dick K Yue, and Mr. F. C. Frimm, and lab. manager, M. S. Drooker, in the Design Laboratory, Department of Ocean Engineering, MIT.

Thanks are due to Korean Government for financial support and I want to thank President Kwan Lee and Professors in Ship Building and Ocean Engineering, Ulsan University (Korea), and specially Professor Jong H. Hwang, my previous research supervisor, and Professors in Seoul National University (Korea) for their encouragement.

5. Cable with Intermediate Attached Buoys For Offshore Applications	90
5.1 Introduction	90
5.2 Statics	90
5.3 Dynamics	93
5.3.1 Drag Forces on a Submerged Buoy	93
5.3.2 Dynamic Equations of a Submerged Intermediate Buoy	96
5.3.3 Linearized Dynamic Equations of a Submerged Intermediate Buoy	96
5.4 Numerical Application	99
6. Combined Effects of the Geometric Nonlinearity, Large Tensile Forces and Nonlinear Drag Forces	119
6.1 Introduction	119
6.2 Nonlinear Governing Equations	119
6.3 Numerical Application	120
7. Extreme Tensions in a Snapping Cable	133
7.1 Introduction	133
7.2 Behaviour of a Cable subject to Negative Tension	133
7.3 Clipping-Off Model	137
7.4 Effects of Small Cable Bending Stiffness on its Dynamic Behaviour	139
7.5 Qualitative Analysis of Extreme Tensions in a Snapping Cable	139
7.5.1 Principal Parameters to Increase the Free-Falling Velocity lu_c^*	145
7.5.2 Other Ways to Reduce the Peak Tension in a Snapping Hawser	146
7.6 Applications and Comparisons with Experimental Data	148
7.6.1 NSFI Experiment	148
7.6.2 MIT Experiment	156
Conclusion	166
Appendix A. Classical Wave Equation	169

List of Figures

Figure 1-1: Coordinate Systems for Velocities and Drag Forces	16
Figure 3-1: a Taut String with Nondimensionalized Variables	45
Figure 3-2: String Hitting an Elastic Foundation	50
Figure 3-3: Initial position of the string and Excitation imposed at the end	53
Figure 3-4: Comparison between the Nondimensionalized Transverse Displacements at the Middle of a Damped and an Undamped String [$\pi/4$ (rad/sec) and 1 Dia.]	56
Figure 3-5: Nondimensionalized Transverse Displacement at the Middle of an Undamped String [Period/20 and 20 terms ; $\pi/4$ (rad/sec)]	57
Figure 3-6: Nondimensionalized Transverse Displacement at the Middle of an Undamped String [Period/40 and 20 terms ; $\pi/4$ (rad/sec)]	58
Figure 3-7: Nondimensionalized Transverse Displacement at the Middle of an Undamped String [Period/100 and 20 terms ; $\pi/4$ (rad/sec)]	59
Figure 3-8: Nondimensionalized Transverse Displacement at the Middle of an Undamped String [Period/40 and 30 terms ; $\pi/4$ (rad/sec)]	60
Figure 3-9: Nondimensionalized Transverse Displacement at the Middle of an Undamped String [Period/40 and 10 terms ; $\pi/4$ (rad/sec)]	61
Figure 3-10: Nondimensionalized Transverse Displacement at the Middle of an Undamped String [Period/20 and 30 terms ; $\pi/4$ (rad/sec)]	62
Figure 3-11: Transverse Displacement at the Middle of an Damped String [Excitation ; $\pi/2$ (rad/sec) and 1 Diameter]	63
Figure 3-12: Time History of Transverse Displacement along a Damped String [Excitation ; $\pi/2$ (rad/sec) and 1 Diameter]	64
Figure 3-13: Time History of Transverse Displacement along a Damped String [Excitation ; $\pi/2$ (rad/sec) and 1 Diameter]	65
Figure 3-14: Time History of Transverse Displacement along a Damped String with a Object of $k=15$ and $c=10$ [Excitation ; $\pi/2$ (rad/sec) and 1 Diameter]	66
Figure 3-15: Time History of Transverse Displacement along a Damped String with a Object of $k=15$ and $c=10$ [Excitation ; $\pi/2$ (rad/sec) and 1 Diameter]	67
Figure 3-16: Time History of Transverse Displacement along a Damped String with a Object of $k=1000$ and $c=1000$ [Excitation ; $\pi/2$ (rad/sec) and 1 Diameter]	68
Figure 4-1: Static configuration and Lagrangian Coordinates	73
Figure 4-2: Collocation Points	78
Figure 4-3: Static configuration of GUYSTA	82
Figure 4-4: Dynamic Tensions of GUYSTA without damping in normal excitation of amplitude equal to 10 diameters at the first natural frequency	83
Figure 4-5: Normal displacements of GUYSTA without damping in normal excitation of amplitude equal to 10 diameters at the first natural frequency	84
Figure 4-6: Tangential Displacement of GUYSTA without damping in normal excitation of amplitude equal to 10 diameters at the first natural frequency	85
Figure 4-7: Dynamic Tensions of GUYSTA with damping in normal excitation of amplitude equal to 10 diameters at the first natural frequency	86
Figure 4-8: Normal displacements of GUYSTA with damping in normal excitation of amplitude equal to 10 diameters at the first natural frequency	87
Figure 4-9: Tangential Displacement of GUYSTA with damping in normal excitation of amplitude equal to 10 diameters at the first natural frequency	88

Figure 4-10: Comparison of dynamic tensions of GUYSTA between the predicted results and Bliiek's results with damping in normal excitation of amplitude equal to 10 diameters at its first natural frequency	89
Figure 5-1: Static Forces at an Attachment Point	92
Figure 5-2: Total Drag Force on a Buoy	95
Figure 5-3: Dynamic Variables in a Multi-segmented Cable	99
Figure 5-4: Static configuration of the inclined cable with a neutral buoy	103
Figure 5-5: Dynamic tension at the top of the cable with a neutral intermediate buoy [10 Dia. 0.9rad/sec, Normal excitation, No window function]	104
Figure 5-6: Dynamic tension at the bottom of the cable with a buoy [10 Dia. 0.9rad/sec, Normal excitation, No window function]	104
Figure 5-7: Displacement at the attachment of the cable with a buoy [10 Dia. 0.9rad/sec, Normal excitation, No window function, Left side]	105
Figure 5-8: Displacement at the attachment of the cable with a buoy [10 Dia. 0.9rad/sec, Normal excitation, No window function, Right side]	105
Figure 5-9: Dynamic tension at the attachment of the cable with a buoy [10 Dia. 0.9rad/sec, Normal excitation, No window function]	106
Figure 5-10: Displacement at the attachment of the cable with a buoy [10 Dia. 0.9rad/sec, Normal excitation, No window function]	106
Figure 5-11: Dynamic tensions of a cable with a very small buoy with damping in normal excitation of amplitude equal to 10 diameters at the first natural frequency	107
Figure 5-12: Normal displacements of a cable with a very small buoy with damping in normal excitation of amplitude equal to 10 diameters at the first natural frequency	108
Figure 5-13: Tangential displacements of a cable with a very small buoy with damping in normal excitation of amplitude equal to 10 diameters at the first natural frequency	109
Figure 5-14: Comparison between the dynamic tensions of a cable with a very small buoy and a cable without buoy [excitation of amplitude equal to 10 diameters, at the first natural frequency]	110
Figure 5-15: Comparison of dynamic tensions at the top of the inclined cable between with a very small buoy and without buoy and Bliiek's results at excitation of amplitude equal to 10 dia. and its first natural frequency	111
Figure 5-16: Dynamic tension at the top of the cable with a very small buoy [10 Dia. 0.9rad/sec, Normal excitation, No window function]	112
Figure 5-17: Dynamic tension at the bottom of the cable with a very small buoy [10 Dia. 0.9rad/sec, Normal excitation, No window function]	112
Figure 5-18: Dynamic tension at the attachment of the cable with a very small buoy [10 Dia. 0.9rad/sec, Normal excitation, No window function]	113
Figure 5-19: Dynamic tensions at several points of the cable with a very small buoy [10 Dia. 0.9rad/sec, Normal excitation, No window function]	113
Figure 5-20: First expansion coefficient of nondimensionalized dynamic tension at the lower segment of the cable with a very small buoy [10 Dia. 0.9rad/sec, Normal excitation, No window function]	114
Figure 5-21: First expansion coefficient of nondimensionalized dynamic tension at the upper segment of the cable with a very small buoy [10 Dia. 0.9rad/sec, Normal excitation, No window function]	114
Figure 5-22: Dynamic tension at the top of the cable with a very small buoy [10 Dia. 0.9rad/sec, Normal excitation, Window = 0.5]	115
Figure 5-23: Dynamic tension at the bottom of the cable with a very small buoy [10 Dia. 0.9rad/sec, Normal excitation, Window = 0.5]	115

Figure 5-24: First expansion coefficient of nondimensionalized dynamic tension at the lower segment of the cable with a very small buoy [10 Dia. 0.9rad/sec, Normal excitation, Window = 0.5]	116
Figure 5-25: First expansion coefficient of nondimensionalized dynamic tension at the upper segment of the cable with a very small buoy [10 Dia. 0.9rad/sec, Normal excitation, Window = 0.5]	116
Figure 5-26: Dynamic tension at the top of the cable with a very small buoy [10 Dia. 0.9rad/sec, Normal excitation, Window = 1.5]	117
Figure 5-27: Dynamic tension at the bottom of the cable with a very small buoy [10 Dia. 0.9rad/sec, Normal excitation, Window = 1.5]	117
Figure 5-28: First expansion coefficient of nondimensionalized dynamic tension at the lower segment of the cable with a very small buoy [10 Dia. 0.9rad/sec, Normal excitation, Window = 1.5]	118
Figure 5-29: First expansion coefficient of nondimensionalized dynamic tension at the upper segment of the cable with a very small buoy [10 Dia. 0.9rad/sec, Normal excitation, Window = 1.5]	118
Figure 6-1: Dynamic tension at the middle of GUYSTA, subjected to only nonlinear drag forces [10 diameters, 0.9rad/sec]	124
Figure 6-2: Normal displacement at the middle of GUYSTA, subjected to only nonlinear drag forces [10 diameters, 0.9rad/sec]	125
Figure 6-3: Dynamic tension at the top of GUYSTA, subjected to only nonlinear drag forces [10 diameters, 0.9rad/sec]	126
Figure 6-4: Dynamic tension at the middle of GUYSTA, subjected to geometric nonlinearity and large tensile forces as well as nonlinear drag forces [10 diameters, 0.9rad/sec]	127
Figure 6-5: Normal displacement at the middle of GUYSTA, subjected to geometric nonlinearity and large tensile forces as well as nonlinear drag forces [10 diameters, 0.9rad/sec]	128
Figure 6-6: Dynamic tension at the top of GUYSTA, subjected to geometric nonlinearity and large tensile forces as well as nonlinear drag forces [10 diameters, 0.9rad/sec]	129
Figure 6-7: Comparison between dynamic tensions at the middle of a cable subjected to nonlinear drag forces and a cable subjected to geometric nonlinearity and large tensile forces, as well as nonlinear drag forces [10 diameters, 0.9rad/sec]	130
Figure 6-8: Comparison between normal displacements at the middle of a cable subjected to nonlinear drag forces and a cable subjected to geometric nonlinearity and large tensile forces, as well as nonlinear drag forces [10 diameters, 0.9rad/sec]	131
Figure 6-9: Comparison between dynamic tensions at the top of a cable subjected to nonlinear drag forces and a cable subjected to geometric nonlinearity and large tensile forces, as well as nonlinear drag forces [10 diameters, 0.9rad/sec]	132
Figure 7-1: Variation of Total Tension during Consecutive Time Steps	135
Figure 7-2: Normal velocity at the middle of the cable in the clipping-off region	140
<p>the cable with the clip-off model ; $u_c^* < (u_{nc})_{min}$ the cable with the clip-off model ; $u_c^* > (u_{nc})_{min}$ the cable without the clip-off model</p>	
Figure 7-3: Dynamic configuration in slack condition	141

Figure 7-4:	Dynamic configuration in snap condition	141
Figure 7-5:	Dynamic Tension in the clipping-off area	143
Figure 7-6:	Normal displacement in the clipping-off area	143
Figure 7-7:	Dynamic Tension when $ (u_{nc})_{min} > u_c^* $	144
Figure 7-8:	Normal displacement when $ (u_{nc})_{min} > u_c^* $	144
Figure 7-9:	Dynamic Tension when $ (u_{nc})_{min} < u_c^* $	145
Figure 7-10:	Comparison of extreme tensions : NSFI-5d	152
Figure 7-11:	Comparison of extreme tensions : NSFI-7.5d	153
Figure 7-12:	Comparison of extreme tensions : NSFI-10d	154
Figure 7-13:	Time history of predicted dynamic tension ; 1.5hz_5d_1.0Cd	155
Figure 7-14:	Time history of predicted dynamic tension ; cable with spring [0.1hz, 25d]	162
Figure 7-15:	Time history of predicted normal displacement at the middle ; cable with spring [0.1hz, 25d]	162
Figure 7-16:	Time history of predicted dynamic tension ; cable with spring [1hz, 25d]	163
Figure 7-17:	Time history of predicted normal displacement at the middle ; cable with spring [1hz, 25d]	163
Figure 7-18:	Time history of predicted normal velocity at the middle ; cable with spring [1hz, 25d]	164
Figure 7-19:	Effect of the drag coefficient on predicted dynamic tensions	164
Figure 7-20:	Effect of the drag coefficient on predicted normal displacement at the middle	165
Figure 7-21:	Effect of the drag coefficient on predicted normal velocity at the middle	165

List of Tables

Table 3-I: Nondimensionalized Parameters of the String used in Figures 3-4 to 3-10	52
Table 3-II: Nondimensionalized Parameters of the String used in Figures 3-11 to 3-16	55
Table 4-I: Cable used in Figures 4-3 to 4-10	80
Table 5-I: Characteristics of the neutral buoy and the segments of the cable	102
Table 6-I: Comparison of the maximum dynamic response of GUYSTA with only nonlinear drag forces, with respect to the case of including both geometric nonlinearity and large tensile forces, as well as nonlinear drag forces	122
Table 6-II: Comparison of minimum dynamic responses of GUYSTA with only nonlinear drag forces with respect to the case of both geometric nonlinearity and large tensile forces, as well as nonlinear drag forces	123
Table 7-I: Sensitivity of the maximum total tension to the number of time steps per period [$C_d=1.5$, Chebyshev terms=11]	148
Table 7-II: Sensitivity of the maximum total tension to the number of Chebyshev polynomials [$C_d=1.5$, time steps per period=200]	149
Table 7-III: Effect of the drag coefficient on the maximum total tension [time steps per period=200, Chebyshev terms=11]	150
Table 7-IV: Cable used in the experiment of the Ship Research Institute of Norway [11].	151
Table 7-V: Comparison of the dynamic tension of the cable with a spring [0.1hz, 25d]	157
Table 7-VI: Comparison of the dynamic tension of the cable with a spring [1hz, 25d]	157
Table 7-VII: Comparison between numerical results and experimental data for the dynamic tension in the cable without spring	158
Table 7-VIII: Effect of the drag coefficient on the dynamic tension and comparison with experimental data	158
Table 7-IX: Comparison of the methodologies used in M. S. Triantafyllou's Analysis and in author's Analysis	159
Table 7-X: Comparison between M.S. Triantafyllou's result, Author's prediction and experimental data [0.1hz, 25d]	160
Table 7-XI: Comparison between M.S. Triantafyllou's result, Author's prediction and experimental data [1hz, 12.5d]	160
Table 7-XII: Cable used in MIT experiment [10].	161

Introduction

The recent move by the offshore industry towards deeper water, made mooring systems very attractive, and created an interest in studying such systems. Semi-submersibles, for example, are normally positioned with a multi-leg mooring system.

Two typical offshore applications, deeper water moorings and open sea towing, suffer from very large cable dynamic tension amplification in rough seas, necessitating a detailed analysis. This in turn requires a complete understanding of the effect of the nonlinearities involved. Also the dynamic analysis of the cable-buoy systems is necessary to ensure safe operation in deeper water.

Researchers have studied the nonlinear dynamics of a mooring line in various coordinate systems [9], [16] and [6]. Recently, Blik derived the cable dynamic equations by considering the kinematics and dynamics of a mooring line in three dimensions [4]. Shin has extended the dynamic equations derived by Blik, using a coordinate system which is based on the moving configuration (dynamic reference) of a mooring line [23].

In this thesis, great attention is paid to the time domain simulation methods for the analysis of nonlinear cable dynamics. The time domain simulation method employed here is based on the collocation method spatially and Newmark's method for time integration.

We focus on three important topics in nonlinear cable dynamics. The first topic is the motion of a cable in water when buoys are attached along its length. The second topic is the combined effect of the geometric nonlinearity, having a large dynamic tension, and nonlinear drag force. The third topic is the effect of zero total tension due to large dynamic tension amplification.

In chapter 1, we derive the fully nonlinear two dimensional dynamic equations, expressed in terms of the displacements p and q , relative to the static configuration of cable.

In chapter 2, these nonlinear equations are simplified, in order to use efficient nonlinear numerical schemes. An order of magnitude analysis is performed to justify the simplification of the equations.

As a first step in the time domain analysis of cable dynamics, the taut string is studied in chapter 3 in detail, subject to nonlinear drag forces and a string-obstacle interaction, because its simplicity allows a clearer understanding of the effect of the nonlinearities involved. The taut string serves also to check the numerical schemes used in this thesis. Researchers in fields such as mathematics, physics and acoustics have treated the taut string problem as a basic example of wave propagation and fundamental vibration theory. [27], [14], [19], [7], [8], [13] and [4], etc.

In chapter 4, a cable subjected to nonlinear drag forces is studied. Time domain simulations are carried out by expanding the cable motions in a set of Chebyshev polynomials. Due to the presence of space-varying terms in the governing equations of the cable, the collocation method is used, because it is superior to Galerkin's method as a spatial integration scheme [22]. Migliore and McReynolds studied the dynamic effects of paying out and reeling in a cable system using the orthogonal collocation method [21] and [20].

A time domain simulation of a cable subject to nonlinear drag forces has been done by Blik [4] and Burgess [5]. Blik used the natural modes of the cable as the set of orthogonal functions, and Burgess used sine functions. Burgess found sine functions have computational advantages over the natural modes of the cable. Both used Galerkin's method, rather than the collocation method used in this thesis. The author has used the equivalent linearization method to treat the nonlinear drag forces by employing frequency domain techniques and an iterative procedure, so that the linear term has the same overall effect as the term it replaces [23].

In chapter 5, the nonlinear static and linearized dynamic equations of a cable with

intermediate buoys are derived. Small motions of a mooring line with buoys attached on it around a mean position, are then simulated. The analysis of a mooring line with attached buoys is necessary to assess the safety of the cable-buoy system in deeper water.

The cable-buoy system appears to be very useful in solving the problems associated with the large self-weight of a mooring line in deep water. By adding appropriate buoys to the mooring line, it is possible to reduce the top tensile force and, therefore, to decrease the diameter of the cable. So far, most analyses are restricted to a cable without buoys and only a few papers refer to the mooring line with buoys.

The fully nonlinear two-dimensional governing equations were derived in Chapter 2, and the simplification of the nonlinear equations was carried out in Chapter 3, in order to use efficient nonlinear numerical schemes.

In chapter 6, we study the combined effects of the geometric nonlinearity, large dynamic tension and nonlinear drag forces on the cable dynamic response, with the limitation that the total tension remains positive at all times.

In chapter 7, we develop a model for a slack-and-snapping cable, which clips off large negative dynamic tensions. The theoretical predictions are then compared with experimental results from [11] and [10].

Negative overall tensions, caused by large dynamic tension build-up, force a cable to go completely slack. Immediately after the cable goes slack, it is forced to go taut in a rapid motion (snapping of cable). Until now, few papers on extreme tensions of a cable have been presented because of the numerical difficulties involved [11] and [18].

Chapters 3 through 7 contain the numerical applications and comparisons with experimental data and some conclusions are drawn from these comparisons.

Chapter 1

Nonlinear Dynamic Equations

1.1 Introduction

Researchers have studied the nonlinear dynamics of a mooring line in various coordinate systems [9], [16] and [6].

Recently, Blik derived the cable dynamic equations by considering the kinematics and dynamics of a mooring line in three dimensions [4]. Shin has extended the dynamic equations derived by Blik, using a coordinate system which is based on the moving configuration (dynamic reference) of a mooring line [23].

In this chapter we deal with the dynamics of a mooring line with coplanar static configuration, when we can study the in-plane dynamics separately, because the out-of-plane motion is uncoupled from the in-plane motions [24].

In the next chapter, a simplification of the two-dimensional nonlinear hydrodynamic force is investigated.

1.2 Decomposition of (Relative) Velocity and Drag Force

We employ two different coordinate systems ; one based on the static configuration of a mooring line (static reference system), and the other based on the moving configuration (dynamic reference system). The former will be denoted by (p,q) , the latter by (x,y) . See Figure (1-1). We project the drag forces and velocities along both coordinate systems, and relations between the corresponding components are derived.

- **Two Coordinate Systems**

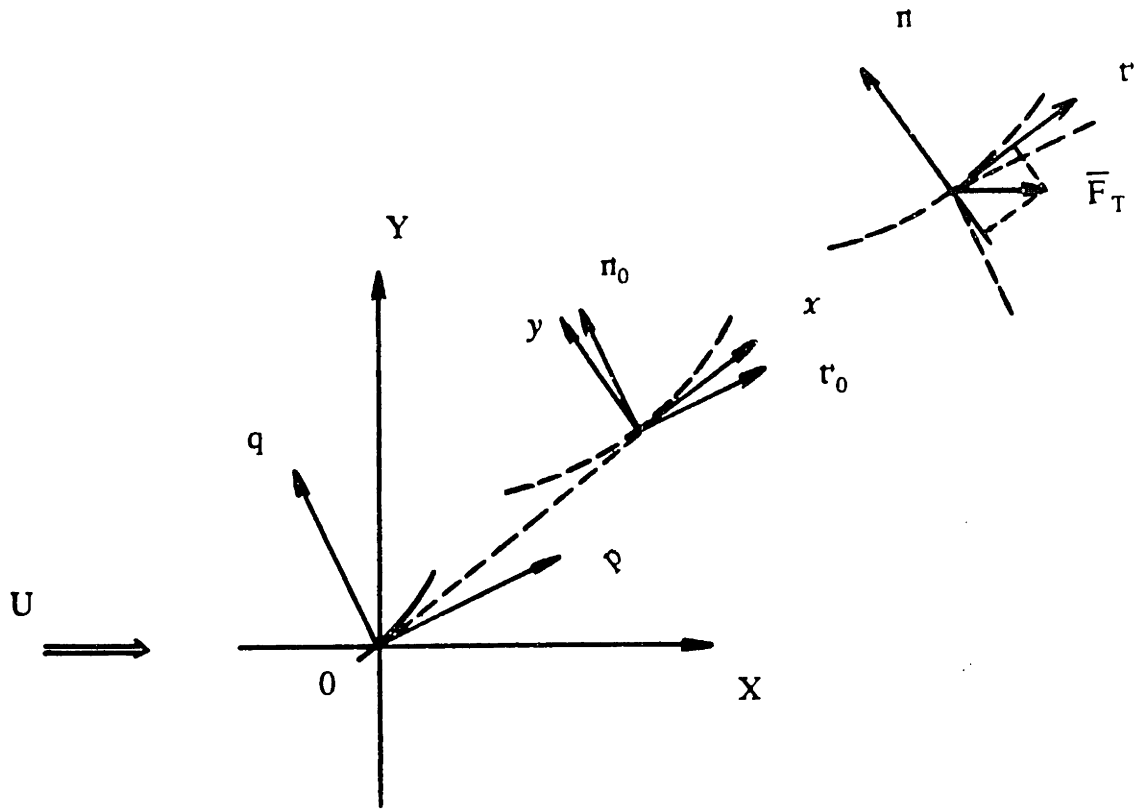


Figure 1-1: Coordinate Systems for Velocities and Drag Forces

(p,q) : coordinate system fixed on the static configuration
unit vectors (r_0, n_0)

(x,y) : coordinate system fixed on the dynamic configuration
unit vectors (r, n)

• **Relations between Unit Vectors**

$$r = r_0 \cos \phi_1 + n_0 \sin \phi_1 \tag{1.1}$$

$$n = -r_0 \sin \phi_1 + n_0 \cos \phi_1$$

• **Velocity**

Direction	Cable	Current
r	$v_t = \frac{\partial p}{\partial t} \cos \phi_1 + \frac{\partial q}{\partial t} \sin \phi_1$	$U \cos(\phi_1 + \phi_0)$
n	$v_n = -\frac{\partial p}{\partial t} \sin \phi_1 + \frac{\partial q}{\partial t} \cos \phi_1$	$-U \sin(\phi_1 + \phi_0)$

(1.2)

where :

ϕ_0 : static component of the angle ϕ

ϕ_1 : dynamic component of the angle ϕ

v_t : tangential component of cable velocity

v_n : normal component of cable velocity

• **Relative Velocity**

r	$\frac{\partial p}{\partial t} \cos \phi_1 + \frac{\partial q}{\partial t} \sin \phi_1 - U \cos(\phi_1 + \phi_0)$
n	$-\frac{\partial p}{\partial t} \sin \phi_1 + \frac{\partial q}{\partial t} \cos \phi_1 - [-U \cos(\phi_1 + \phi_0)]$

(1.3)

• **Damping Force**

$$\bar{F}_T = \bar{F}_{t1} + \bar{F}_{n1} \quad (1.4)$$

$$= \bar{F}_p + \bar{F}_q$$

Note that by relative velocity we mean the relative velocity between the cable and the fluid particles.

Drag Force = - f (Relative Velocity)

1.3 Nonlinear Dynamic Equations

The dynamic equations, obtained from the equilibrium of forces acting on a mooring line in a moving coordinate system (x,y), including the nonlinear hydrodynamic forces, are as follows [Blick 84] :

$$m \left[\frac{\partial v_t}{\partial t} - v_n \frac{\partial \phi}{\partial t} \right] = \frac{\partial T_e}{\partial s} - w_0 \sin \phi + F_{t1}$$

$$m \left[\frac{\partial v_n}{\partial t} + v_t \frac{\partial \phi}{\partial t} \right] = T_e \frac{\partial \phi}{\partial s} - w_0 \cos \phi + F_{n1} - m_a \frac{\partial v_n}{\partial t} \quad (1.5)$$

with :

$$F_{t1} = 0.5 \pi \rho_w C_{Dt} D_0 (U \cos \phi - v_t) |U \cos \phi - v_t| (1+e/2)$$

$$F_{n1} = 0.5 \rho_w C_{Dt} D_0 (-U \sin \phi - v_n) |-U \sin \phi - v_n| (1+e/2)$$

$$v_t = \frac{\partial p}{\partial t} \cos \phi_1 + \frac{\partial q}{\partial t} \sin \phi_1$$

$$v_n = -\frac{\partial p}{\partial t} \sin \phi_1 + \frac{\partial q}{\partial t} \cos \phi_1$$

where :

m = Mass per unit unstretched length

T_e = Effective tension

e = Strain

The compatibility equations for the mooring lines must be satisfied. :

$$\frac{\partial v_t}{\partial s} - \frac{\partial \phi}{\partial s} v_n = \frac{\partial e}{\partial t}$$

(1.6)

$$\frac{\partial v_n}{\partial s} + \frac{\partial \phi}{\partial s} v_t = (1+e) \frac{\partial \phi}{\partial t}$$

Finally, a constitutive equation for the cable must be added :

$$T_e = f\left(e, \frac{\partial e}{\partial t}, s\right)$$

(1.7)

Equations (1.5), (1.6) and (1.7) constitute a complete set of the nonlinear two-dimensional dynamic equations (5 equations with 5 unknowns).

1.4 Reformulation of Equations of Motion

Using relations (1.1) and (1.2), we can reformulate the governing equations (1.5). The following two equations are obtained using (1.1).

t_0 direction :

$$\begin{aligned}
 & m \left[\frac{\partial v_t}{\partial t} - v_n \frac{\partial \phi}{\partial t} \right] \cos \phi_1 - m \left[\frac{\partial v_n}{\partial t} + v_t \frac{\partial \phi}{\partial t} \right] \sin \phi_1 \\
 & = \frac{\partial T_e}{\partial s} \cos \phi_1 - w_0 \sin \phi \cos \phi_1 + F_{t1}(1+e) \cos \phi_1 - T_e \frac{\partial \phi}{\partial s} \sin \phi_1 \\
 & + w_0 \cos \phi \sin \phi_1 - F_{n1}(1+e) \sin \phi_1 + m_a \frac{\partial v_n}{\partial t} \sin \phi_1
 \end{aligned} \tag{1.8}$$

n_0 direction :

$$\begin{aligned}
 & m \left[\frac{\partial v_t}{\partial t} - v_n \frac{\partial \phi}{\partial t} \right] \sin \phi_1 + m \left[\frac{\partial v_n}{\partial t} + v_t \frac{\partial \phi}{\partial t} \right] \cos \phi_1 \\
 & = \frac{\partial T_e}{\partial s} \sin \phi_1 - w_0 \sin \phi \sin \phi_1 + F_{t1}(1+e) \sin \phi_1 + T_e \frac{\partial \phi}{\partial s} \cos \phi_1 \\
 & - w_0 \cos \phi \cos \phi_1 + F_{n1}(1+e) \cos \phi_1 - m_a \frac{\partial v_n}{\partial t} \cos \phi_1
 \end{aligned}$$

The above equations (1.8) can be rewritten, using relations (1.2) with $\phi = \phi_0 + \phi_1$, as :

$$\begin{aligned}
 m \frac{\partial^2 p}{\partial t^2} &= \frac{\partial T_e}{\partial s} \cos \phi_1 - w_0 \sin \phi_0 - T_e \frac{\partial \phi}{\partial s} \sin \phi_1 \\
 &+ F_{t1}(1+e) \cos \phi_1 - F_{n1}(1+e) \sin \phi_1 \\
 &+ m_a \left[-\left(\frac{\partial^2 p}{\partial t^2} + \frac{\partial q}{\partial t} \frac{\partial \phi_1}{\partial t} \right) \sin^2 \phi_1 - \left(\frac{\partial p}{\partial t} \frac{\partial \phi_1}{\partial t} - \frac{\partial^2 q}{\partial t^2} \right) \sin \phi_1 \cos \phi_1 \right] \quad (1.9)
 \end{aligned}$$

$$\begin{aligned}
 m \frac{\partial^2 q}{\partial t^2} &= \frac{\partial T_e}{\partial s} \sin \phi_1 - w_0 \cos \phi_0 - T_e \frac{\partial \phi}{\partial s} \cos \phi_1 \\
 &+ F_{t1}(1+e) \sin \phi_1 + F_{n1}(1+e) \cos \phi_1 \\
 &- m_a \left[-\left(\frac{\partial^2 p}{\partial t^2} + \frac{\partial q}{\partial t} \frac{\partial \phi_1}{\partial t} \right) \sin \phi_1 \cos \phi_1 - \left(\frac{\partial p}{\partial t} \frac{\partial \phi_1}{\partial t} - \frac{\partial^2 q}{\partial t^2} \right) \cos^2 \phi_1 \right]
 \end{aligned}$$

These governing equations, expressed in terms of p and q, are based on coordinates fixed on static configuration of the cable (quasi-static reference).

We need the following static equations and the decomposition $T_e = T_0 + T_1$, in order to obtain the governing equations in final form.

$$\begin{aligned} r_0 & : \frac{dT_0}{ds} = w_0 \sin \phi_0 - F_{i0} (1 + \epsilon_0) \\ n_0 & : T_0 \frac{d\phi_0}{ds} = w_0 \cos \phi_0 - F_{n0} (1 + \epsilon_0) \end{aligned} \quad (1.10)$$

$$\frac{dx}{ds} = (1 + \epsilon_0) \cos \phi_0$$

$$\frac{dy}{ds} = (1 + \epsilon_0) \sin \phi_0$$

$$T_0 = EA_0 \epsilon_0$$

(Refer to [Blick 84]).

Inserting static equations (1.10) into (1.9), we obtain the reformulation of (1.5).

$$\begin{aligned} m \frac{\partial^2 p}{\partial t^2} &= \frac{\partial T_1}{\partial s} \cos \phi_1 - T_0 \frac{d\phi_0}{ds} \sin \phi_1 \\ &+ [F_{n1} \cos \phi_1 - F_{n1} \sin \phi_1] (1 + \epsilon) - F_{i0} (1 + \epsilon_0) \\ &+ m_a [- \left(\frac{\partial^2 p}{\partial t^2} + \frac{\partial q}{\partial t} \frac{\partial \phi_1}{\partial t} \right) \sin^2 \phi_1 - \left(\frac{\partial p}{\partial t} \frac{\partial \phi_1}{\partial t} - \frac{\partial^2 q}{\partial t^2} \right) \sin \phi_1 \cos \phi_1] \\ &+ \frac{dT_0}{ds} (\cos \phi_1 - 1) - T_0 \frac{\partial \phi_1}{\partial s} \sin \phi_1 - T_1 \frac{d\phi_0}{ds} \sin \phi_1 - T_1 \frac{\partial \phi_1}{\partial s} \sin \phi_1 \end{aligned} \quad (1.11)$$

$$\begin{aligned}
 m \frac{\partial^2 q}{\partial t^2} &= \frac{dT_0}{ds} \sin \phi_1 + T_0 \frac{\partial \phi_1}{\partial s} \cos \phi_1 + T_1 \frac{d\phi_0}{ds} \cos \phi_1 \\
 &+ [F_{t1} \sin \phi_1 + F_{n1} \cos \phi_1] (1+e) - F_{n0}(1+e_0) \\
 &+ m_s [(\frac{\partial^2 p}{\partial t^2} + \frac{\partial q}{\partial t} \frac{\partial \phi_1}{\partial t}) \sin \phi_1 \cos \phi_1 + (\frac{\partial p}{\partial t} \frac{\partial \phi_1}{\partial t} - \frac{\partial^2 q}{\partial t^2}) \cos^2 \phi_1] \\
 &+ \frac{\partial T}{\partial s} \sin \phi_1 - T_0 \frac{d\phi_0}{ds} (\cos \phi_1 - 1) + T_1 \frac{\partial \phi_1}{\partial s} \cos \phi_1
 \end{aligned}$$

1.5 Reformulation of Compatibility Equations

Similarly, we can reformulate compatibility equations (1.6) using relations (1.1) and (1.2)

Using (1.1),

r_0 :

$$\begin{aligned}
 &\frac{\partial v_1}{\partial s} \cos \phi_1 - \phi_s v_2 \cos \phi_1 - \frac{\partial v_2}{\partial s} \sin \phi_1 - \phi_s v_1 \sin \phi_1 \\
 &= \frac{\partial e}{\partial t} \cos \phi_1 - (1+e) \phi_t \sin \phi_1
 \end{aligned} \tag{1.12}$$

n_0 :

$$\begin{aligned} & \frac{\partial v_1}{\partial s} \sin \phi_1 - \phi_s v_2 \sin \phi_1 + \frac{\partial v_2}{\partial s} \cos \phi_1 + \phi_s v_1 \cos \phi_1 \\ & = \frac{\partial e}{\partial t} \sin \phi_1 - (1+e) \phi_t \cos \phi_1 \end{aligned}$$

Using (1.2),

$$\frac{\partial}{\partial s} \left(\frac{\partial p}{\partial t} \right) - \phi_s \frac{\partial q}{\partial t} + \frac{\partial q}{\partial t} \frac{\partial \phi_1}{\partial s} = \frac{\partial e}{\partial t} \cos \phi_1 - (1+e) \frac{\partial \phi_1}{\partial t} \sin \phi_1 \quad (1.13)$$

$$\frac{\partial}{\partial s} \left(\frac{\partial q}{\partial t} \right) + \phi_s \frac{\partial p}{\partial t} - \frac{\partial p}{\partial t} \frac{\partial \phi_1}{\partial s} = \frac{\partial e}{\partial t} \sin \phi_1 + (1+e) \frac{\partial \phi_1}{\partial t} \cos \phi_1$$

After manipulating some terms and using $\phi = \phi_0 + \phi_1$, we obtain the following simpler equations.

$$\frac{\partial}{\partial s} \left(\frac{\partial p}{\partial t} \right) - \frac{\partial q}{\partial t} \frac{d\phi_0}{ds} = \frac{\partial}{\partial t} [(1+e) \cos \phi_1] \quad (1.14)$$

$$\frac{\partial}{\partial s} \left(\frac{\partial q}{\partial t} \right) + \frac{\partial p}{\partial t} \frac{d\phi_0}{ds} = \frac{\partial}{\partial t} [(1+e) \sin \phi_1]$$

Since the two operators $\frac{\partial}{\partial s}$ and $\frac{\partial}{\partial t}$ are commutative, it follows that

$$\frac{\partial}{\partial t} \left[\frac{\partial p}{\partial s} - q \frac{d\phi_0}{ds} \right] = \frac{\partial}{\partial t} [(1+e)\cos\phi_1] \quad (1.15)$$

$$\frac{\partial}{\partial t} \left[\frac{\partial q}{\partial s} + p \frac{d\phi_0}{ds} \right] = \frac{\partial}{\partial t} [(1+e)\sin\phi_1]$$

Finally, we can make the above equations (1.15) independent of time.

$$\frac{\partial p}{\partial s} - q \frac{d\phi_0}{ds} = (1+e)\cos\phi_1 + C_1(s) \quad (1.16)$$

$$\frac{\partial q}{\partial s} + p \frac{d\phi_0}{ds} = (1+e)\sin\phi_1 + C_2(s)$$

where $C_1(s)$ and $C_2(s)$ are integration constants and are independent of time t .

In order to determine $C_1(s)$ and $C_2(s)$, we use initial conditions.

If $\phi_1 = 0$, $p = 0$ and $q = 0$ at time $t = 0$,

$$e = e_0 \quad (1.17)$$

Under the initial condition (1.17),

$$\frac{\partial p}{\partial s} - q \frac{d\phi_0}{ds} = 0 = (1+e_0) + C_1(s) \quad (1.18)$$

$$\frac{\partial q}{\partial s} + p \frac{d\phi_0}{ds} = 0 = 0 + C_2(s)$$

Therefore we can derive $C_1(s)$ and $C_2(s)$ from (1.18)

$$C_1(s) = -(1+e_0) \quad (1.19)$$

$$C_2(s) = 0$$

In terms of p and q , the compatibility equations can be cast in the following simple form.

$$\frac{\partial p}{\partial s} - q \frac{d\phi_0}{ds} = (1+e)\cos\phi_1 - (1+e_0) \quad (1.20)$$

$$\frac{\partial q}{\partial s} + p \frac{d\phi_0}{ds} = (1+e)\sin\phi_1$$

1.6 Summary of Fully Nonlinear Two-Dimensional Governing Equations

$$\begin{aligned}
 m \frac{\partial^2 p}{\partial t^2} &= \frac{\partial T_1}{\partial s} \cos \phi_1 - T_0 \frac{d\phi_0}{ds} \sin \phi_1 \\
 &+ [F_{n1} \cos \phi_1 - F_{n1} \sin \phi_1] (1+e) - F_{t0}(1+e_0) \\
 &+ m_a [-(\frac{\partial^2 p}{\partial t^2} + \frac{\partial q}{\partial t} \frac{\partial \phi_1}{\partial t}) \sin^2 \phi_1 - (\frac{\partial p}{\partial t} \frac{\partial \phi_1}{\partial t} - \frac{\partial^2 q}{\partial t^2}) \sin \phi_1 \cos \phi_1] \\
 &+ \frac{dT_0}{ds} (\cos \phi_1 - 1) - T_0 \frac{\partial \phi_1}{\partial s} \sin \phi_1 - T_1 \frac{d\phi_0}{ds} \sin \phi_1 - T_1 \frac{\partial \phi_1}{\partial s} \sin \phi_1
 \end{aligned} \tag{1.21}$$

$$\begin{aligned}
 m \frac{\partial^2 q}{\partial t^2} &= \frac{dT_0}{ds} \sin \phi_1 + T_0 \frac{\partial \phi_1}{\partial s} \cos \phi_1 + T_1 \frac{d\phi_0}{ds} \cos \phi_1 \\
 &+ [F_{t1} \sin \phi_1 + F_{n1} \cos \phi_1] (1+e) - F_{n0}(1+e_0) \\
 &+ m_a [(\frac{\partial^2 p}{\partial t^2} + \frac{\partial q}{\partial t} \frac{\partial \phi_1}{\partial t}) \sin \phi_1 \cos \phi_1 + (\frac{\partial p}{\partial t} \frac{\partial \phi_1}{\partial t} - \frac{\partial^2 q}{\partial t^2}) \cos^2 \phi_1] \\
 &+ \frac{\partial T}{\partial s} \sin \phi_1 - T_0 \frac{d\phi_0}{ds} (\cos \phi_1 - 1) + T_1 \frac{\partial \phi_1}{\partial s} \cos \phi_1
 \end{aligned} \tag{1.22}$$

$$\frac{\partial p}{\partial s} - q \frac{d\phi_0}{ds} = (1+e) \cos \phi_1 - (1+e_0) \tag{1.23}$$

$$\frac{\partial q}{\partial s} + p \frac{d\phi_0}{ds} = (1+e) \sin \phi_1 \tag{1.24}$$

Chapter 2

Simplification of Nonlinear Dynamic Equations

2.1 Introduction

In chapter 1, we derived the fully nonlinear dynamic equations, which are expressed in terms of the displacements p and q , based on the static configuration of cable. These nonlinear equations may be simplified, in order to use efficiently nonlinear numerical schemes, but care should be taken not to oversimplify and hence omit important nonlinear mechanisms.

The author has used the equivalent linearization method to treat the nonlinear drag forces by employing frequency domain techniques and an iterative procedure, so that the linear term has the same overall effect as the term it replaces [Shin 85]. This procedure is employed often to simplify complex nonlinear equations without losing their particular properties [2].

2.2 Assumptions

In order to simplify the nonlinear equations of motion, we make the following assumptions.

- In case of harmonic excitation we assume that each dynamic quantity is also harmonic (just for estimating the order of magnitude of the nonlinear terms). We write it in the form of a complex amplitude times a complex exponential, but we mean always the real part of it.

$$\begin{aligned} p &= p_a e^{i\omega t} & q &= q_a e^{i\omega t} \\ \phi_1 &= \phi_{1a} e^{i\omega t} & T_1 &= T_{1a} e^{i\omega t} \end{aligned} \quad (2.1)$$

- T_1 may be large. We can distinguish two cases :

When $\frac{T_p}{T_{1a}} > 1$ we may use a linear approach.

When $\frac{T_p}{T_{1a}} \leq 1$ we must use a nonlinear approach. (2.2)

with $O\left(\frac{T_0}{T_p}\right) = 1$, $T_p =$ pretension

In this chapter we are interested in the latter case.

- ϕ_1 remains small ; for example,

$$\frac{\phi_{1\max}}{\phi_{0\max}} = O(10^{-2}) \quad \text{with} \quad O(\phi_{0\max}) \sim 1 \quad (2.3)$$

Assumption (2.3) leads to the following relations.

$$O(\sin\phi_1) = O(\phi_1) \quad (2.4)$$

$$O(\cos\phi_1 - 1) = O\left(-\frac{\phi_1^2}{2}\right)$$

After higher order terms have been omitted, we can write the following approximate relations.

$$\sin\phi_1 = \phi_1 \quad (2.5)$$

$$\cos\phi_1 - 1 = -\frac{\phi_1^2}{2}$$

Equations (1.21) and (1.22) are considered term by term, in order to eliminate those terms which are not important.

2.3 Simplification of the Equation of Motion in the Tangential Direction

All of terms in equation (1.21) are compared to each other. In case of harmonic excitation, assumptions (2.1) and (2.3) are applicable.

$$A = \frac{m_a \frac{\partial^2 p}{\partial t^2} \sin^2 \phi_1}{m \frac{\partial^2 p}{\partial t^2}} = [\phi_{1a}^2]$$

$$B = \frac{m_a \frac{\partial q}{\partial t} \frac{\partial \phi_1}{\partial t} \sin^2 \phi_1}{m \frac{\partial^2 p}{\partial t^2}} = [\frac{q_a}{p_a} \phi_{1a}^3]$$

$$C = \frac{m_a \frac{\partial p}{\partial t} \frac{\partial \phi_1}{\partial t} \sin \phi_1 \cos \phi_1}{m \frac{\partial^2 p}{\partial t^2}} = [\phi_{1a}^2]$$

$$D = \frac{m_a \frac{\partial^2 q}{\partial t^2} \sin \phi_1 \cos \phi_1}{m \frac{\partial^2 p}{\partial t^2}} = [\frac{q_a}{p_a} \phi_{1a}]$$

Considering the following relation,

$$\frac{\partial T_1}{\partial s} \cos \phi_1 = \frac{\partial T_1}{\partial s} [1 - \frac{\phi_1^2}{2} + O(\phi_1^3)]$$

$$E = \frac{\frac{\partial T_1 \phi_1^2}{\partial s}}{\frac{\partial T_1}{\partial s}} = [\phi_{1a}^2]$$

$$F = \frac{T_0 \frac{d\phi_0}{ds} \sin \phi_1}{\frac{\partial T_1}{\partial s}} = [\frac{T_p}{T_{1a}} \phi_{1a}]$$

$$G = \frac{\frac{dT_0}{ds} (\cos \phi_1 - 1)}{\frac{\partial T_1}{\partial s}} = [\frac{T_p}{T_{1a}} \phi_{1a}^2]$$

$$H = \frac{T_0 \frac{\partial \phi_1}{\partial s} \sin \phi_1}{\frac{\partial T_1}{\partial s}} = [\frac{T_p}{T_{1a}} \phi_{1a}^2]$$

$$I = \frac{T_1 \frac{d\phi_0}{ds} \sin \phi_1}{\frac{\partial T_1}{\partial s}} = [\phi_{1a}]$$

$$J = \frac{T_1 \frac{\partial \phi_1}{\partial s} \sin \phi_1}{\frac{\partial T_1}{\partial s}} = [\phi_{1a}^2]$$

After neglecting the higher order terms $[\phi_{1a}^2]$ - A, B, C, E and J - we get the following equation.

$$\begin{aligned}
 m \frac{\partial^2 p}{\partial t^2} &= \frac{\partial T_1}{\partial s} - T_0 \frac{d\phi_0}{ds} \sin \phi_1 + [F_{dt} \cos \phi_1 - F_{dn} \sin \phi_1] (1 + e) \\
 &- F_{i0} (1 + e_0) + m_a \frac{\partial^2 q}{\partial t^2} \sin \phi_1 \cos \phi_1 \\
 &+ \frac{dT_0}{ds} (\cos \phi_1 - 1) - T_0 \frac{\partial \phi_1}{\partial s} \sin \phi_1 - T_1 \frac{d\phi_0}{ds} \sin \phi_1
 \end{aligned} \tag{2.6}$$

Also, using assumption (2.2), we can eliminate G and H.

$$\begin{aligned}
 m \frac{\partial^2 p}{\partial t^2} &= \frac{\partial T_1}{\partial s} - T_0 \frac{d\phi_0}{ds} \sin \phi_1 + [F_{dt} \cos \phi_1 - F_{dn} \sin \phi_1] (1 + e) \\
 &- F_{i0} (1 + e_0) + m_a \frac{\partial^2 q}{\partial t^2} \sin \phi_1 \cos \phi_1 - T_1 \frac{d\phi_0}{ds} \sin \phi_1
 \end{aligned} \tag{2.7}$$

In order to further simplify equation, we apply assumptions (2.5) to (2.7) again.

$$\begin{aligned}
 m \frac{\partial^2 p}{\partial t^2} &= \frac{\partial T_1}{\partial s} - T_0 \frac{d\phi_0}{ds} \sin \phi_1 + [F_{dt} \cos \phi_1 - F_{dn} \sin \phi_1] (1 + e) \\
 &- F_{i0} (1 + e_0) + m_a \frac{\partial^2 q}{\partial t^2} \phi_1
 \end{aligned} \tag{2.8}$$

2.4 Simplification of the Equation of Motion in the Normal Direction

All of the terms in equation (1.22), are similarly compared to each other. In case of harmonic excitation, assumptions (2.1) and (2.3) are employed.

$$a = \frac{m_a \frac{\partial^2 p}{\partial t^2} \sin \phi_1 \cos \phi_1}{m \frac{\partial^2 q}{\partial t^2}} = \left[\frac{p_a}{q_a} \phi_{1a} \right]$$

$$b = \frac{m_a \frac{\partial q}{\partial t} \frac{\partial \phi_1}{\partial t} \sin \phi_1 \cos \phi_1}{m \frac{\partial^2 q}{\partial t^2}} = \left[\phi_{1a}^2 \right]$$

$$c = \frac{m_a \frac{\partial p}{\partial t} \frac{\partial \phi_1}{\partial t} \cos^2 \phi_1}{m \frac{\partial^2 q}{\partial t^2}} = \left[\frac{p_a}{q_a} \phi_{1a} \right]$$

$$d = \frac{m_a \frac{\partial^2 q}{\partial t^2} \cos^2 \phi_1}{m \frac{\partial^2 q}{\partial t^2}} = O(1)$$

$$e = \frac{\frac{dT_0}{ds} \sin \phi_1}{\frac{\partial T_1}{\partial s}} = \left[\frac{T_p}{T_{1a}} \phi_{1a} \right]$$

$$f = \frac{T_0 \frac{\partial \phi_1}{\partial s} \cos \phi_1}{\frac{\partial T_1}{\partial s}} = \left[\frac{T_p}{T_{1a}} \phi_{1a} \right]$$

$$g = \frac{T_1 \frac{d\phi_0}{ds} \cos \phi_1}{\frac{\partial T_1}{\partial s}} = \left[\frac{T_p}{T_{1a}} \right]$$

$$h = \frac{\frac{\partial T_1}{\partial s} \sin \phi_1}{\frac{\partial T_1}{\partial s}} = \left[\phi_{1a} \right]$$

$$i = \frac{T_0 \frac{d\phi_0}{ds} (\cos \phi_0 - 1)}{\frac{\partial T_1}{\partial s}} = \left[\frac{T_p}{T_{1a}} \phi_{1a}^2 \right]$$

$$j = \frac{T_1 \frac{\partial \phi_1}{\partial s} \cos \phi_1}{\frac{\partial T_1}{\partial s}} = \left[\phi_{1a} \right]$$

Neglecting $[\phi_{1a}^2]$ and considering $O\left(\frac{T_p}{T_{1a}}\right) \leq 1$, we can eliminate b and i.

Using relations (2.5), the following simplified equation is obtained :

$$\begin{aligned} (m + m_a) \frac{\partial^2 q}{\partial t^2} = \frac{dT_0}{ds} \phi_1 + T_0 \frac{\partial \phi_1}{\partial s} + T_1 \frac{d\phi_0}{ds} + [F_{dt} \phi_1 + F_{dn}] (1 + e) \\ - F_{n0} (1 + e_0) + m_a \left[\frac{\partial^2 p}{\partial t^2} \phi_1 + \frac{\partial p}{\partial t} \frac{\partial \phi_1}{\partial t} \right] + \frac{\partial T_1}{\partial s} \phi_1 + T_1 \frac{\partial \phi_1}{\partial s} \end{aligned} \quad (2.9)$$

2.5 A Simplified Version of the Compatibility Relations

We can estimate the order of magnitude of each term in the compatibility relations (1.23) and (1.24). In order to avoid eliminating terms which are small, but which nonetheless represent important nonlinear effects, and to retain consistently terms of similar order of magnitude, we make use of the large physical quantity, E (Young's Modulus) as shown in the sequel. We can rewrite the compatibility equations as follows ;

$$\frac{\partial p}{\partial s} - q \frac{d\phi_0}{ds} = (1+e)(\cos \phi_1 - 1) + e_1 \quad (2.10)$$

$$\frac{\partial q}{\partial s} + p \frac{d\phi_0}{ds} = (1+e)\sin \phi_1 \quad (2.11)$$

Using relations (2.5), and including terms like $e \frac{\phi_1^2}{2}$ and $e\phi_1$,

we obtain the compatibility relations in the form :

$$\frac{\partial p}{\partial s} - q \frac{d\phi_0}{ds} = (1+e) \left(-\frac{\phi_1^2}{2} \right) + e_1 \quad (2.12)$$

$$\frac{\partial q}{\partial s} + p \frac{d\phi_0}{ds} = (1+e)\phi_1 \quad (2.13)$$

Since the linear tension-extension relation is,

$$e_1 = \frac{T_1}{EA} \quad (2.14)$$

we must multiply by EA each term in the compatibility relations, to estimate their order of magnitude, when expressed as forces :

$$EA \frac{\partial p}{\partial s} - EA q \frac{d\phi_0}{ds} = EA(1+e) \left(-\frac{\phi_1^2}{2} \right) + EA e_1 \quad (2.15)$$

$$EA \frac{\partial q}{\partial s} + EA p \frac{d\phi_0}{ds} = EA(1+e) \phi_1 \quad (2.16)$$

Comparing each term in (2.15) and (2.16) with $\frac{\partial T_1}{\partial s}$, as found in sections (2.3) and (2.4), we find that there is no trivial term in the equation above.

2.6 Nonlinear Terms in the Governing Equations

We distinguish between linear governing equations and simplified nonlinear governing equations. From equations (2.8), (2.9), (2.15) and (2.16), we identify the following nonlinear terms.

$$m_a \frac{\partial^2 q}{\partial t^2} \phi_1 \text{ and } T_1 \frac{d\phi_0}{ds} \phi_1 \quad \text{in (2.8)}$$

$$m_a \frac{\partial^2 p}{\partial t^2} \phi_1, m_a \frac{\partial p}{\partial t} \frac{\partial \phi_1}{\partial t}, \frac{\partial T_1}{\partial s} \phi_1 \text{ and } T_1 \frac{\partial \phi_1}{\partial s} \quad \text{in (2.9)}$$

$$(1+e) \left(-\frac{\phi_1^2}{2} \right) \quad \text{in (2.15)}$$

$$e \phi_1 \quad \text{in (2.16)}$$

nonlinear drag terms in (2.8) and (2.9)

An iterative method, together with an equivalent linearization procedure, can give good results as found in the case of studying nonlinear drag forces [25].

The displacement p in the tangential direction is much smaller than the displacement q in the normal direction. This means that

$m_s \frac{\partial^2 p}{\partial t^2}$ and $m_s \frac{\partial p}{\partial t} \frac{\partial \phi_1}{\partial t}$ in (2.9) can be neglected.

2.7 Summary of Nonlinear Governing Equations after Higher Order Terms are Omitted

$$m \frac{\partial^2 p}{\partial t^2} = \frac{\partial T_1}{\partial s} - T_0 \frac{d\phi_0}{ds} \phi_1 + [F_{dt} - F_{dn} \phi_1] (1 + e) - F_{t0} (1 + e_0) + m_a \frac{\partial^2 q}{\partial t^2} \phi_1 \quad (2.17)$$

$$(m + m_a) \frac{\partial^2 q}{\partial t^2} = \frac{dT_0}{ds} \phi_1 + T_0 \frac{\partial \phi_1}{\partial s} + T_1 \frac{d\phi_0}{ds} + [F_{dt} \phi_1 + F_{dn}] (1 + e) - F_{n0} (1 + e_0) + \frac{\partial T_1}{\partial s} \phi_1 + T_1 \frac{\partial \phi_1}{\partial s} \quad (2.18)$$

$$EA \frac{\partial p}{\partial s} - EA q \frac{d\phi_0}{ds} = EA (1 + e) \left(-\frac{\phi_1^2}{2} \right) + EA e_1 \quad (2.19)$$

$$EA \frac{\partial q}{\partial s} + EA p \frac{d\phi_0}{ds} = EA (1 + e) \phi_1 \quad (2.20)$$

Chapter 3

Nonlinear Dynamics of a String

3.1 Introduction

As a first step in the time domain analysis of cable dynamics, the taut string will be studied in detail, subject to nonlinear drag forces and a string-obstacle interaction, because its simplicity allows a clearer understanding of the nonlinearities involved. The taut string will serve also to check the numerical schemes used in this thesis.

Many researchers in fields such as mathematics, physics and acoustics have studied the taut string problem as a basic example for describing wave propagation and fundamental vibration theory [27], [14], [19], [7], [8], [13] and [4], etc.

3.2 Dynamic Equations

3.2.1 Linearized Dynamic Equations of a Taut String in Air

We assume that the dynamic tension T_1 , caused by a small disturbance around the static configuration of a taut string, is very small with respect to the static tension T_0 .

From dynamic equilibrium conditions and the assumption of small displacements, we obtain linearized equations for the taut string in air as follows (refer to equations (2.17) through (2.20))

$$m \frac{\partial^2 q}{\partial t^2} = \frac{T_0}{1+e_0} \frac{\partial^2 q}{\partial s^2} \quad (3.1)$$

$$m \frac{\partial^2 p}{\partial t^2} = EA_0 \frac{\partial^2 q}{\partial s^2}$$

where m : mass per unit length

p : axial displacement

q : transverse displacement

T_0 : static tension

e_0 : static strain

s : Lagrangian coordinate

E : Young's modulus

A_0 : Cross-sectional Area

The two equations (3.1) are uncoupled from each other and hence Elasticity is not important quantitatively for the transverse motion of a taut string. However, Young's modulus E should be finite in order to have any vibrations at all.

3.2.2 Dynamic Equations of a Taut String in Water

The motions of a string in water differ basically from those of a string in air, due to the presence of large hydrodynamic forces. In this thesis, a Morison type of loading is used to model the hydrodynamic forces. The mass of the string is augmented by an added mass, which represents a weighted integral of the kinetic energy in its surrounding water. Because the added mass of a flexible body in unsteady shear flow is difficult to obtain, we

employ the approximation of using at each section the added mass per unit length of a rigid cylinder with the same cross-section and two-dimensional flow conditions. The drag force is assumed to be a quadratic function of the relative velocity between the string and the ambient fluid. The linearized dynamic equations with one additional nonlinear term, the drag force, are written as follows :

$$M \frac{\partial^2 q}{\partial t^2} = \frac{T_0}{1+e_0} \frac{\partial^2 q}{\partial s^2} + F_n \quad (3.2)$$

$$m \frac{\partial^2 p}{\partial t^2} = EA_0 \frac{\partial^2 p}{\partial s^2} + F_t$$

with

$$F_n = -0.5 \rho_w C_{d_n} D_0 \left| \frac{\partial q}{\partial t} - U_q \right| \left(\frac{\partial q}{\partial t} - U_q \right)$$

$$F_t = -0.5 \rho_w C_{d_t} D_0 \left| \frac{\partial p}{\partial t} - U_p \right| \left(\frac{\partial p}{\partial t} - U_p \right)$$

$$M = m + a$$

where a : added mass per unit length

D_0 : unstretched diameter of the string

F_n : transverse component of the drag force

F_t : axial component of the drag force

U_q : transverse component of the velocity of the ambient water

U_p : axial component of the velocity of the ambient water

$\frac{\partial q}{\partial t}$: transverse component of the velocity of the string

$\frac{\partial p}{\partial t}$: axial component of the velocity of the string

ρ_w : water density

C_{dn} : transverse drag coefficient

C_{dt} : frictional drag coefficient

3.2.3 Nondimensionalized Dynamic Equations

The linearized dynamic equations which include the nonlinear drag forces, are nondimensionalized by introducing the following nondimensionalized variables :

$$\frac{\partial^2 q'}{\partial t'^2} = \frac{\partial^2 q'}{\partial s'^2} - C_{d_n} \left| \frac{\partial q'}{\partial t'} - U_{q'} \right| \left(\frac{\partial q'}{\partial t'} - U_{q'} \right) \quad (3.3)$$

$$\frac{\partial^2 p'}{\partial t''^2} = \frac{\partial^2 p'}{\partial s'^2} - C_{d_t} \left| \frac{\partial p'}{\partial t''} - U_{p'} \right| \left(\frac{\partial p'}{\partial t''} - U_{p'} \right)$$

where

$$s' = \frac{s}{l/2} \quad t' = \frac{t}{l/2 \sqrt{(m+a)(1+e_0)} / T_0}$$

$$t'' = \frac{t}{l/2 \sqrt{(m+a)} / EA_0} \quad k = \frac{(m+a)}{0.5\rho_w D_0}$$

$$K' = \frac{kt'}{t} \quad K'' = \frac{kt''}{t}$$

$$q' = \frac{q}{k} \quad p' = \frac{p}{k}$$

$$U_{q'} = \frac{U_q}{K'} \quad U_{p'} = \frac{U_p}{K''}$$

The nondimensionalized equations (3.3) have the form of the classical wave equations with the addition of nonlinear drag forces.

3.3 Classical Wave Equation with Inhomogeneous Boundary Conditions

The classical wave equation with inhomogeneous boundary conditions in the transverse direction can be transformed into an equation with homogeneous boundary conditions by introducing a quasi-static solution. After dropping primes, the governing equation in the transverse direction is :

$$\frac{\partial^2 q}{\partial t^2} = \frac{\partial^2 q}{\partial s^2} \quad (3.4)$$

Initial conditions are :

$$q(s,0) = f(s)$$

$$\frac{\partial q}{\partial t}(s,0) = g(s)$$

Inhomogeneous boundary conditions are (see Fig. 3-1) :

$$q(-1,t) = 0$$

$$q(1,t) = h(t)$$

where $f(s)$: initial position

$g(s)$: initial velocity

$h(t)$: a nondimensionalized excitation

The quasi-static solution is assumed to be in the form

$$v(s,t) = \frac{s+1}{2} h(t) \quad (3.5)$$

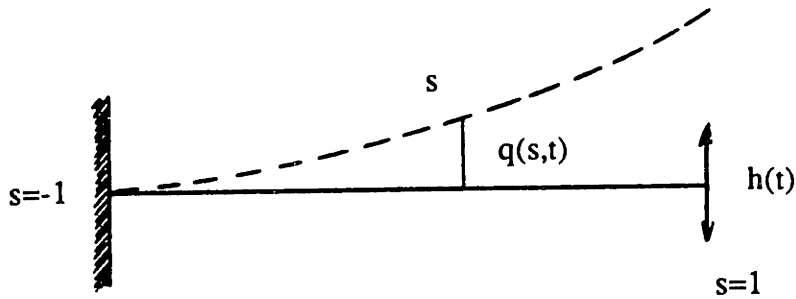


Figure 3-1: a Taut String with Nondimensionalized Variables

After a transformation, we obtain the following equation which is inhomogeneous.

$$\frac{\partial^2 w}{\partial t^2} = \frac{\partial^2 w}{\partial s^2} - \frac{s+1}{2} \frac{d^2 h}{dt^2} \quad (3.6)$$

with $w(s,t) = g(s,t) - v(s,t)$

where the initial conditions are

$$w(s,0) = F(s) = f(s) - \frac{s+1}{2} h(0)$$

$$\frac{\partial w}{\partial t}(s,0) = g(s) - \frac{s+1}{2} \frac{dh}{dt}(0)$$

and the boundary conditions (homogeneous) are :

$$w(-1,t) = 0$$

$$w(1,t) = 0$$

3.4 Classical Wave Equation with Forcing Function

In equations (3.3) and (3.4), nonlinear drag forces or inhomogeneous boundary conditions are represented by a forcing term $H(s,t)$. Without loss of generality, we can set up the initial conditions in equation (3.6) as follows :

$$f(s) = \frac{s+1}{2} h(0) \tag{3.7}$$

$$g(s) = \frac{s+1}{2} \frac{dh}{dt}(0)$$

Finally, we obtain a linearized equation with a forcing term and homogeneous conditions :

$$\frac{\partial^2 w}{\partial t^2} = \frac{\partial^2 w}{\partial s^2} + H(s,t) \tag{3.8}$$

$$w(s,0) = 0$$

$$\frac{\partial w}{\partial t}(s,0) = 0$$

$$w(-1,t) = 0$$

$$w(1,t) = 0$$

with

$$H(s,t) = -\frac{s+1}{2} \frac{d^2h}{dt^2} - Cd_n \left| \frac{\partial w}{\partial t} + \frac{s+1}{2} \frac{dh}{dt} - U_q \right| \left(\frac{\partial w}{\partial t} + \frac{s+1}{2} \frac{dh}{dt} - U_q \right)$$

3.5 Application of a Spectral Method to the Classical Wave Equation

An approximate solution of the governing equation (3.8) of a taut string in the transverse direction is sought in the form of a truncated series.

$$w_N(s,t) = \sum_{n=1}^N a_n(t) b_n(s) \quad (3.9)$$

where

a_n : expansion coefficients of $w(s,t)$

b_n : time independent orthogonal functions

For this expansion, we use Chebyshev polynomials $T_n(s)$ which are orthogonal to each other in the interval $-1 \leq s \leq 1$, based on the Galerkin approximation [22], [12], [15] and [Hamming].

In the Galerkin method, for $b_n(s)$ to satisfy all boundary conditions and contain Chebyshev polynomials $T_n(s)$, we set up linearly independent functions $b_n(s)$ as follows :

$$b_m(s) = T_m(s) - \begin{cases} T_0(s) & m \text{ even} \\ T_1(s) & m \text{ odd} \end{cases} \quad (3.10)$$

$$m = 2, 3, 4, \dots, N$$

Therefore, the series can be written as :

$$w_N(s,t) = \sum_{m=2}^N a_m(t) b_m(s) \quad (3.11)$$

Using the orthogonality of the Chebyshev polynomials $T_n(s)$ with a Galerkin approximation, ordinary differential equations of the expansion coefficients $a_n(t)$ are obtained.

$$\frac{d^2 a_n(t)}{dt^2} = \frac{1}{C_n} \sum_{p=n+2; p+n=\text{even}}^N p(p^2 - n^2) a_p(t) + \frac{B_1(t)}{C_n} + \frac{B_2(t)}{C_n} (-1)^n$$

$$+ H_n(t)$$

$$n = 0, 1, 2, \dots, N$$

where :

$$B_1(t) = \xi \alpha + \rho(\eta) \beta$$

$$B_2(t) = x \beta + g(h) \alpha \quad (3.12)$$

$$\alpha = \frac{\partial^2 w}{\partial s^2} \Big|_{s=1} + \sum_{n=0}^N H_n(t)$$

$$\beta = \frac{\partial^2 w}{\partial s^2} \Big|_{s=-1} + \sum_{n=0}^N (-1)^n H_n(t)$$

$$\xi = -\frac{(N+0.5)}{N^2+N}$$

$$\eta = \frac{0.5(-1)^N}{N^2+N}$$

$H_n(t)$: Chebyshev Series Coefficient of $H(s,t)$

$$C_n = \begin{cases} 2, & n = 1 \\ 1, & \text{otherwise} \end{cases}$$

As the time integration scheme of (3.12), we use the Newmark method which is unconditionally stable [1].

$$\begin{aligned} \frac{d^2 a_n}{dt^2}(t + \Delta t) = & \frac{1}{C_n} \sum_{p=n+2; p+n=\text{even}}^N p(p^2 - n^2) a_p(t + \Delta t) + \frac{B_1(t+\Delta t)}{C_n} \\ & + \frac{B_2(t+\Delta t)}{C_n} (-1)^n + H_n(t+\Delta t) \end{aligned} \quad (3.13)$$

The left side of equation (3.13) can be calculated from results of the previous time step.

$$\frac{d^2 a_n}{dt^2}(t + \Delta t) = \frac{1}{a\Delta t^2} [a_n(t + \Delta t) - a_n(t)] - \frac{1}{a\Delta t} \frac{da_n(t)}{dt} - \left(\frac{1}{2a} - 1 \right) \frac{d^2 a_n(t)}{dt^2}$$

$$\text{with } a = \frac{1}{4} \tag{3.14}$$

Therefore, the only unknown $a_n(t + \Delta t)$ in both equations (3.13) and (3.14) can be determined by time domain simulation.

3.6 String-Object Interaction

We consider an elastic foundation to model an object obstructing the motion of the string, excited at one end as shown in (Fig. 3-2).

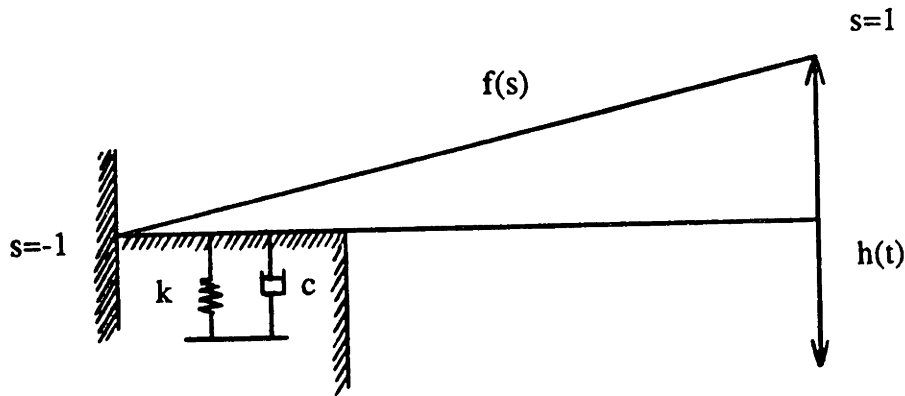


Figure 3-2: String Hitting an Elastic Foundation

The effect of the object can be modelled through an equivalent spring-damper system, i.e. an elastic foundation with an appropriate damper. The continuous distribution

of a spring-damper system can describe properly the effects of the object on the motion of a taut string by adjusting the values of the constants k and c .

In a time domain analysis, these interactions can be included in the forcing term $H(s,t)$ of the classical wave equation (3.8) and this can change the values of α and β in the equation (3.12).

3.7 Results and Comparisons of a Time Domain Analysis of the Taut String

We calculate three different solutions of a taut string from equations (3.13), (A.15) and (A.16) and compare those results.

$$\begin{aligned} \frac{d^2 a_n}{dt^2}(t + \Delta t) = & \frac{1}{C_n} \sum_{p=n+2; p+n=\text{even}}^N p(p^2 - n^2) a_p(t + \Delta t) + \frac{B_1(t+\Delta t)}{C_n} \\ & + \frac{B_2(t+\Delta t)}{C_n} (-1)^n + H_n(t+\Delta t) \quad \text{from (3.13)} \end{aligned}$$

$$u(x,t) = -\sum_{n=1}^{\infty} \frac{C_n}{\omega^2 - (n\pi/l)^2} \left[\cos \omega t - \cos \frac{n\pi}{l} t \right] \sin \frac{n\pi}{l} x$$

$$\text{with } C_n = \frac{2}{l} \int_0^l f(x) \sin \frac{n\pi}{l} x \, dx \quad \text{from (A.15)}$$

$$\frac{d^2 q_n}{dt^2} = -\left(\frac{n\pi}{l}\right)^2 q_n(t) + C_n \cos \omega t \quad \text{from (A.16)}$$

The principal nondimensionalized parameters of the string and the excitation used for comparisons of Fig. (3-4) to Fig. (3-10) are shown in Table 3-I (see Fig. 3-3).

Fig. (3-4) shows the comparison between the transverse displacements of the middle

Table 3-I: Nondimensionalized Parameters of the String used in Figures 3-4 to 3-10

length = 2

first natural frequency = $\pi/2$

frequency of excitation = $\pi/4$

amplitude of excitation = 1

excitation function = $\cos(\pi t/4)$

initial velocity along the string = 0

initial position of the string = $(s+1)/2$

where s is a nondimensionalized Lagrangian coordinate : $(-1 \leq s \leq 1)$

of the string subjected to a nonlinear drag force, relative to the displacements of an undamped string. As we expected, the asymmetry and irregularity in the curve of the transverse displacement of an undamped spring, are eliminated in the case of a damped string due to the significant damping action of the fluid drag.

In Figures (3-5), (3-6) and (3-7) we show the sensitivity of the solution to the number of time steps per period for the case of undamped vibration, with the excitation frequency equal to half the first natural frequency.

When the number of orthogonal functions is 20 and the number of time steps is 20,

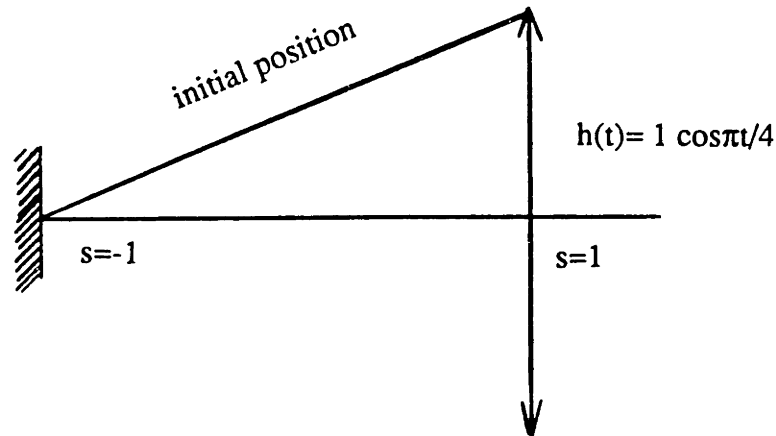


Figure 3-3: Initial position of the string and Excitation imposed at the end

Fig. 3-5 shows disagreement between the exact solution obtained from equation (A.15) in the form of a sine series, and solutions obtained from equations (3.13) and (A.16) using Chebyshev polynomials and sine functions, respectively. Note that the two solutions from equations (3.13) and (A.15) are very close to each other in all cases considered in this chapter (Fig. 3-10). When the number of time steps per period increases to 40, there is little difference relative to the case of using 20 time steps (Fig. 3-6). When we select 100 for the number of time steps per period, Fig. 3-7 showed very good agreement between the numerical solutions and the exact solution.

Next, we investigated the sensitivity of the solution to the number of orthogonal functions used, as shown in Figures (3-6), (3-8), (3-9) and (3-10). With a constant number of time steps per period equal to 40, we changed the number of orthogonal functions. As seen in Figures (3-6), (3-8) and (3-9), the effect of the number of orthogonal functions used on the transverse displacements is very small. As Figures (3-10) and (3-5) show, when the number of time steps per period was reduced to 20, the sensitivity to the number of orthogonal functions was found to be very small also.

Therefore, we can conclude that the effect of the number of time steps per period is more important than the effect of the number of orthogonal functions on the dynamic response of the string for the particular frequency considered. It means that the better way to obtain accurate predictions is to increase the number of time steps per period, rather than the number of orthogonal functions.

In Table 3-II, the principal nondimensionalized parameters of the string and the excitation used for string-object problem, are shown.

Fig. (3-11) shows the transverse displacement at the middle of the string subjected to a nonlinear drag force.

Fig. (3-12) and Fig. (3-13) show the time history of the transverse displacements along the string subjected to nonlinear drag force. Due to the nonlinear drag force, we can find the phase difference between the displacements at the middle and at the top of the string. Figures (3-14) to (3-16) show the transverse displacements of the string when hitting the object, modelled as an elastic foundation with spring constant k and damping coefficient c , as shown in Fig. (3-2).

For lower values of the spring constant, $k=15$, and the damping coefficient, $c=10$, the string penetrated the object, which was relatively soft (Figures 3-14 and 3-15), while, for the higher values of $k=1000$ and $c=1000$, the string did not penetrate the object and bounced back. In the latter case, the object models better a rigid bottom (Fig. 3-16).

In the numerical calculations, the discontinuity due to such a spring-damper system may cause divergence. So, for large values of k and c , the variable time step interval method is recommended in order to get good convergence characteristics as shown in Fig. (3-16).

**Table 3-II: Nondimensionalized Parameters of the String
used in Figures 3-11 to 3-16**

length = 2

first natural frequency = $\pi/2$

frequency of excitation = $\pi/2$

amplitude of excitation = 1 string diameter

excitation function = $1D \cos(\pi t/4)$

initial velocity along the string = 0

initial position of the string = $(s+1)/2$

where

s is a nondimensionalized Lagrangian coordinate : $(-1 \leq s \leq 1)$

D is the string diameter

DISPLACEMENT OF STRING WITH DAMPING
CHEBYSHEV POLYNOMIALS; COSINE TOP EXCITATION

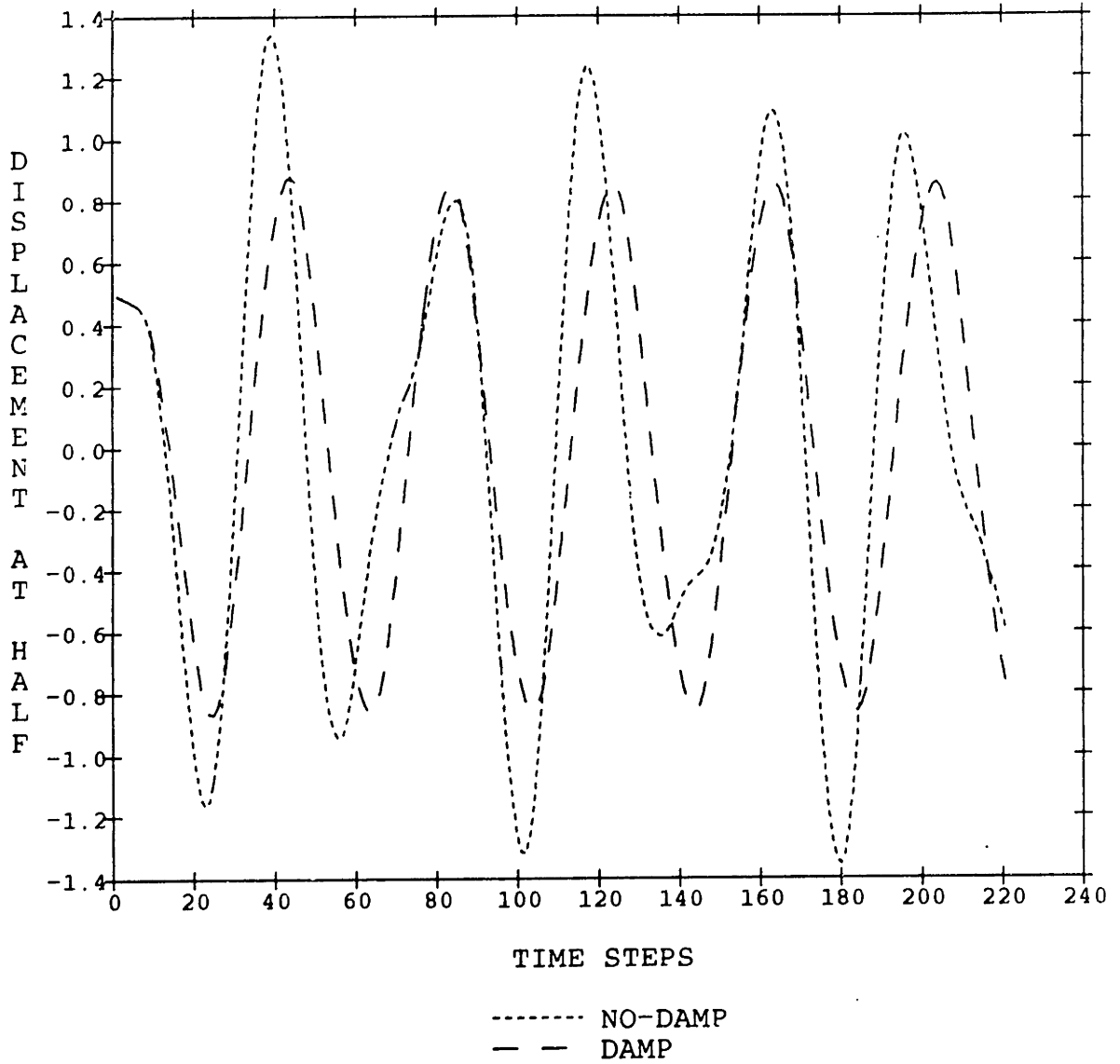


Figure 3-4: Comparison between the Nondimensionalized Transverse Displacements at the Middle of a Damped and an Undamped String [$\pi/4$ (rad/sec) and 1 Dia.]

TRANS. MOTION OF STRING ($1/20 * T, N=20$)

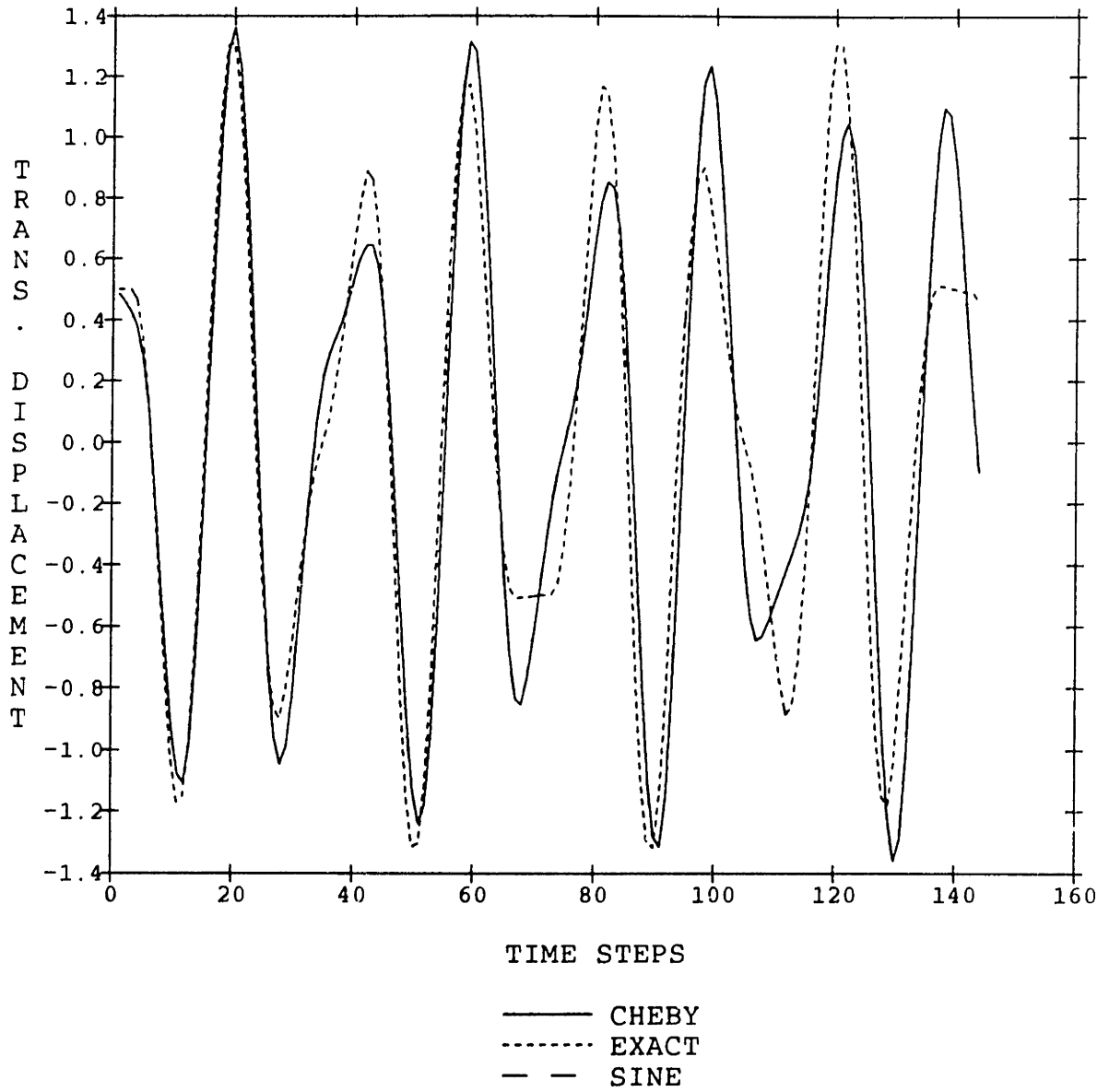


Figure 3-5: Nondimensionalized Transverse Displacement at the Middle of an Undamped String [Period/20 and 20 terms ; $\pi/4$ (rad/sec)]

TRANS. MOTION OF STRING ($1/40 * T, N=20$)

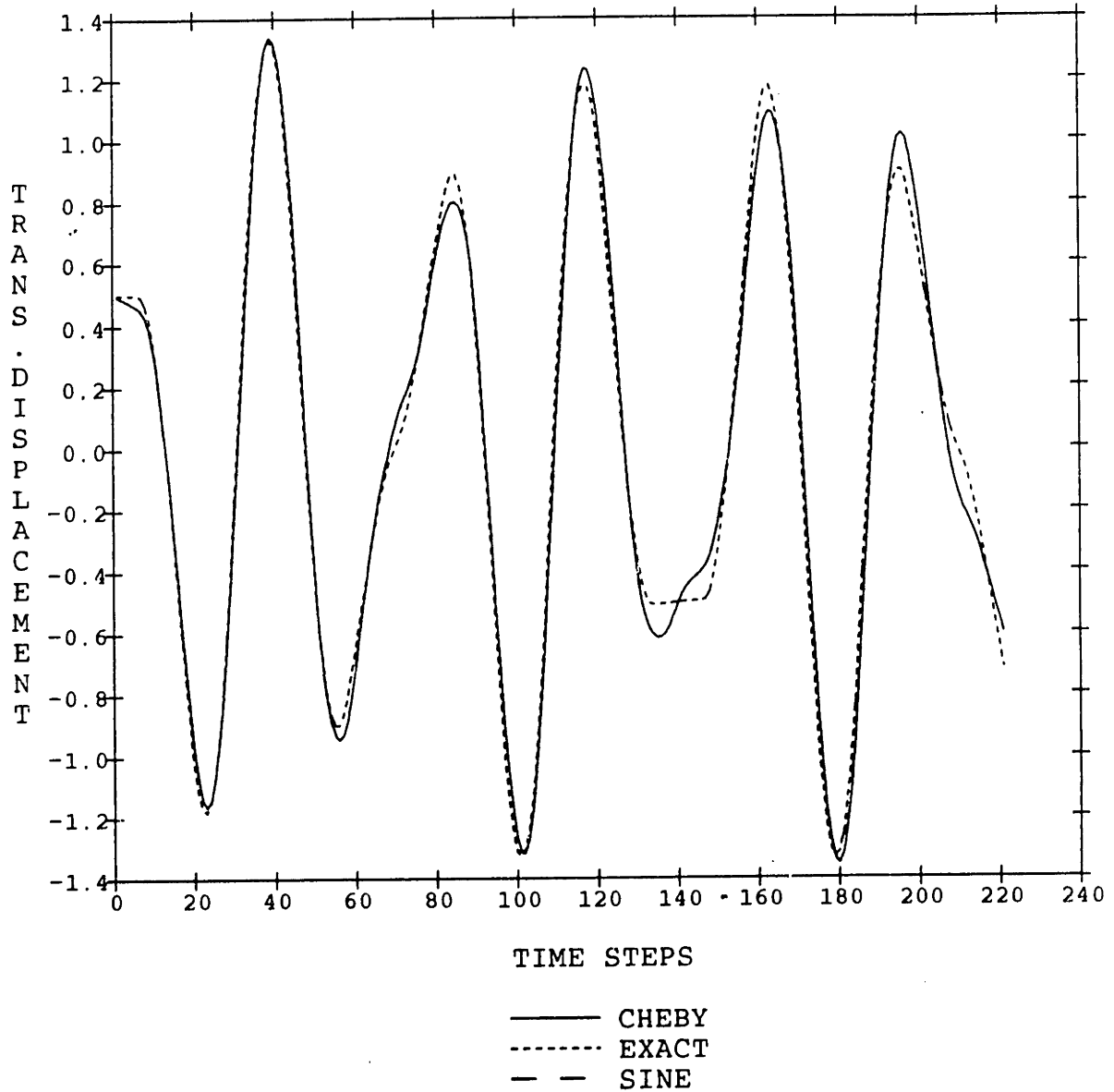


Figure 3-6: Nondimensionalized Transverse Displacement at the Middle of an Undamped String [Period/40 and 20 terms ; $\pi/4$ (rad/sec)]

TRANS.MOTION OF STRING ($1/100 * T, N=20$)

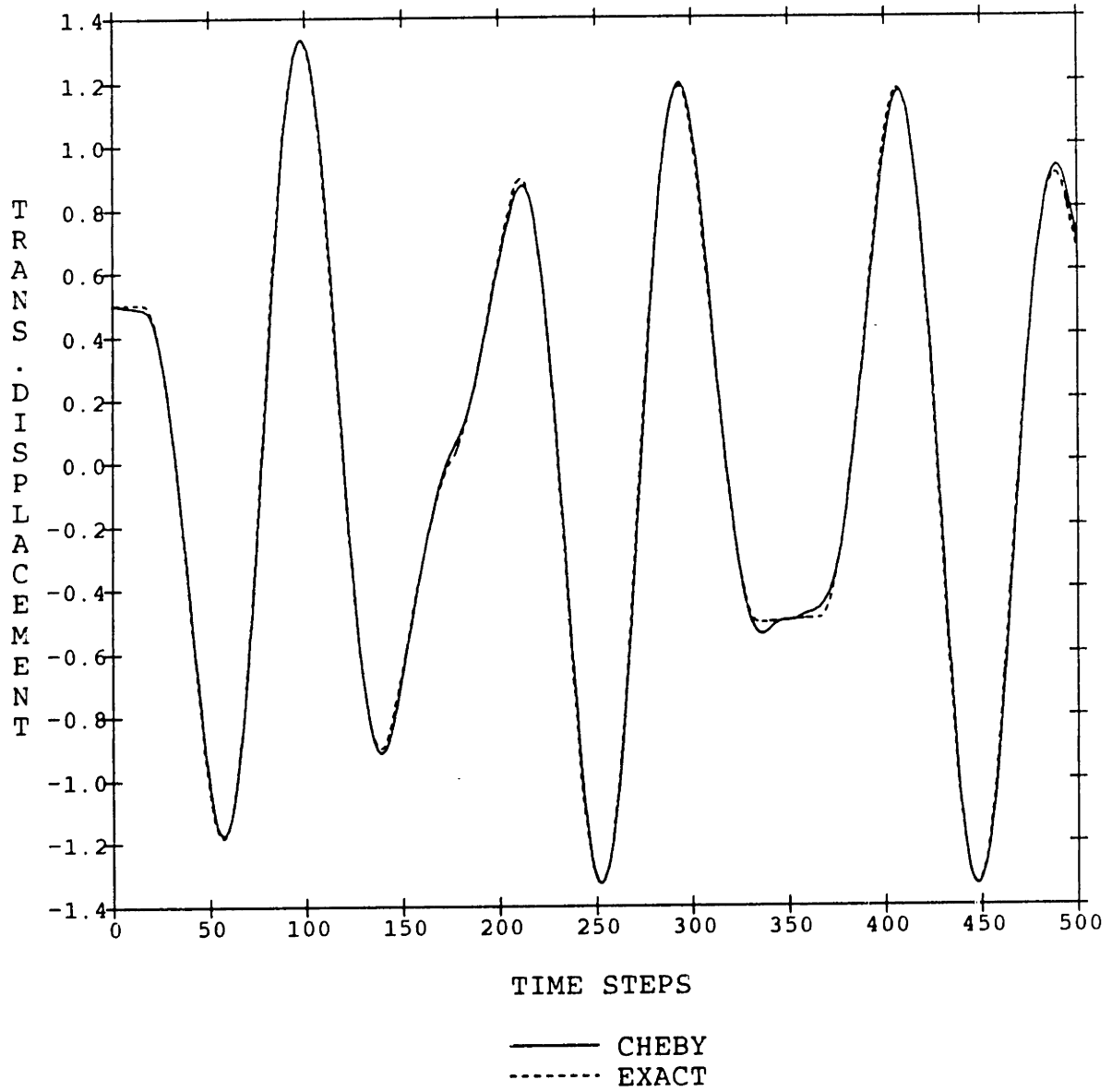


Figure 3-7: Nondimensionalized Transverse Displacement at the Middle of an Undamped String [Period/100 and 20 terms ; $\pi/4$ (rad/sec)]

TRANS. MOTION OF STRING ($1/40 \cdot T, N=30$)

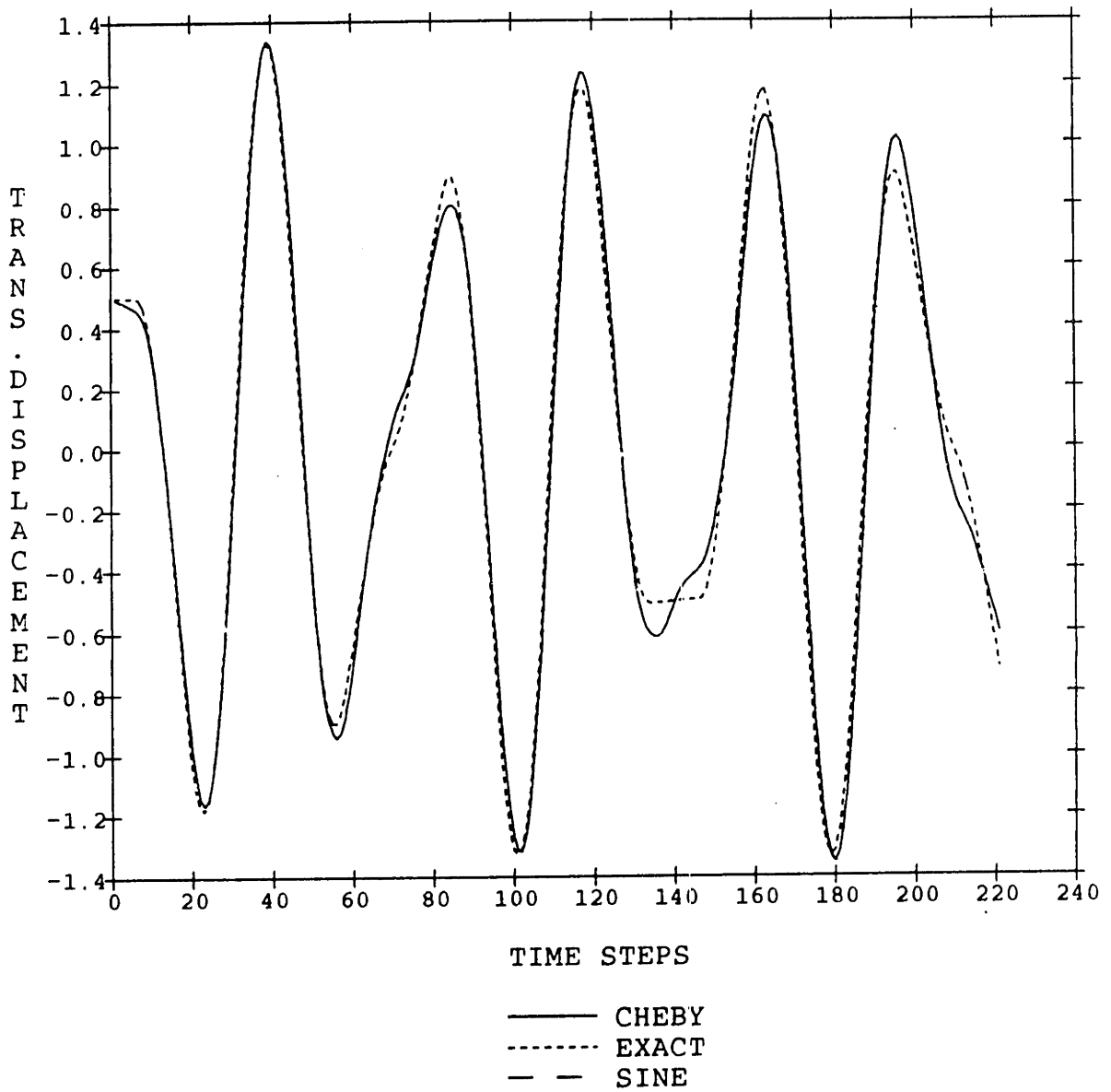


Figure 3-8: Nondimensionalized Transverse Displacement at the Middle of an Undamped String [Period/40 and 30 terms ; $\pi/4$ (rad/sec)]

TRANS. MOTION OF STRING ($1/40 * T, N=10$)

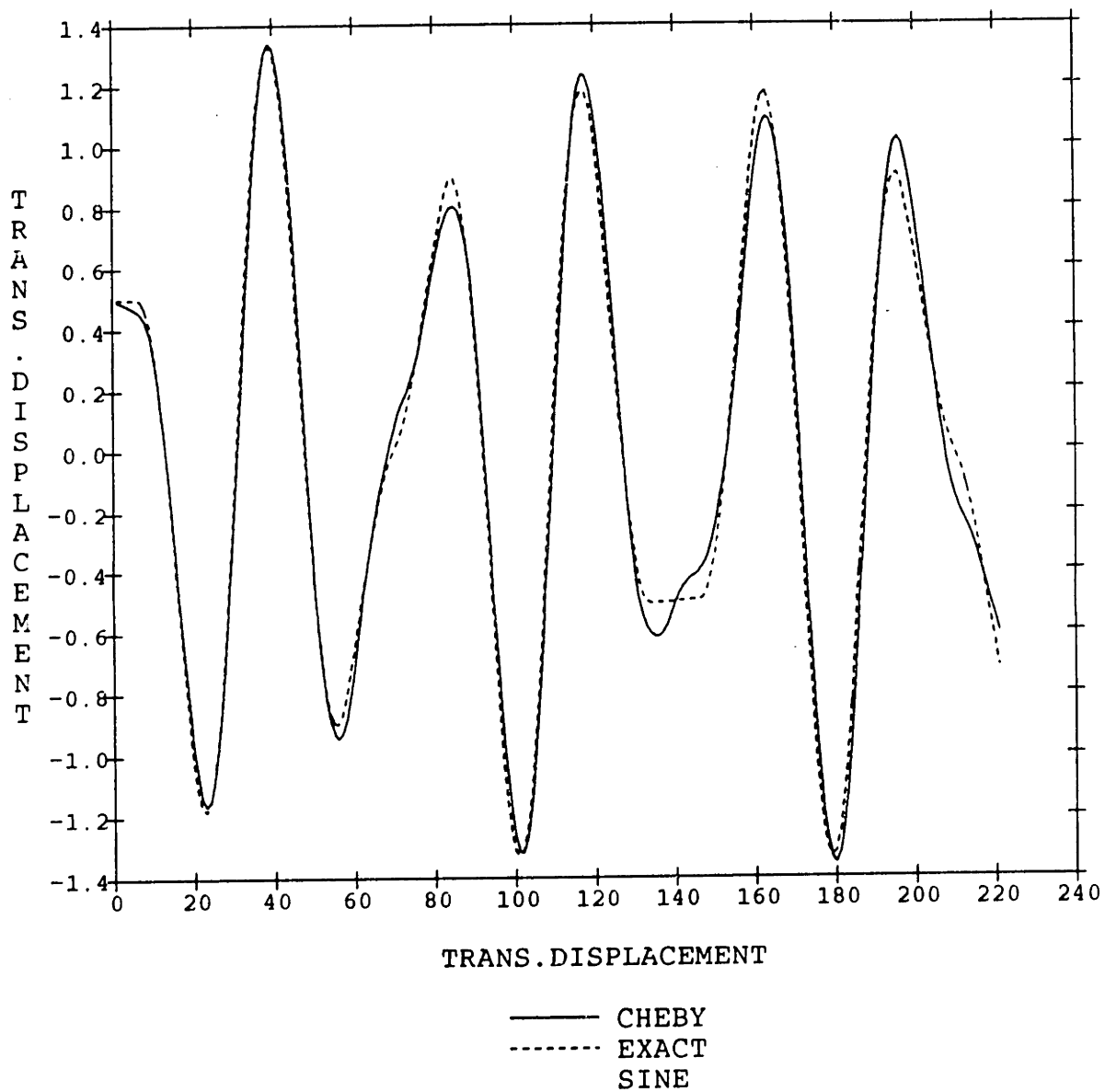


Figure 3-9: Nondimensionalized Transverse Displacement at the Middle of an Undamped String [Period/40 and 10 terms ; $\pi/4$ (rad/sec)]

TRANS. MOTION OF STRING ($1/20 * T, N=30$)

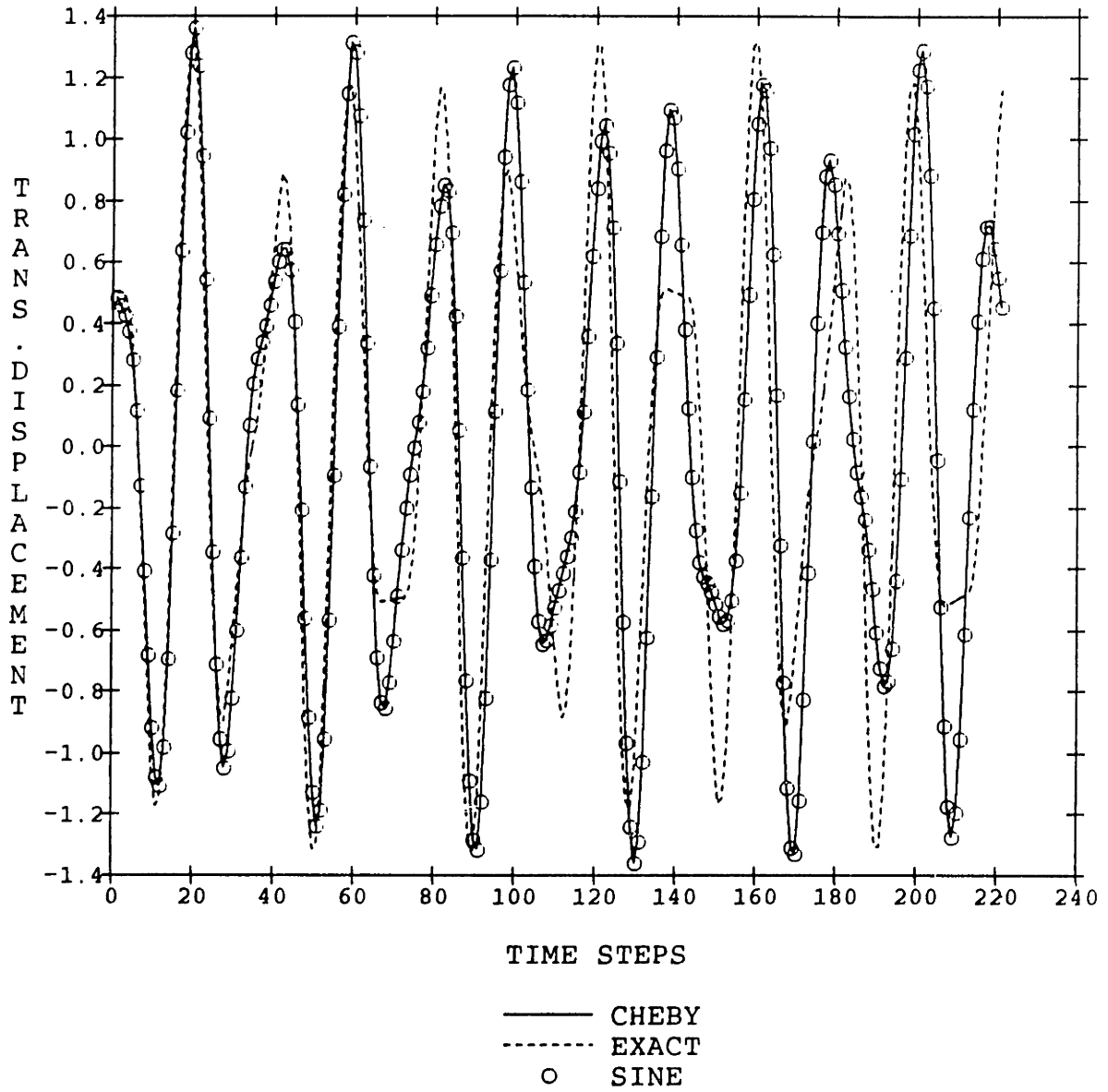
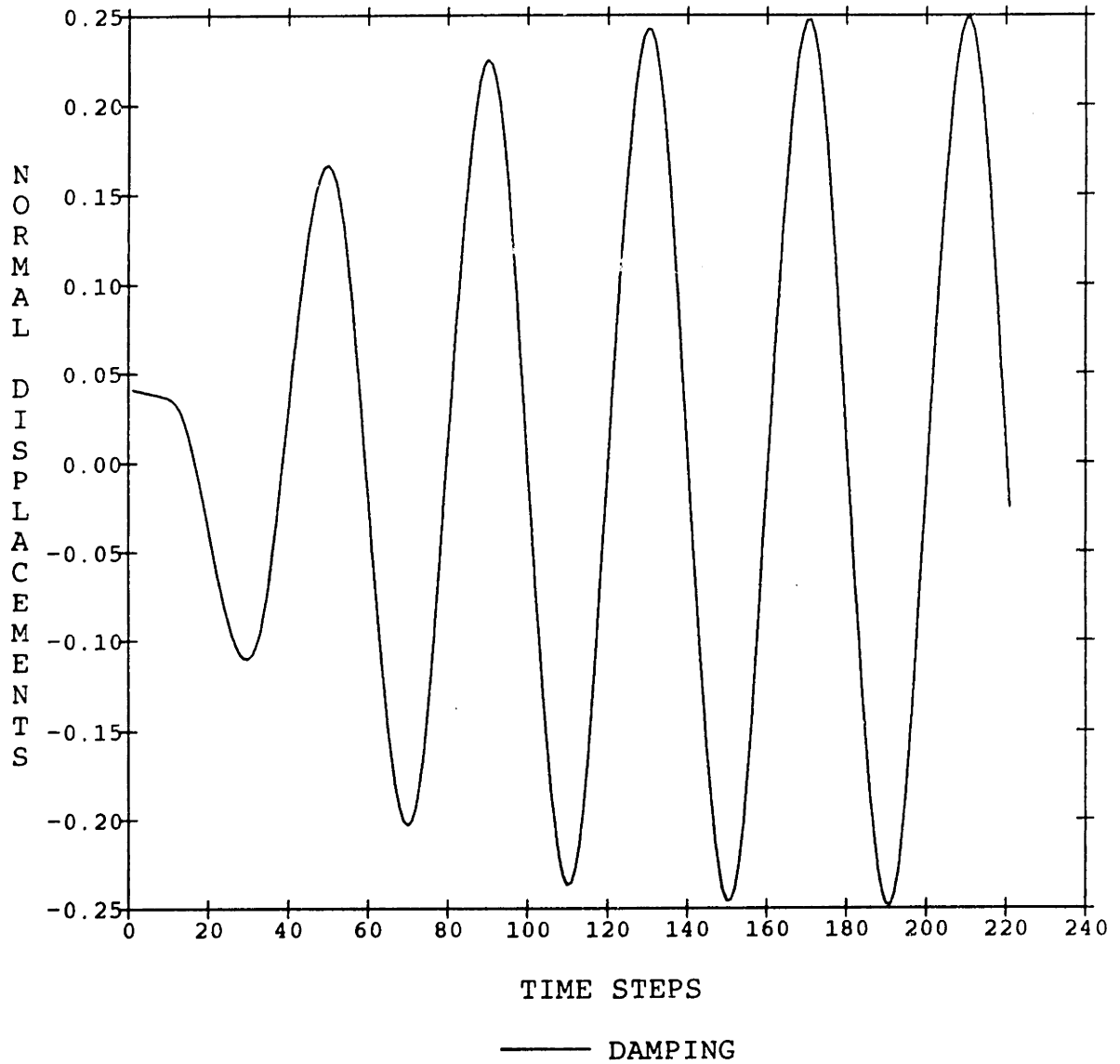


Figure 3-10: Nondimensionalized Transverse Displacement at the Middle of an Undamped String [Period/20 and 30 terms ; $\pi/4$ (rad/sec)]

NORMAL DISPLACEMENT AT MIDPOINT WITH DAMPING AND
FIRST EIGENVALUE (ABS. AMPLITUDE = 1 DIA.)



**Figure 3-11: Transverse Displacement at the Middle of a Damped String
[Excitation ; $\pi/2$ (rad/sec) and 1 Diameter]**

HIT01G

07-OCT-85 13:33 Page 1

DIS. OF STRING HITTING THE RIGID BOTTOM

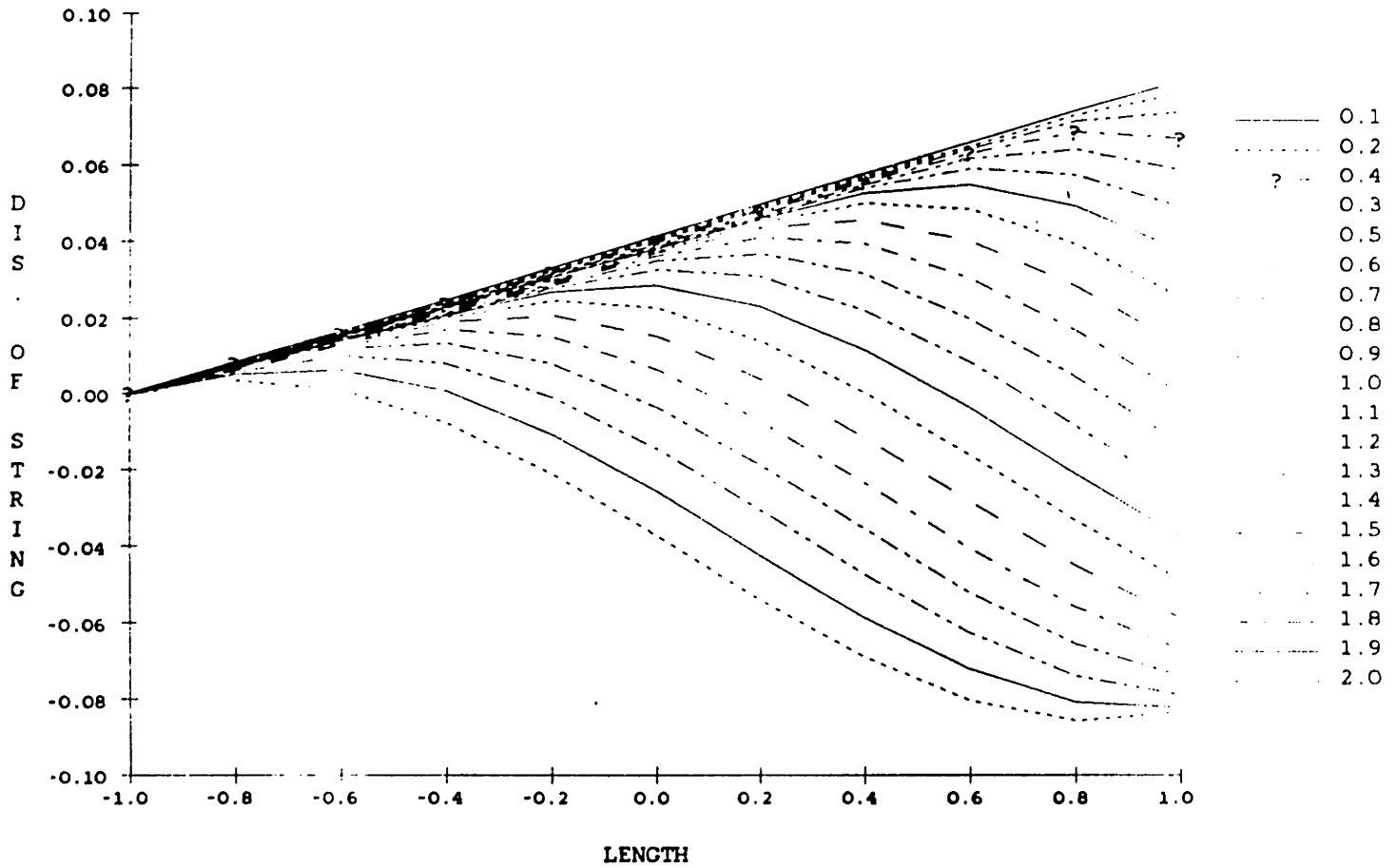


**Figure 3-12: Time History of Transverse Displacement along a Damped String
[Excitation ; $\pi/2$ (rad/sec) and 1 Diameter]**

GNOWALL

24-OCT-85 11:32 Page 1

DISPLACEMENT OF STRING WITH NO WALL

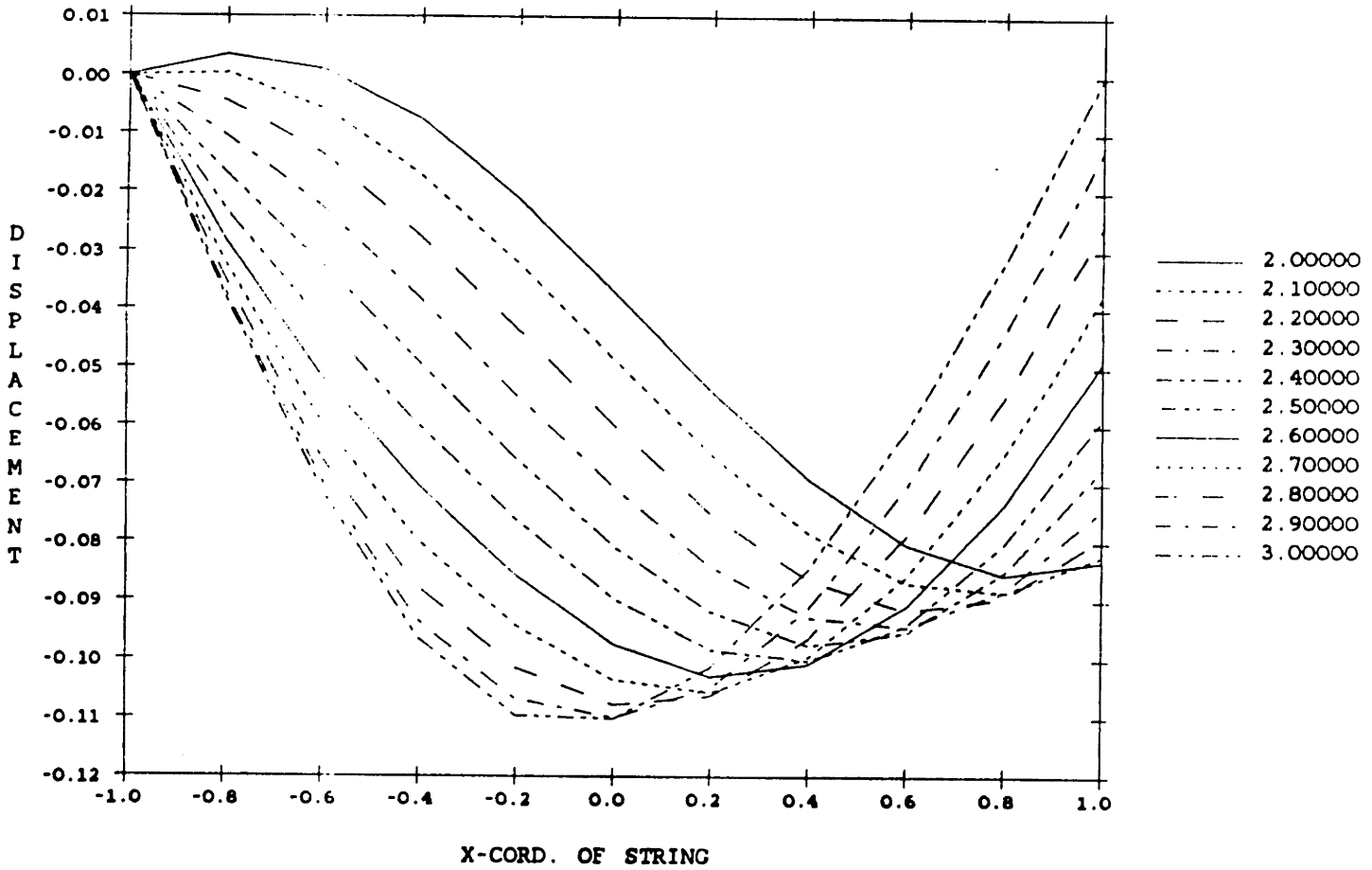


Figure 3-13: Time History of Transverse Displacement along a Damped String [Excitation ; $\pi/2$ (rad/sec) and 1 Diameter]

GMUD15V4

28-OCT-85 11:37 Page 1

DISPLACEMENT OF STRING WITH K=15, C=10 OF MUD

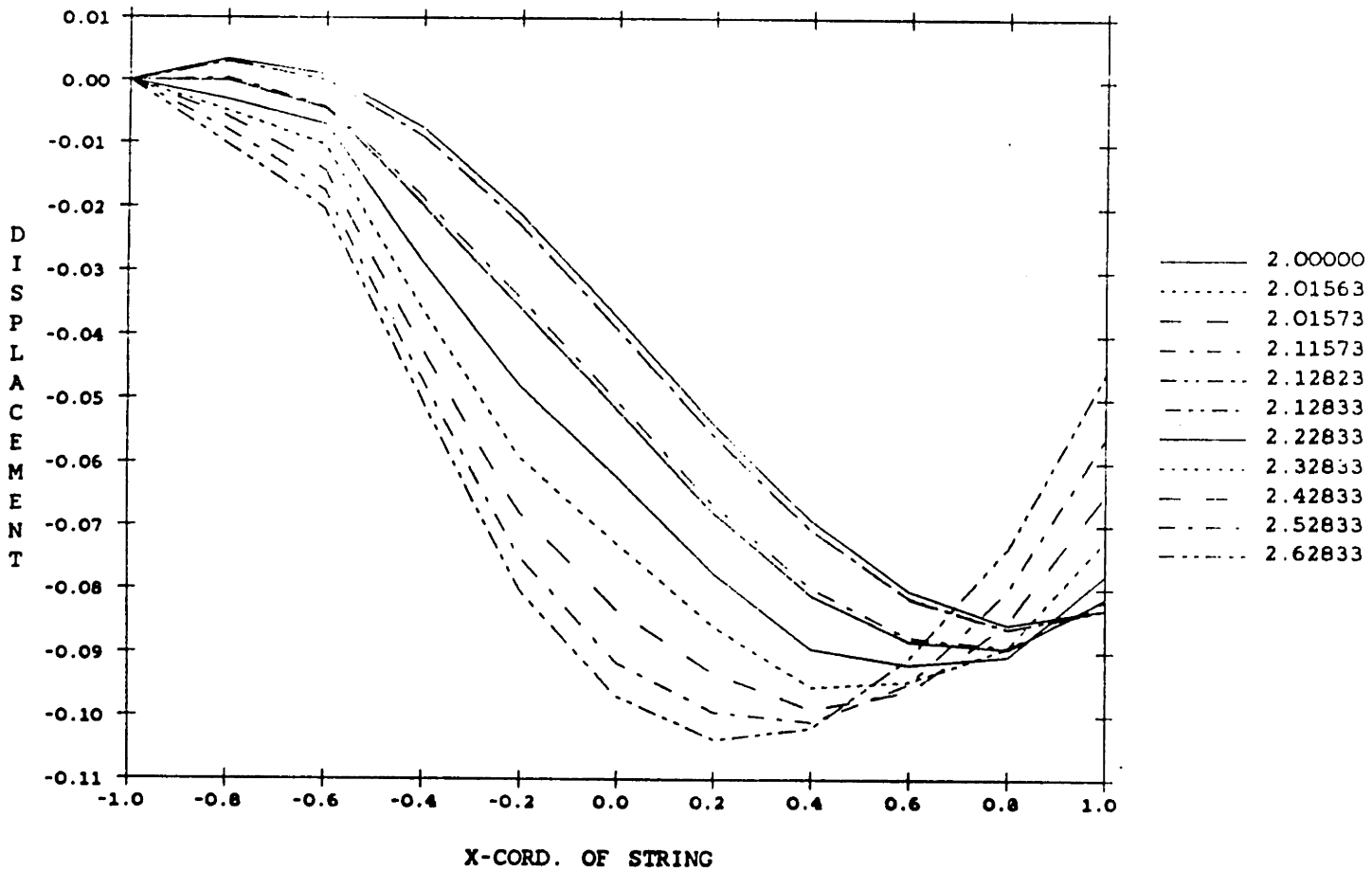


Figure 3-14: Time History of Transverse Displacement along a Damped String with a Object of k=15 and c=10 [Excitation ; $\pi/2$ (rad/sec) and 1 Diameter]

GMUD15V5

28-OCT-85 12:52 Page 1

DISPLACEMENT OF STRING WITH K=15, C=10 OF MUD

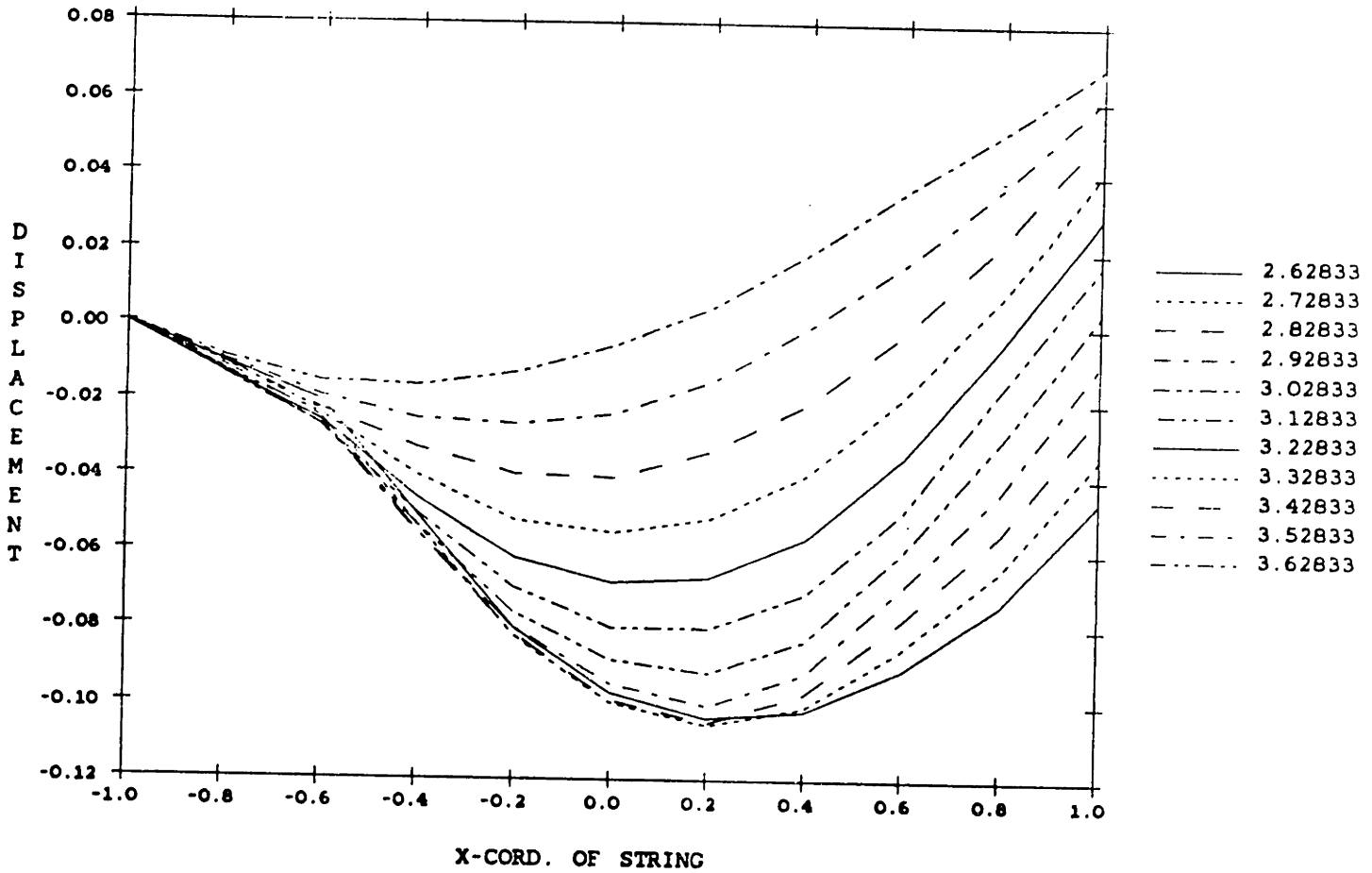


Figure 3-15: Time History of Transverse Displacement along a Damped String with a Object of k=15 and c=10 [Excitation ; $\pi/2$ (rad/sec) and 1 Diameter]

HIT04G

07-OCT-85 14:03 Page 1

DIS. OF STRING HITTING THE RIGID BOTTOM

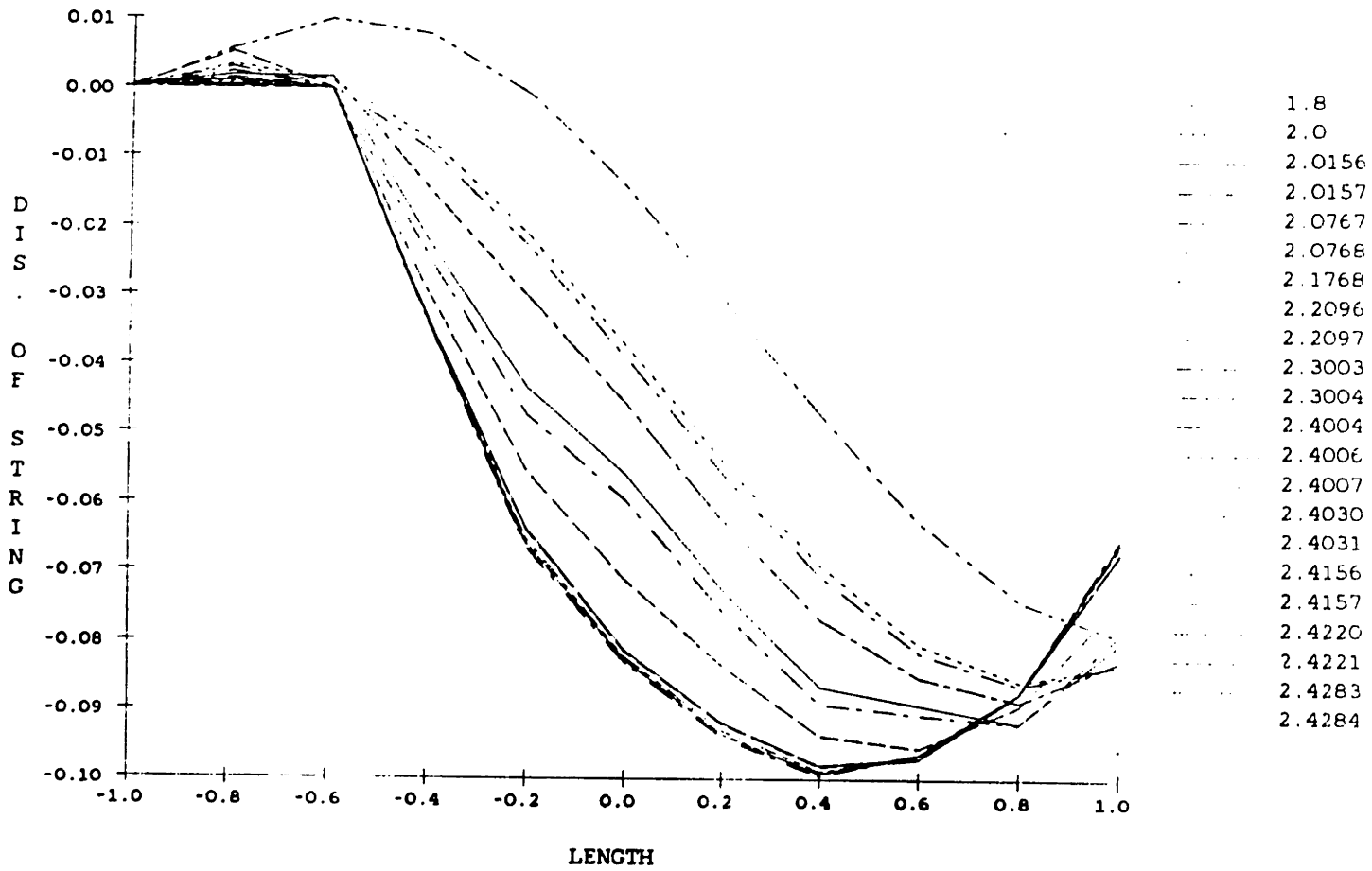


Figure 3-16: Time History of Transverse Displacement along a Damped String with a Object of $k=1000$ and $c=1000$ [Excitation ; $\pi/2$ (rad/sec) and 1 Diameter]

Chapter 4

Cable Subjected To Nonlinear Drag Forces

4.1 Introduction

In this chapter, we study a cable subjected to nonlinear drag forces. Time domain simulations are carried out by expanding the cable motions in a set of Chebyshev polynomials, as in the analysis of a string of Chapter 2. Due to nonconstant terms in the governing equations of the cable, the collocation method is superior to Galerkin's method for a spatial integration scheme [12] and [22].

A time domain simulation of a cable subject to nonlinear drag forces has been done by Blik [4] and Burgess [5]. Blik used the natural modes of the cable as the set of orthogonal functions, and Burgess used sine functions. Burgess found in his thesis some advantages of the sine functions over the natural modes of the cable. Both used Galerkin's method, rather than the collocation method used in this thesis.

Migliore and McReynolds studied the dynamic effects of paying out and reeling in the cable system using the orthogonal collocation method [20] and [21].

4.2 Linearized Governing Equations with Nonlinear Drag Force Terms

The 2-dimensional, linearized equations of motion of a cable, whose static configuration is 2-dimensional, expressed along the local tangential and normal directions [23], are

$$m \frac{\partial^2 p}{\partial t^2} = \frac{\partial T_1}{\partial s} - T_0 \frac{d\phi_0}{ds} \phi_1 + F_{1d}$$

$$M \frac{\partial^2 q}{\partial t^2} = \frac{dT_0}{ds} \phi_1 + T_0 \frac{\partial \phi_1}{\partial s} + T_1 \frac{d\phi_0}{ds} + F_{nd} \quad (4.1)$$

$$\frac{\partial p}{\partial s} - q \frac{d\phi_0}{ds} = \frac{T_1}{EA}$$

$$\frac{\partial q}{\partial s} + p \frac{d\phi_0}{ds} = \phi_1 (1 + e_0)$$

with

$$\phi = \phi_0 + \phi_1$$

$$F_{1d} = \frac{1}{2} \rho_w C_{dn} D_0 (U \sin \phi + V_n) |U \sin \phi + V_n| \left(1 + \frac{e}{2}\right) \sin \phi_1$$

$$+ \frac{1}{2} \pi \rho_w C_{Dt} D_0 (U \cos \phi - V_t) |U \cos \phi - V_t| \left(1 + \frac{e}{2}\right) \cos \phi_1$$

$$- F_{1e} \quad (4.2)$$

$$\begin{aligned} F_{nd} = & -\frac{1}{2} \rho_w C_{dn} D_0 (U \sin \phi + V_n) |U \sin \phi + V_n| \left(1 + \frac{e}{2}\right) \cos \phi_1 \\ & + \frac{1}{2} \pi \rho_w C_{dt} D_0 (U \cos \phi - V_t) |U \cos \phi - V_t| \left(1 + \frac{e}{2}\right) \sin \phi_1 \\ & - F_{ns} \end{aligned}$$

$$V_t = \frac{\partial p}{\partial t} \cos \phi_1 + \frac{\partial q}{\partial t} \sin \phi_1$$

$$V_n = -\frac{\partial p}{\partial t} \sin \phi_1 + \frac{\partial q}{\partial t} \cos \phi_1$$

$$M = m + m_a$$

where

m : mass per unit length of the cable

m_a : added mass per unit length of the cable

E : Young's modulus of the cable

A : cross-sectional area of the cable

D_0 : unstretched diameter of the cable

p : tangential displacement

q : normal displacement

T_1 : dynamic tension

T_0 : static tension

ϕ_1 : dynamic angle

ϕ_0 : static angle

e : total strain ($e = e_1 + e_0$)

e_0 : static strain

e_1 : dynamic strain

U : velocity of current parallel to the x-axis

C_{dn} : tangential drag coefficient

C_{dt} : frictional drag coefficient

F_{td} : tangential dynamic drag force

F_{nd} : normal dynamic drag force

F_{ts} : tangential static drag force

F_{ns} : normal static drag force

ρ_w : water density

Boundary conditions and initial conditions are as follows (see Fig. 4-1) :

• Boundary conditions :

$$p(0,t) = 0$$

$$p(l,t) = h(t) \cos(\phi_{0top} - \theta)$$

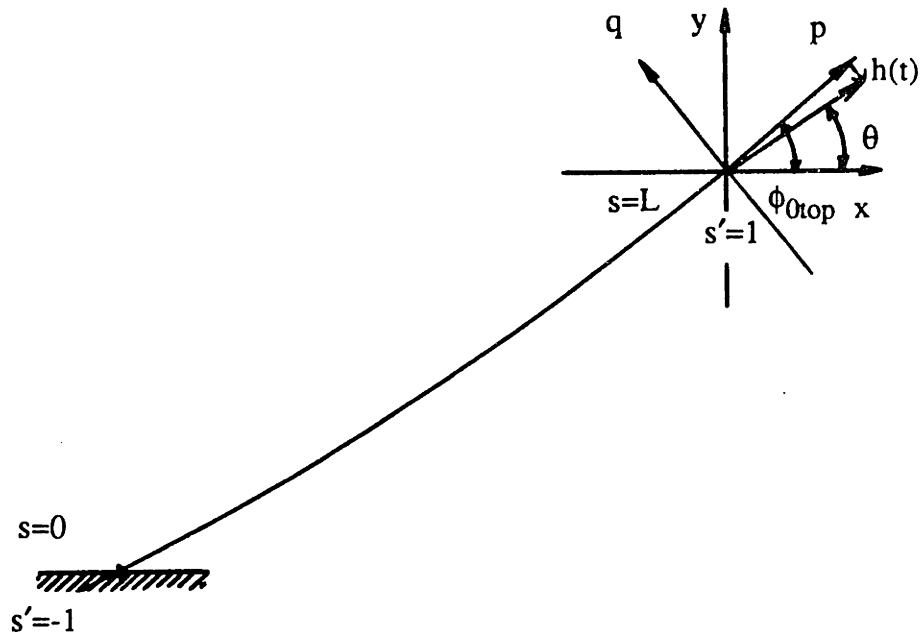


Figure 4-1: Static configuration and Lagrangian Coordinates

$$q(0,t) = 0 \tag{4.3}$$

$$q(l,t) = -h(t) \sin(\phi_{0top} - \theta)$$

where

$h(t)$: arbitrary excitation function of time t

imposed at the top of the cable

ϕ_{0top} : static angle at the top of the cable

θ : angle of direction of the excitation

- Initial conditions :

$$p(s,0) = f_1(s)$$

$$q(s,0) = f_2(s) \tag{4.4}$$

$$\frac{\partial p}{\partial t}(s,0) = f_3(s)$$

$$\frac{\partial q}{\partial t}(s,0) = f_4(s)$$

where $f_1(s)$, $f_2(s)$, $f_3(s)$ and $f_4(s)$ are arbitrary functions of the lagrangian coordinate s .

4.3 Nondimensionalized equations

By introducing nondimensionalized variables, the governing equations (4.1) are transformed into the following nondimensionalized equations :

$$\frac{\partial^2 p'}{\partial t^2} = \frac{T_p}{mD_0 L/2} \frac{\partial T'}{\partial s'} - \frac{T_0}{mD_0} \frac{d\phi_0}{ds} \phi_1 + \frac{1}{mD_0} F_{ld}$$

$$-1 < s' < 1$$

$$\frac{\partial^2 q'}{\partial t^2} = \frac{T_p}{MD_0} \frac{d\phi_0}{ds} T' + \frac{T_0}{MD_0 L/2} \frac{\partial \phi_1}{\partial s'} + \frac{1}{MD_0} \frac{dT_0}{ds} \phi_1 + \frac{1}{MD_0} F_{nd}$$

$$T' = \frac{D_0 EA}{T_p L/2} \frac{\partial p'}{\partial s'} - \frac{D_0 EA}{T_p} \frac{d\phi_0}{ds} q'$$

$$-1 \leq s' \leq 1$$

$$\phi_1 = \frac{1}{1+e_0} \frac{D_0}{L/2} \frac{\partial q'}{\partial s'} + \frac{D_0}{1+e_0} \frac{d\phi_0}{ds} p' \quad (4.5)$$

with

$$p' = \frac{p}{D_0}$$

$$q' = \frac{q}{D_0}$$

$$s' = \frac{s}{L/2} - 1$$

$$T' = \frac{T_1}{T_p}$$

where

L : total length of the cable

T_p : pretension at the top of the cable

Also, the boundary conditions and initial conditions are nondimensionalized (see Fig. 4-1).

• **Boundary Condition :**

$$p'(-1,t) = 0$$

$$p'(1,t) = \frac{h(t)}{D_0} \cos(\phi_{0top} - \theta) \quad (4.6)$$

$$q'(-1,t) = 0$$

$$q'(1,t) = -\frac{h(t)}{D_0} \sin(\phi_{0top} - \theta)$$

• Initial conditions :

$$p'(s',0) = f_1(s')$$

$$q'(s',0) = f_2(s') \quad (4.7)$$

$$\frac{\partial p'}{\partial t}(s',0) = f_3(s')$$

$$\frac{\partial q'}{\partial t}(s',0) = f_4(s')$$

4.4 Application of the Collocation Method to Cable Dynamics

4.4.1 Residual Equations

The residual equations resulting from the trial solutions, i. e., expansion along the set of orthogonal functions, can be expressed, using Chebyshev polynomials $T_n(s')$, as :

$$\begin{aligned}
 R_1(s',t) &= \frac{\partial^2 p'}{\partial t^2} - \frac{T_p}{mD_0 L/2} \frac{\partial T'}{\partial s'} + \frac{T_0}{mD_0} \frac{d\phi_0}{ds} \phi_1 - \frac{1}{mD_0} F_{ud} \\
 R_2(s',t) &= \frac{\partial^2 q'}{\partial t^2} - \frac{T_p}{MD_0 L/2} \frac{d\phi_0}{ds} T' - \frac{T_0}{MD_0 L/2} \frac{\partial \phi_1}{\partial s'} \\
 &\quad - \frac{1}{MD_0} \frac{dT_0}{ds} \phi_1 - \frac{1}{MD_0} F_{nd}
 \end{aligned} \tag{4.8}$$

$$R_3(s',t) = T' - \frac{D_0 EA}{T_p L/2} \frac{\partial p'}{\partial s'} + \frac{D_0 EA}{T_p} \frac{d\phi_0}{ds} q'$$

$$R_4(s',t) = \phi_1 - \frac{1}{1+e_0} \frac{D_0}{L/2} \frac{\partial q'}{\partial s'} - \frac{D_0}{1+e_0} \frac{d\phi_0}{ds} p'$$

where

$$\begin{aligned}
 p'(s',t) &= \sum_{n=0}^{N+1} p_n(t) T_n(s') \\
 q'(s',t) &= \sum_{n=0}^{N+1} q_n(t) T_n(s') \\
 T'(s',t) &= \sum_{n=0}^{N+1} t_n(t) T_n(s') \\
 \phi_1(s',t) &= \sum_{n=0}^{N+1} a_n(t) T_n(s')
 \end{aligned} \tag{4.9}$$

There are (N+2) unknown expansion coefficients for each of the expansions (4.9) and, in total, 4(N+2) unknowns must be determined.

In order to set up $4(N+2)$ equations we choose N collocation points along the cable excluding both end boundary points (Fig. 4-2). At each collocation point, 4 residual equations (4.8) are forced to be zero and, at the two boundary points, the boundary conditions are required to be satisfied instead of $R_1(s',t)$ and $R_2(s',t)$.

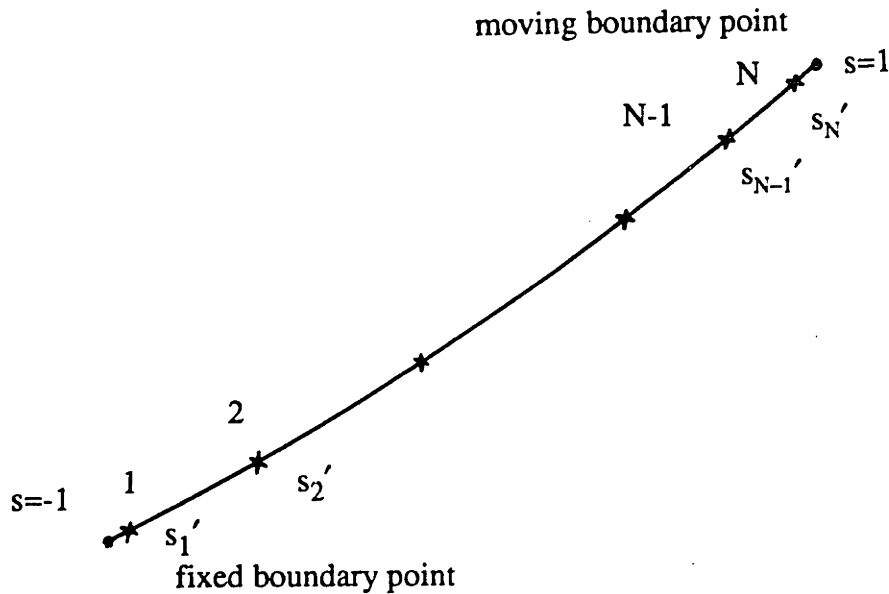


Figure 4-2: Collocation Points

In summary,

- $4N$ equations at the collocation points

$$R_j(S'_k, t) = 0 \tag{4.10}$$

where $j = 1, 2, 3, 4$

$k = 1, 2, 3, \dots, N$

8 equations at the two boundary points

$$\begin{array}{ll} \text{at } s = -1 & \text{at } s = 1 \\ R_3(-1,t) = 0 & R_3(1,t) = 0 \\ R_4(-1,t) = 0 & R_4(1,t) = 0 \\ p'(-1,t) = 0 & p'(1,t) = \frac{h(t)}{D_0} \cos(\phi_{0top} - \theta) \\ q'(-1,t) = 0 & q'(1,t) = -\frac{h(t)}{D_0} \sin(\phi_{0top} - \theta) \end{array} \quad (4.11)$$

Thus $4(N+2)$ equations are formulated in (4.10) and (4.11) and, therefore, $4(N+2)$ unknown coefficients in (4.9) can be determined as solutions of (4.10) and (4.11).

Solutions of $4(N+2)$ simultaneous equations can be calculated numerically through matrix manipulations. Then the Newmark method becomes an appropriate tool as a time integration scheme.

4.5 Numerical Applications

In order to compare our numerical predictions with the existing data, we employed the inclined cable used in Blied's thesis [4]. Also, this cable is used in Chapters 5 and 6. The principal parameters of the inclined cable are found in Table 4-I.

Fig. (4-3) shows the static configuration of the inclined cable in Table 4-3. We calculated the natural frequencies of this cable, using the computer code "CAEIG.EIG" which was developed in the Design Laboratory, Ocean Engineering, MIT.

First Natural Frequency = 0.9001219 rad/sec

Second Natural Frequency = 1.193369 rad/sec

$$T_0 = 1332000 \text{ N}$$

$$m = 48.7 \text{ kg/m}$$

$$m_a = 6.3 \text{ kg/m}$$

$$w_{\text{water}} = 414.98 \text{ N/m}$$

$$EA = 1.3 \times 10^9$$

$$L = 67.6656 \text{ m}$$

$$D_0 = 0.0889 \text{ m}$$

$$\text{depth} = 427.7 \text{ m}$$

$$C_{dn} = 1.2$$

Table 4-I: Cable used in Figures 4-3 to 4-10

The dynamic responses of the cable to excitation at the top, in the normal direction, of amplitude equal to 10 cable diameters, and frequency equal to its first natural frequency (0.9 rad/sec) are shown in Figures (4-4) to (4-10).

Without the effect of the nonlinear drag force, the cable is subject to undamped free vibrations and resonance phenomena should be observed at its natural frequency. Figures (4-4), (4-5) and (4-6) show indeed the resonance phenomena at the first natural frequency as expected. As time goes on, the amplitude of normal displacement at intermediate points ($s = -1, -0.5, 0, 0.5, 1$) of the cable increases without bound. Comparison between dynamic tensions at several points along the cable, showed that the dynamic tension is uniform along the cable (Fig. 4-4).

When the cable is subjected to nonlinear drag forces, we obtain eventually a steady-state response (Fig. 4-8). Figure (4-7) shows a comparison of the dynamic tensions at several points of the inclined cable subjected to nonlinear drag forces. In Fig. (4-7), we find high frequency fluctuations around the peaks of the dynamic tension at the bottom and the top. This results from the strong singularity of the initial velocity, which was imposed at the top in the form of a cosine function starting at time zero. Such a discontinuity, due to initial conditions, can be alleviated by introducing a time window function, which produces a gradual increase from zero to the desired value in velocity within a few periods. The effect of the time window function is discussed, in detail, in the next chapter. In Figure (4-10), the comparison between our numeric predictions and Bliet's results show good agreement. The effect of an artificial small intermediate buoy on the dynamic tension in Figure (4-10) is shown in the next chapter.

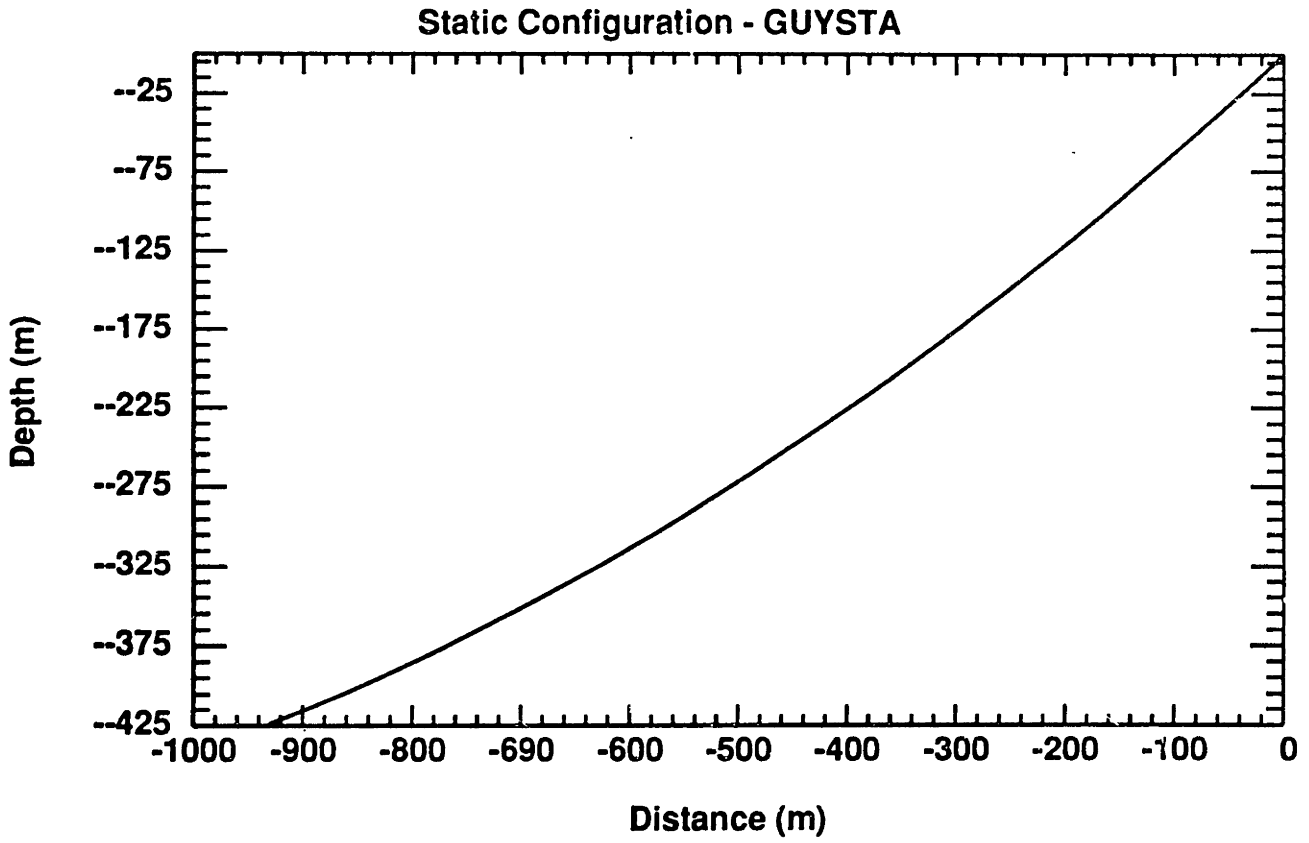


Figure 4-3: Static configuration of GUYSTA

normal excitation ; dynamic tension OF CABLE ; NO DAMPING

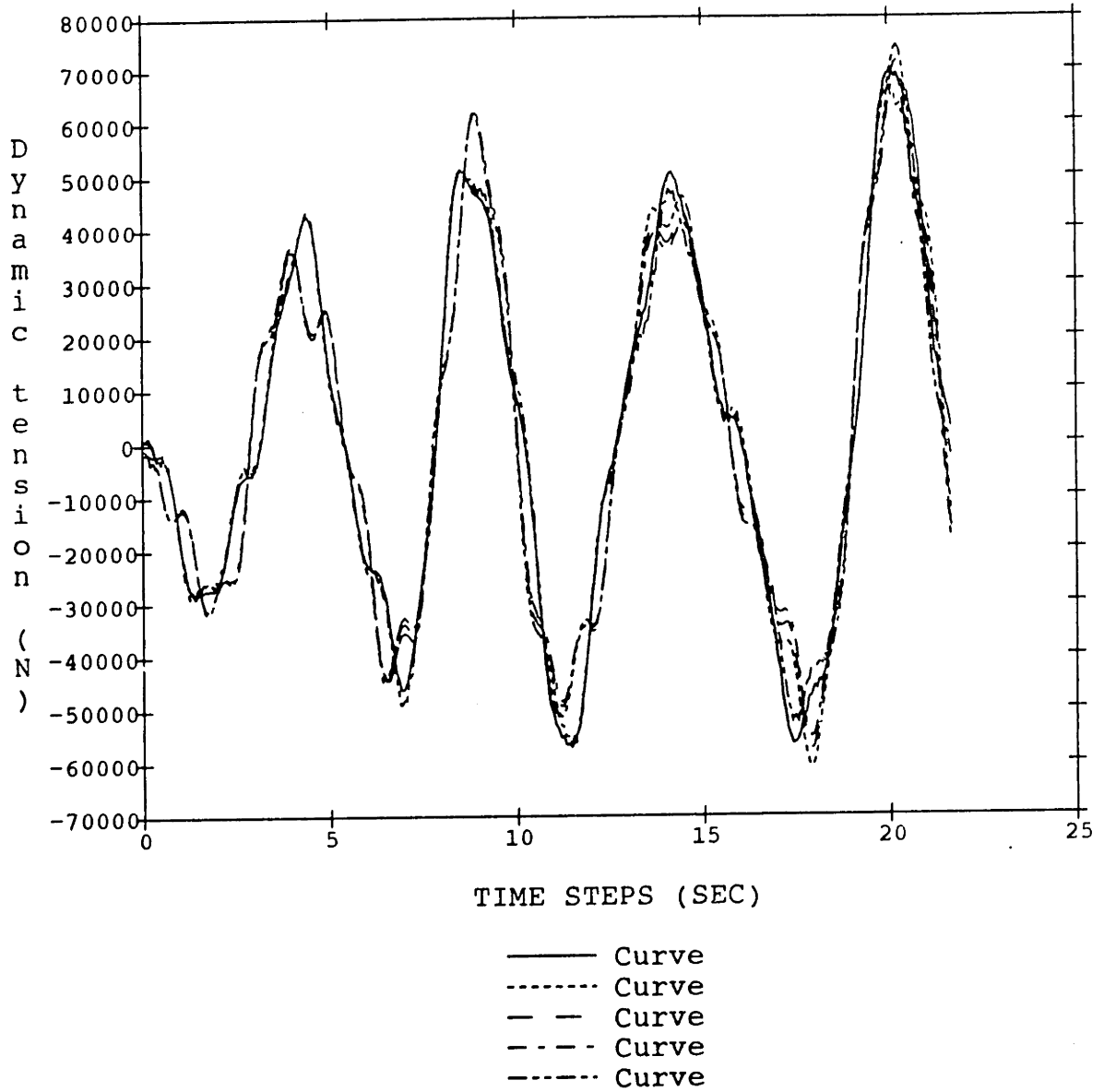


Figure 4-4: Dynamic Tensions of GUYSTA without damping in normal excitation of amplitude equal to 10 diameters at the first natural frequency

normal excitation ; NOMAL DISPLACEMENT OF CABLE ; NO DAMPING

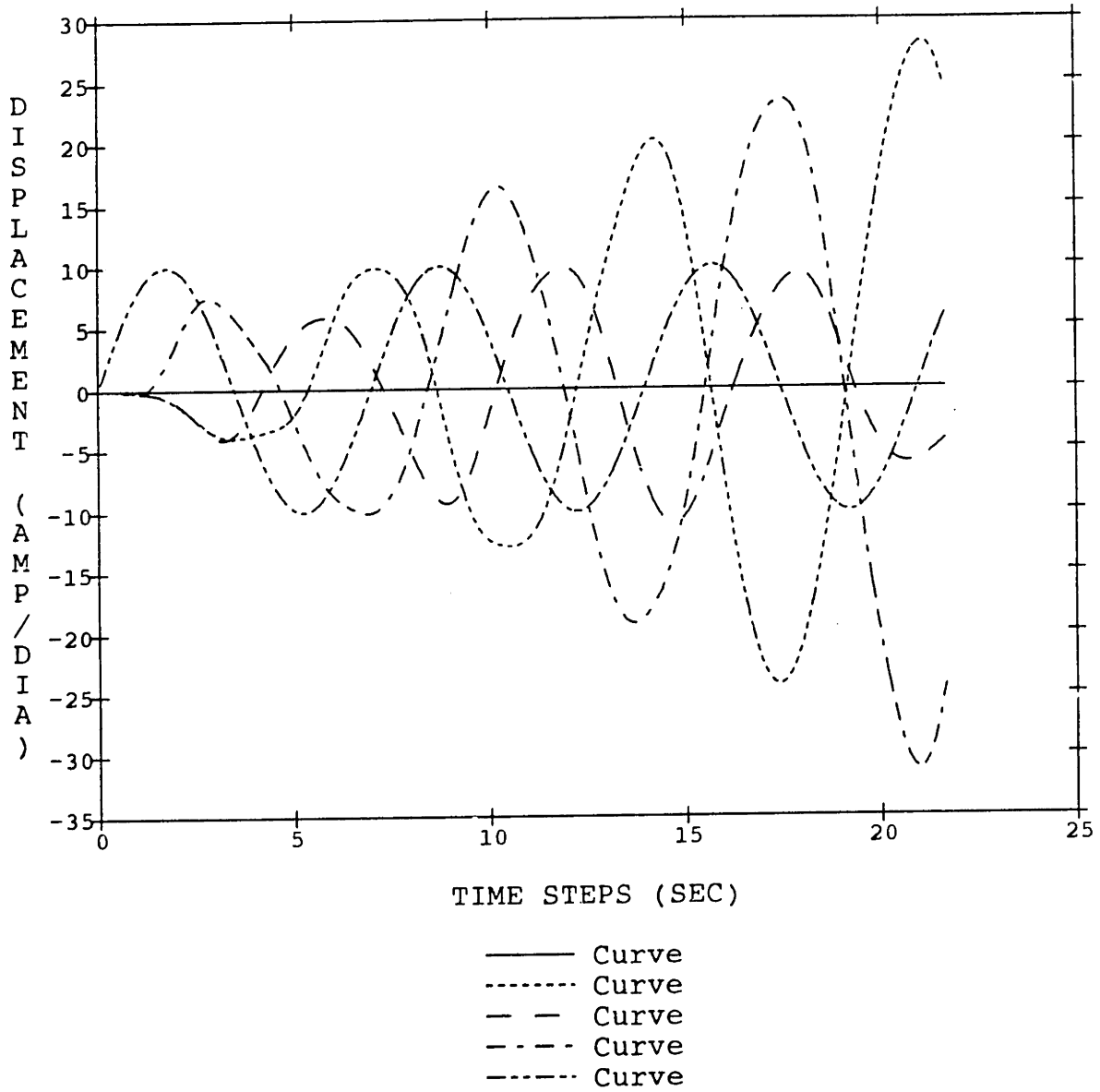


Figure 4-5: Normal displacements of GUYSTA without damping in normal excitation of amplitude equal to 10 diameters at the first natural frequency

normal excitation ; TANGENTIAL DISPLACEMENT OF CABLE ; NO DAMPING

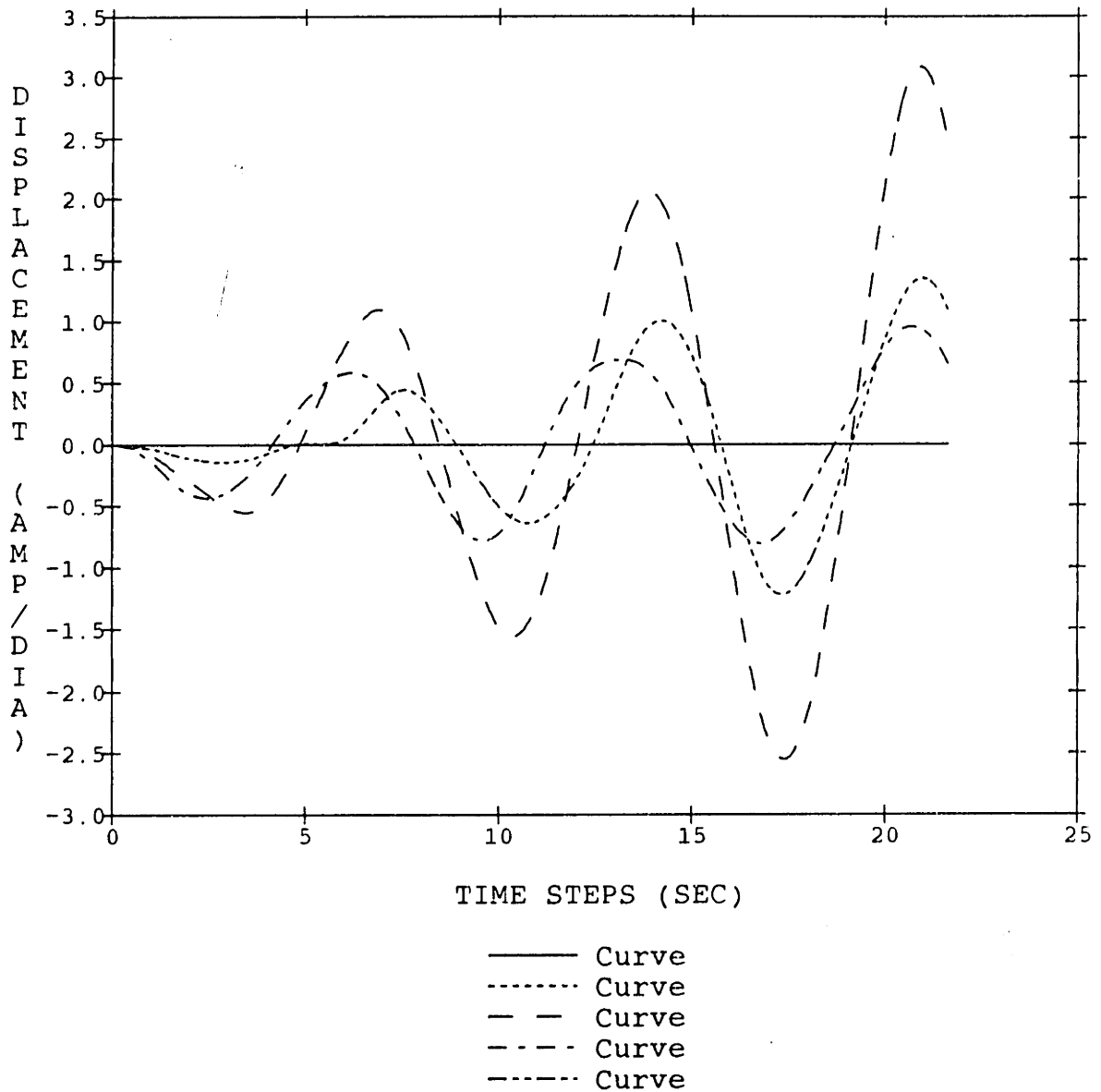


Figure 4-6: Tangential Displacement of GUYSTA without damping in normal excitation of amplitude equal to 10 diameters at the first natural frequency

nomal excitation ; dynamic tension OF CABLE ; with DAMPING

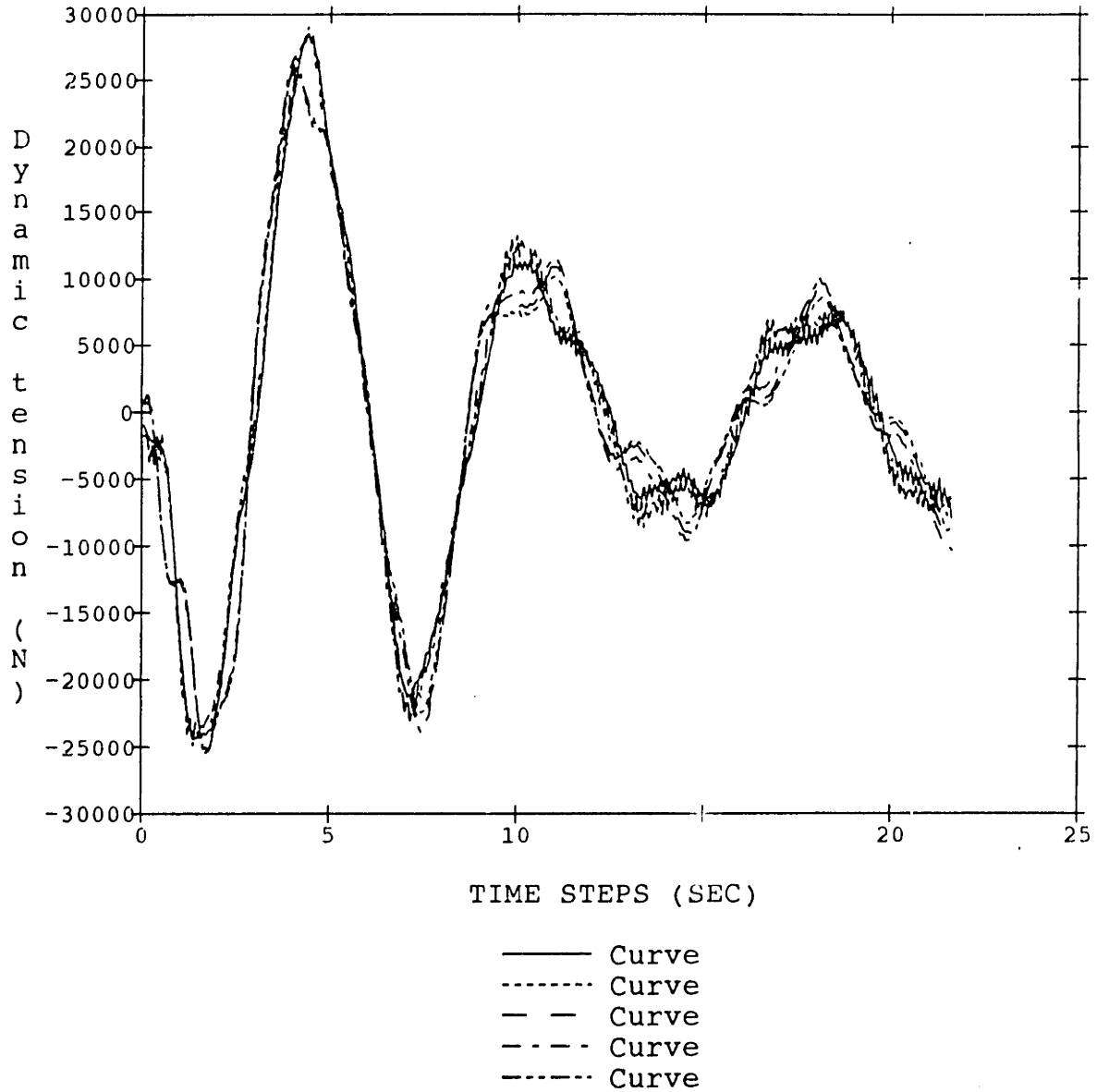


Figure 4-7: Dynamic Tensions of GUYSTA with damping in normal excitation of amplitude equal to 10 diameters at the first natural frequency

nomal excitation ; normal DISPLACEMENT OF CABLE ; with DAMPING

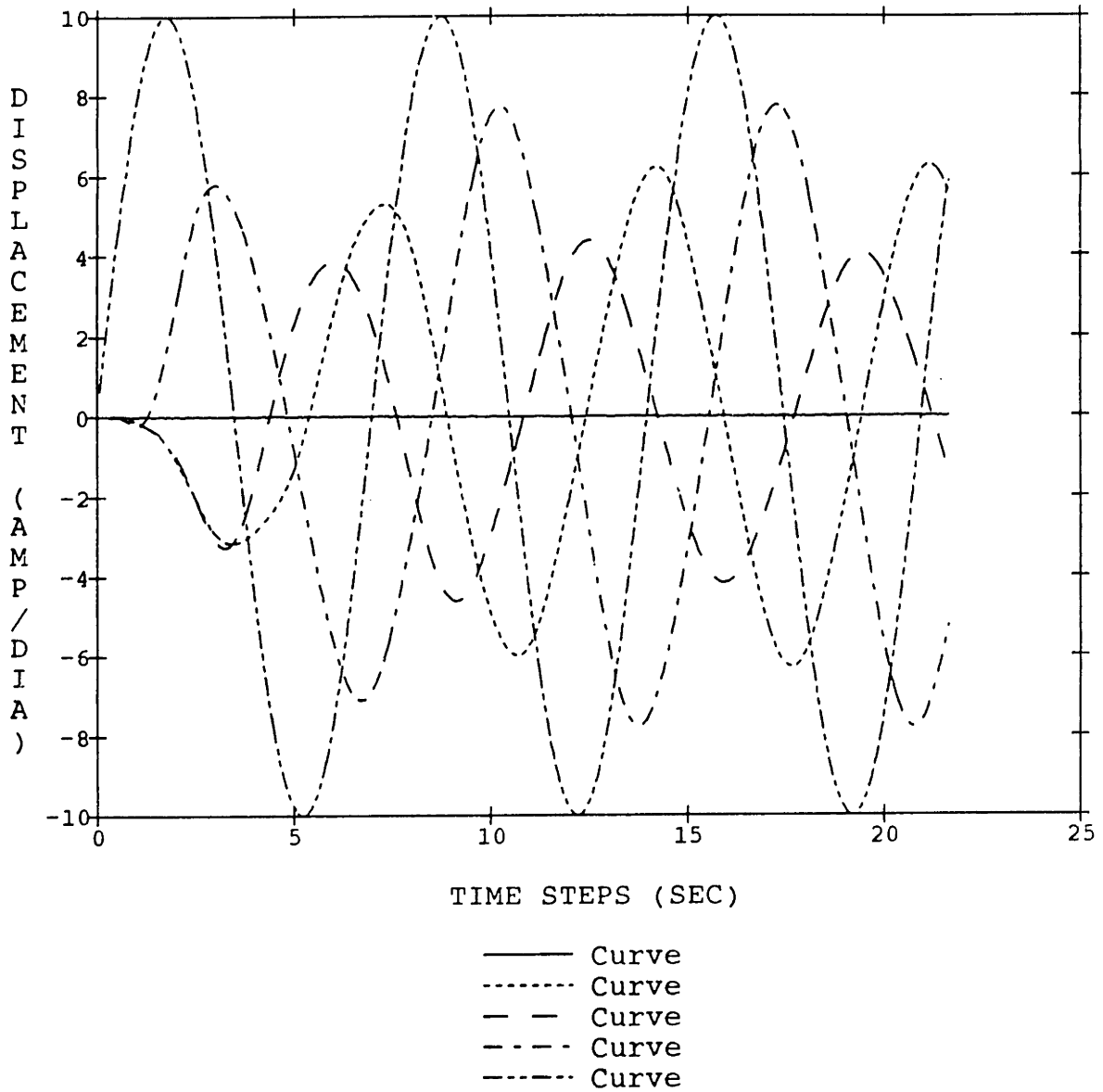


Figure 4-8: Normal displacements of GUYSTA with damping in normal excitation of amplitude equal to 10 diameters at the first natural frequency

normal excitation ; TANGENTIAL DISPLACEMENT OF CABLE ; with DAMPING

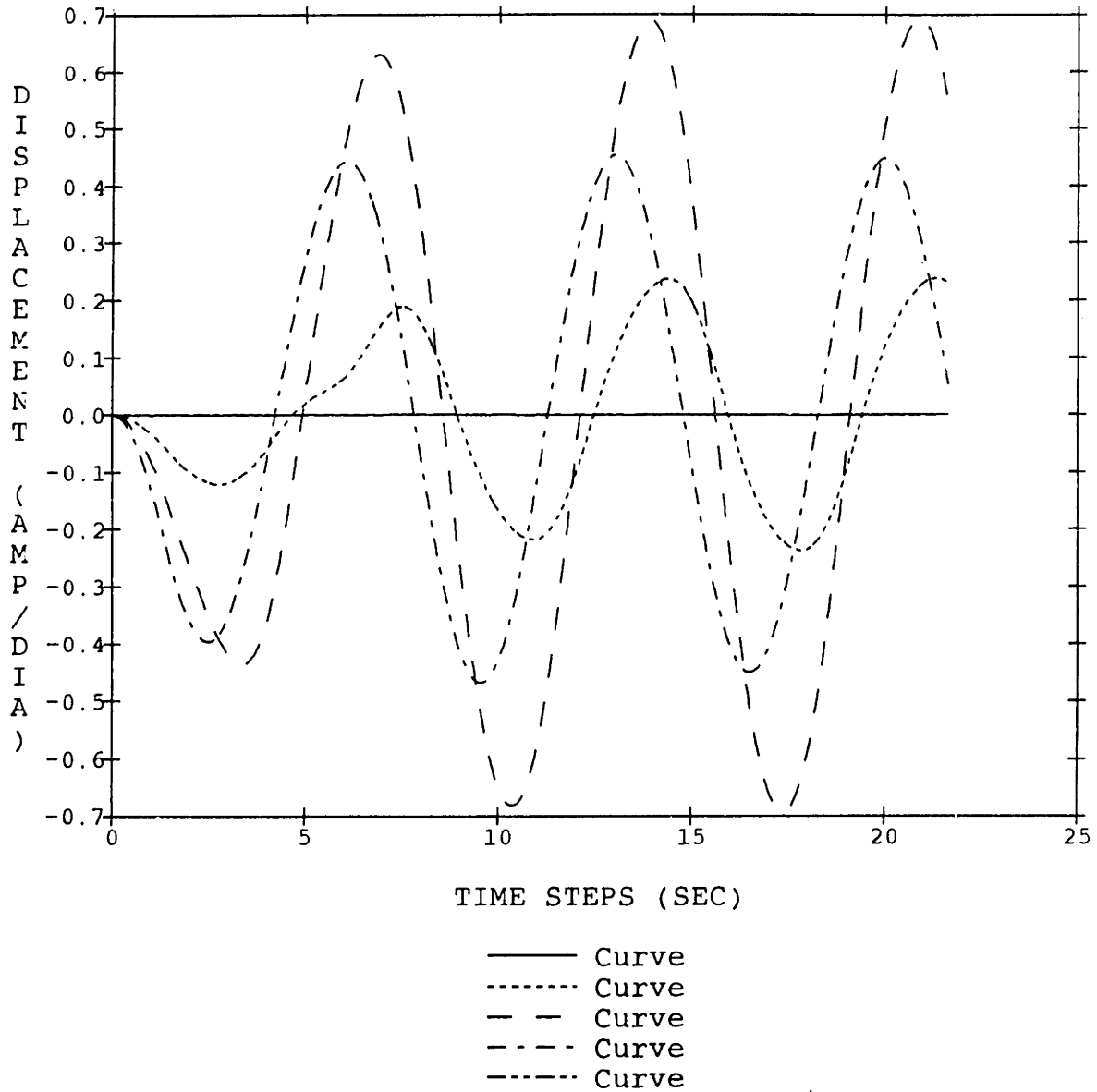


Figure 4-9: Tangential Displacement of GUYSTA with damping in normal excitation of amplitude equal to 10 diameters at the first natural frequency

COMPARISON BETWEEN COLLOCATION AND MODAL METHOD
DYNAMIC TENSILE FORCE AT TOP OF CABLE WITH DAMPING ; NORMAL EXCITATION

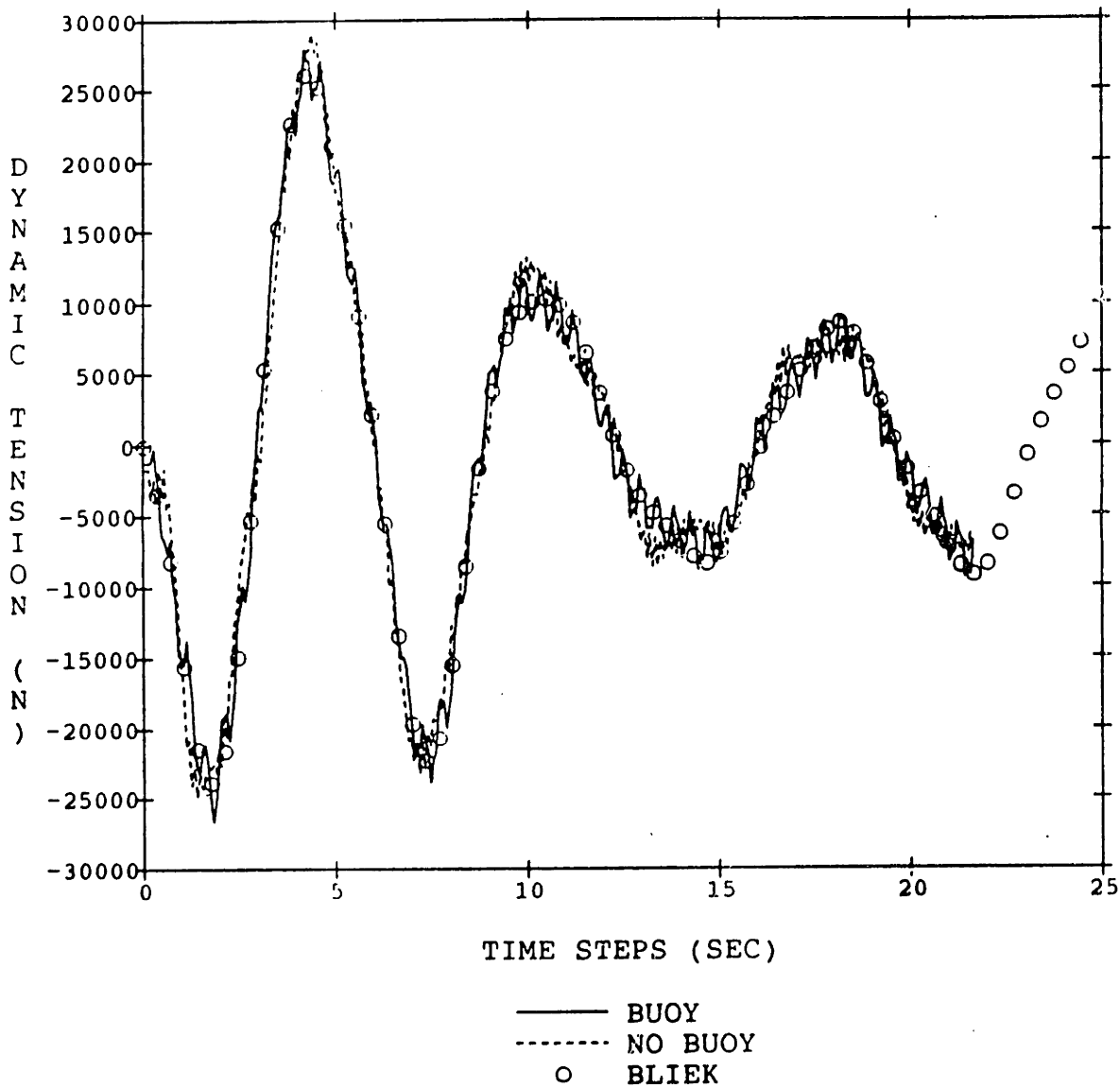


Figure 4-10: Comparison of dynamic tensions of GUYSTA between the predicted results and Bliiek's results with damping in normal excitation of amplitude equal to 10 diameters at its first natural frequency

Chapter 5

Cable with Intermediate Attached Buoys For Offshore Applications

5.1 Introduction

Attaching buoys along the length of the cable appears to be very useful in solving the problems associated with the heavy weight of a mooring line used in deep water. By adding buoys in appropriate points along the mooring line, it is possible to reduce the top tensile force and, therefore, to decrease the diameter of the cable.

So far, most analyses are restricted to a cable without buoys and only a few papers refer to the mooring line with buoys [3].

In this chapter, the nonlinear static and dynamic equations of a cable with intermediate buoys are derived, and small motions of the mooring line around its static configuration are simulated. The analysis of the mooring line with buoys is necessary to assess the safety of the cable-buoy system in deeper water.

5.2 Statics

We assume that each buoy is connected to the cable by a hinge at the attachment point. At each attachment point, we should consider equilibrium of the forces due to the buoy and the forces from the adjacent cable elements (Fig. 5-1).

Except at the end points, the following static equations must be satisfied along the mooring line :

$$\begin{aligned}
 T_0 \frac{d\phi_0}{ds} &= (w_0 - B_0) \cos\phi_0 + F_{n0} \left(1 + \frac{e_0}{2}\right) \\
 \frac{dT_0}{ds} &= (w_0 - B_0) \sin\phi_0 - F_{t0} \left(1 + \frac{e_0}{2}\right) \\
 \frac{dx}{ds} &= \cos\phi_0 \cdot (1 + e_0) \\
 \frac{dy}{ds} &= \sin\phi_0 \cdot (1 + e_0)
 \end{aligned}
 \tag{5.1}$$

where

w_0 : weight per unit length of the cable

B_0 : Buoyancy force per unit length of the cable

e_0 : static strain

F_{n0} : Normal static drag force per unit length of the cable

F_{t0} : Tangential static frictional force per unit length of the cable

s : Lagrangian coordinate

Also, the following relations must be satisfied at each attachment point.

$$\begin{aligned}
 T_0^+ \cos\phi_0^+ - T_0^- \cos\phi_0^- + F_R \cos\psi &= 0 \\
 T_0^+ \sin\phi_0^+ - T_0^- \sin\phi_0^- + F_R \sin\psi &= 0 \\
 F_R \cos\psi &= D_{xbs} \\
 F_R \sin\psi &= B_b - W_b + D_{ybs}
 \end{aligned}
 \tag{5.2}$$

In addition to (5.2), the continuity condition at an attachment point requires the following equalities in displacements.

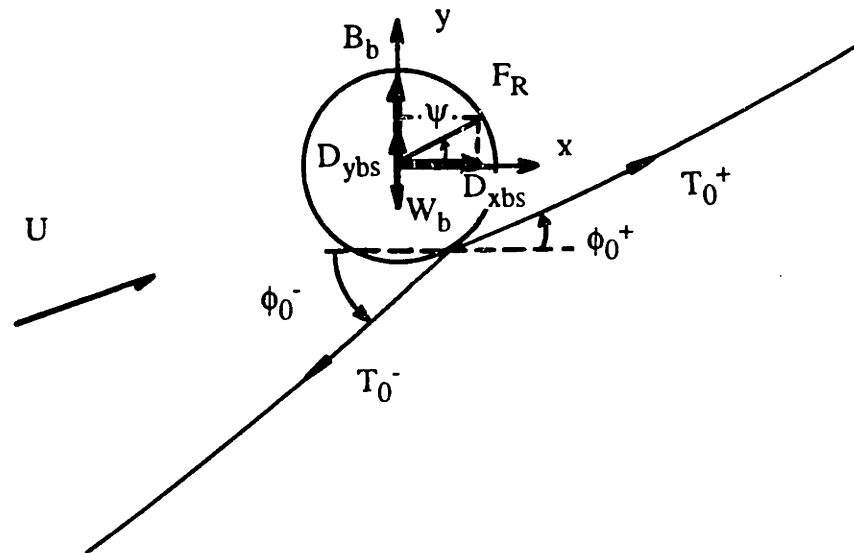


Figure 5-1: Static Forces at an Attachment Point

ϕ_0 : static angle of the cable

T_0 : static tension of the cable

F_R : resultant force of the buoy

ψ : angle of the resultant force F_R

U : current velocity

B_b : buoyancy of the buoy

W_b : weight of the buoy

D_{xbs} : x-component of the static drag force of the buoy

D_{ybs} : y-component of the static drag force of the buoy

$$\begin{aligned}x^+ &= x^- \\y^+ &= y^-\end{aligned}\tag{5.3}$$

Finally static continuity conditions at an attachment point are as follows :

$$\begin{aligned}T_0^- \cos\phi_0^- &= T_0^+ \cos\phi_0^+ + D_{xbs} \\T_0^- \sin\phi_0^- &= T_0^+ \sin\phi_0^+ + B_b - w_b + D_{ybs}\end{aligned}\tag{5.4}$$
$$\begin{aligned}x^+ &= x^- \\y^+ &= y^-\end{aligned}$$

5.3 Dynamics

We assume that each submerged intermediate buoy is fixed on the cable, and we do not allow buoy rotation about the attachment point. The hydrodynamic forces on the buoy are described by a Morison type loading, based on the relative motions between the buoy and the surrounding fluid.

In order to simplify the dynamic problem, the incident current velocity is assumed to be parallel to the x-axis.

5.3.1 Drag Forces on a Submerged Buoy

The drag forces on a submerged buoy are described as follows : (see Fig. 5-2)

$$\bar{D}_T = \frac{1}{2} \rho_w C_{sp} \frac{\pi}{4} D_b^2 (\bar{U} - \bar{V}) |\bar{U} - \bar{V}| \quad (5.5)$$

The total drag force is decomposed into two components :

$$\begin{aligned} D_{xb} &= D_T \cos\gamma \\ &= \frac{1}{2} \rho_w C_{sp} \frac{\pi}{4} D_b^2 (U - V) |U - V| \cos\gamma \end{aligned} \quad (5.6)$$

$$\begin{aligned} D_{yb} &= D_T \sin\gamma \\ &= \frac{1}{2} \rho_w C_{sp} \frac{\pi}{4} D_b^2 (U - V) |U - V| \sin\gamma \end{aligned}$$

with

$$\gamma = \tan^{-1} \frac{-V_y}{U - V_x}$$

$$\bar{V} = (V_x, V_y)$$

$$\bar{U} = (U, 0)$$

where

D_{xb} : x-component of the total drag force of the buoy

D_{yb} : y-component of the total drag force of the buoy

\bar{U} : current velocity assumed to be parallel to the x-axis

\bar{V} : Velocity of the buoy

ρ_w : water density

C_{sp} : damping coefficient of a sphere

D_b : diameter of the buoy

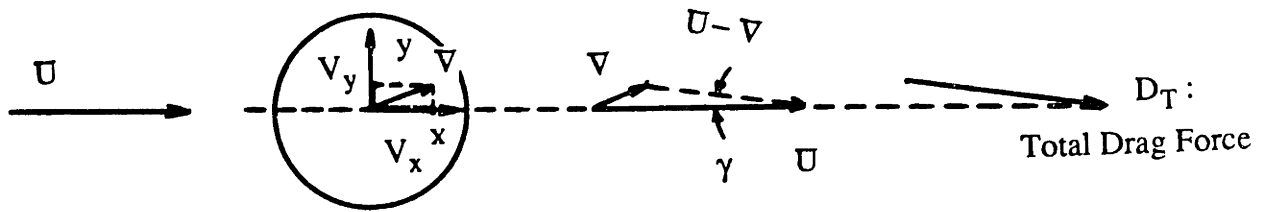


Figure 5-2: Total Drag Force on a Buoy

Therefore the drag forces on a buoy are obtained from (5.6) as :

$$D_{xbd} = D_{xb} - D_{xbs}$$

$$D_{ybd} = D_{yb}$$

(5.7)

with

$$D_{xbs} = \frac{1}{2} \rho_w C_{sp} \frac{\pi}{4} D_b^2 U^2$$

5.3.2 Dynamic Equations of a Submerged Intermediate Buoy

From the dynamic equilibrium condition at an attachment point, we obtain the following equations :

$$m_b \ddot{x} = -a_b \ddot{x} + T^+ \cos\phi^+ - T^- \cos\phi^- + D_{xb}$$

$$m_b \ddot{y} = -a_b \ddot{y} + T^+ \sin\phi^+ - T^- \sin\phi^- + B_b - W_b + D_{yb} \quad (5.8)$$

$$x^+ = x^-$$

$$y^+ = y^-$$

where

T : total tension of the cable

ϕ : Total angle of the cable

m_b : mass of the buoy

a_b : added mass of the buoy

5.3.3 Linearized Dynamic Equations of a Submerged Intermediate Buoy

After neglecting higher order terms in (5.8) and subtracting the static relations (5.2), we obtain the linearized dynamic equations at an attachment point.

$$(m_b + a_b)\ddot{x} = T_d^+ \cos \phi^+ - T_d^+ \phi_d^+ \sin \phi_0^+ - T_d^- \cos \phi_0^- + T_d^- \phi_d^- \sin \phi_0^- + D_{xbd}$$

$$(m_b + a_b)\ddot{y} = T_d^+ \sin \phi^+ + T_d^+ \phi_d^+ \cos \phi_0^+ - T_d^- \sin \phi_0^- - T_d^- \phi_d^- \cos \phi_0^- + D_{ybd}$$

$$x^+ = x^- \tag{5.9}$$

$$y^+ = y^-$$

with

$$x = p \cos \phi_0 - q \sin \phi_0 \tag{5.10}$$

$$y = p \sin \phi_0 + q \cos \phi_0$$

The above continuity conditions (5.9) and (5.10) at an attachment point are expressed in the following matrix form :

$$\begin{pmatrix} \ddot{p}^+ \\ \ddot{q}^+ \\ T_d^+ \\ \phi_d^+ \end{pmatrix} + \begin{pmatrix} 0 \\ 0 \\ D_{xbd} \cos \phi_0^+ + D_{ybd} \sin \phi_0^+ \\ \frac{D_{ybd} \cos \phi_0^+}{T_0^+} - \frac{D_{xbd} \sin \phi_0^+}{T_0^+} \end{pmatrix} = \begin{pmatrix} \cos \tau & -\sin \tau & 0 & 0 \\ \sin \tau & \cos \tau & 0 & 0 \\ M_b \cos \tau & -M_b \sin \tau & \cos \tau & -T_0^- \sin \tau \\ \frac{M_b \sin \tau}{T_0^+} & \frac{M_b \cos \tau}{T_0^+} & \frac{\sin \tau}{T_0^+} & \frac{T_0^- \cos \tau}{T_0^+} \end{pmatrix} \begin{pmatrix} \ddot{p}^- \\ \ddot{q}^- \\ T_d^- \\ \phi_d^- \end{pmatrix}$$

with

$$\tau = \phi_0^- - \phi_0^+ \quad (5.11)$$

$$M_b = m_b + a_b$$

In the case of a cable consisting of several segments with different properties from each other ($D_1 \neq D_2$, etc.), the nondimensionalized variables of each segment are also different.

$$\begin{pmatrix} \frac{\ddot{p}_d^+}{D_2} \\ \frac{\ddot{q}_d^+}{D_2} \\ \frac{T_d^+}{T_p} \\ \phi_d^+ \end{pmatrix} + \begin{pmatrix} 0 \\ 0 \\ \frac{D_{xbd} \cos \phi_0^+}{T_p} + \frac{D_{ybd} \sin \phi_0^+}{T_p} \\ \frac{D_{ybd} \cos \phi_0^+}{T_0^+} - \frac{D_{xbd} \sin \phi_0^+}{T_0^+} \end{pmatrix} = \begin{pmatrix} \frac{D_1 \cos \tau}{D_2} & -\frac{D_1 \sin \tau}{D_2} & 0 & 0 \\ \frac{D_1 \sin \tau}{D_2} & \frac{D_1 \cos \tau}{D_2} & 0 & 0 \\ \frac{D_1 M_b \cos \tau}{T_p} & -\frac{D_1 M_b \sin \tau}{T_p} \cos \tau & -\frac{T_0^- \sin \tau}{T_p} \\ \frac{D_1 M_b \sin \tau}{T_0^+} & \frac{D_1 M_b \cos \tau}{T_0^+} & \frac{\sin \tau}{T_0^+} & \frac{T_0^- \cos \tau}{T_0^+} \end{pmatrix} \begin{pmatrix} \frac{\ddot{p}_d^-}{D_1} \\ \frac{\ddot{q}_d^-}{D_1} \\ \frac{T_d^-}{T_p} \\ \phi_d^- \end{pmatrix}$$

with

$$\tau = \phi_0^- - \phi_0^+ \quad (5.12)$$

$$M_b = m_b + a_b$$

Then the above matrix can be nondimensionalized by using different reference variables (Fig. 5-3).

where

$$\tau = \phi_0^- - \phi_0^+ \quad (5.11)$$

$$M_b = m_b + a_b$$

In the case of a cable consisting of several segments with different properties from each other ($D_1 \neq D_2$, etc.), the nondimensionalized variables of each segment are also different.

$$\begin{pmatrix} \frac{\ddot{p}^+}{D_2} \\ \frac{\ddot{q}^+}{D_2} \\ \frac{T_d^+}{T_p} \\ \phi_d^+ \end{pmatrix} + \begin{pmatrix} 0 \\ 0 \\ \frac{D_{xbd} \cos \phi_0^+}{T_p} + \frac{D_{ybd} \sin \phi_0^+}{T_p} \\ \frac{D_{ybd} \cos \phi_0^+}{T_0^+} - \frac{D_{xbd} \sin \phi_0^+}{T_0^+} \end{pmatrix} = \begin{pmatrix} \frac{D_1 \cos \tau}{D_2} & -\frac{D_1 \sin \tau}{D_2} & 0 & 0 \\ \frac{D_1 \sin \tau}{D_2} & \frac{D_1 \cos \tau}{D_2} & 0 & 0 \\ \frac{D_1 M_b \cos \tau}{T_p} & -\frac{D_1 M_b \sin \tau}{T_p} & \cos \tau & -\frac{T_0^-}{T_p} \sin \tau \\ \frac{D_1 M_b \sin \tau}{T_0^+} & \frac{D_1 M_b \cos \tau}{T_0^+} & \frac{\sin \tau}{T_0^+} & \frac{T_0^- \cos \tau}{T_0^+} \end{pmatrix} \begin{pmatrix} \frac{\ddot{p}^-}{D_1} \\ \frac{\ddot{q}^-}{D_1} \\ \frac{T_d^-}{T_p} \\ \phi_d^- \end{pmatrix}$$

with

$$\tau = \phi_0^- - \phi_0^+ \quad (5.12)$$

$$M_b = m_b + a_b$$

Then the above matrix can be nondimensionalized by using different reference variables (Fig. 5-3).

where

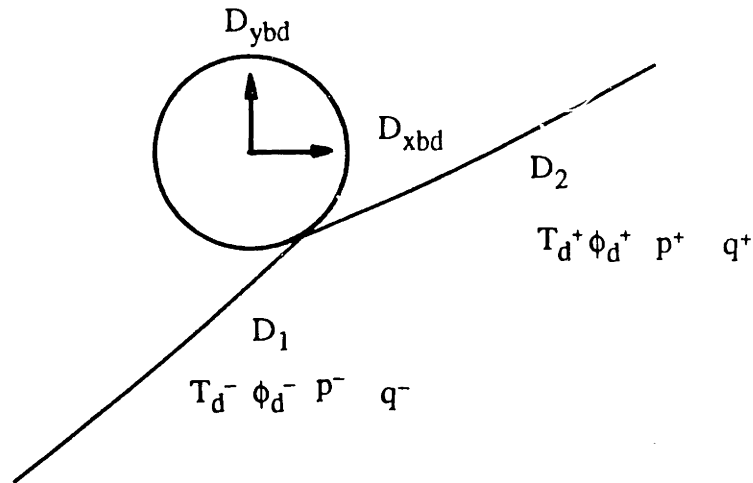


Figure 5-3: Dynamic Variables in a Multi-segmented Cable

D_1 : diameter of a left segment

D_2 : diameter of a right segment

The final continuity condition (5.12) should be assigned as a boundary condition at each attachment point of the cable with submerged intermediate buoys.

In the development of a computer code to simulate the effects of an intermediate buoy, the above condition (5.12) implies complex manipulations of the matrices involved.

5.4 Numerical Application

For the numerical application, we used the same cable as in Chapter 4 and its principal parameters are found in Table 4-I.

In order to establish the validity of our theory, first, we put a very small artificial buoy (diameter=0.0000001 m) in the middle of the inclined cable and we investigate its

effects. We expect that the very small buoy should have very little effect on the dynamic tensions of the cable. This is in fact the case, as comparison with a cable without the buoy shows in (Figures 4-7, 4-8 and 4-9) and (Figures 5-11, 5-12 and 5-13) and our numerical scheme proved to be efficient in solving the cable-buoy system. Also the comparison between our predictions and Bliet's results, mentioned in Chapter 4, show good agreement except for some small, high frequency fluctuations (Figures 5-14 and 5-15).

To investigate the effect of the discontinuity of the initial velocity, imposed as a cosine function at the top of the inclined cable, we introduced the following time window function.

$$sqw = 1 - e^{-\frac{\text{time}}{\text{window}}} \quad (5.13)$$

where

time : the elapsed time

window : the time window constant

We changed the value of 'window' and checked the dynamic tensions at the middle, at the top and the bottom of the inclined cable and the coherence of the phase between the dynamic tensions and their corresponding expansion coefficients. In Figures 5-16 to 5-20, we did not include the window function, that is, $sqw=1.0$ and $window=0.0$. When we used $window=0.5$ in equation (5.13), we found that the high frequency fluctuations in the dynamic tensions at the bottom and the top and their corresponding expansion coefficients became small, due to the gradual change in the initial velocity (Figures 5-22 to 5-24). For larger values of the window, such as 1.5, the high frequency fluctuations were reduced significantly (Figures 5-26 to 5-28). Through this investigation, it was found that it is of great profit to use the time window function to avoid the strong singularity of the imposed initial velocity.

STATIC ANALYSIS

OUTPUT OF STATIC ANALYSIS

NUMBER OF SEGMENTS = 2
TOTAL LENGTH OF THE CABLE = 0.104e+04M

CHARACTERISTICS OF THE CABLE

SEGMENT NUMBER 1
COORDINATES = 0. M - 518.0000 M
LENGTH SEGMENT = 518.0000 M
MASS PER UNIT LENGTH = 48.70000 KG/M
ADDED MASS PER UNIT LENGTH = 6.300000 KG/M
WEIGHT PER UNIT LENGTH = 414.9800 N/M
DIAMETER = 0.8890000e-01 M
EA = 0.1300000e+10 N
BREAKING TENSION = 4950000. N

SEGMENT NUMBER 2
COORDINATES = 518.0000 M - 1036.000 M
LENGTH SEGMENT = 518.0000 M
MASS PER UNIT LENGTH = 48.70000 KG/M
ADDED MASS PER UNIT LENGTH = 6.300000 KG/M
WEIGHT PER UNIT LENGTH = 414.9800 N/M
DIAMETER = 0.8890000e-01 M
EA = 0.1300000e+10 N
BREAKING TENSION = 4950000. N

NUMBER OF BUOYS = 1

CHARACTERISTICS OF THE BUOY

BUOY NUMBER 1
AFTER WHICH SEGMENT, PLACED= 1
MASS = 0.1000000e-05 KG
ADDED MASS = 21934.70 KG
BUOYANCY FORCE = 429919.0 N
VISCIOUS DRAG FORCE = 0. N
DIAMETER = 4.339900 M
TENSION(+) AT THE CONNECTING POINT = 1257887. N
TENSION(-) AT THE CONNECTING POINT = 1434776. N
ANGLE(+) AT THE CONNECTING POINT = 15.63373 DEGREES
ANGLE(-) AT THE CONNECTING POINT = 32.40527 DEGREES
DIFFEREN TENSION(+) AT THE POINT = 112.4879 N/M
DIFFEREN TENSION(-) AT THE POINT = 222.3896 N/M
DIFFERENTI ANGLE(+) AT THE POINT = 0.1818585e-01 DEGREES/M
DIFFERENTI ANGLE(-) AT THE POINT = 0.1399109e-01 DEGREES/M

STATIC DATA INPUT

NUMBER OF DISCRETIZATION POINTS = 101
TENSION AT THE TOP = 1332000.000(N)
DEPTH = 426.700(M)
CURRENT VELOCITY AT THE SURFACE = 0. (M/S)
NORMAL DRAGCOEFFICIENT = 1.20000
TANGENTIAL DRAG COEFFICIENT = 0.05000
ERROR IN DEPTH = 0.
NUMBER OF ITERATIONS = 7
LINE CAN LAY ON THE BOTTOM

SUMMARY OF STATIC RESULTS

Table 5-I: Characteristics of the neutral buoy and the segments of the cable

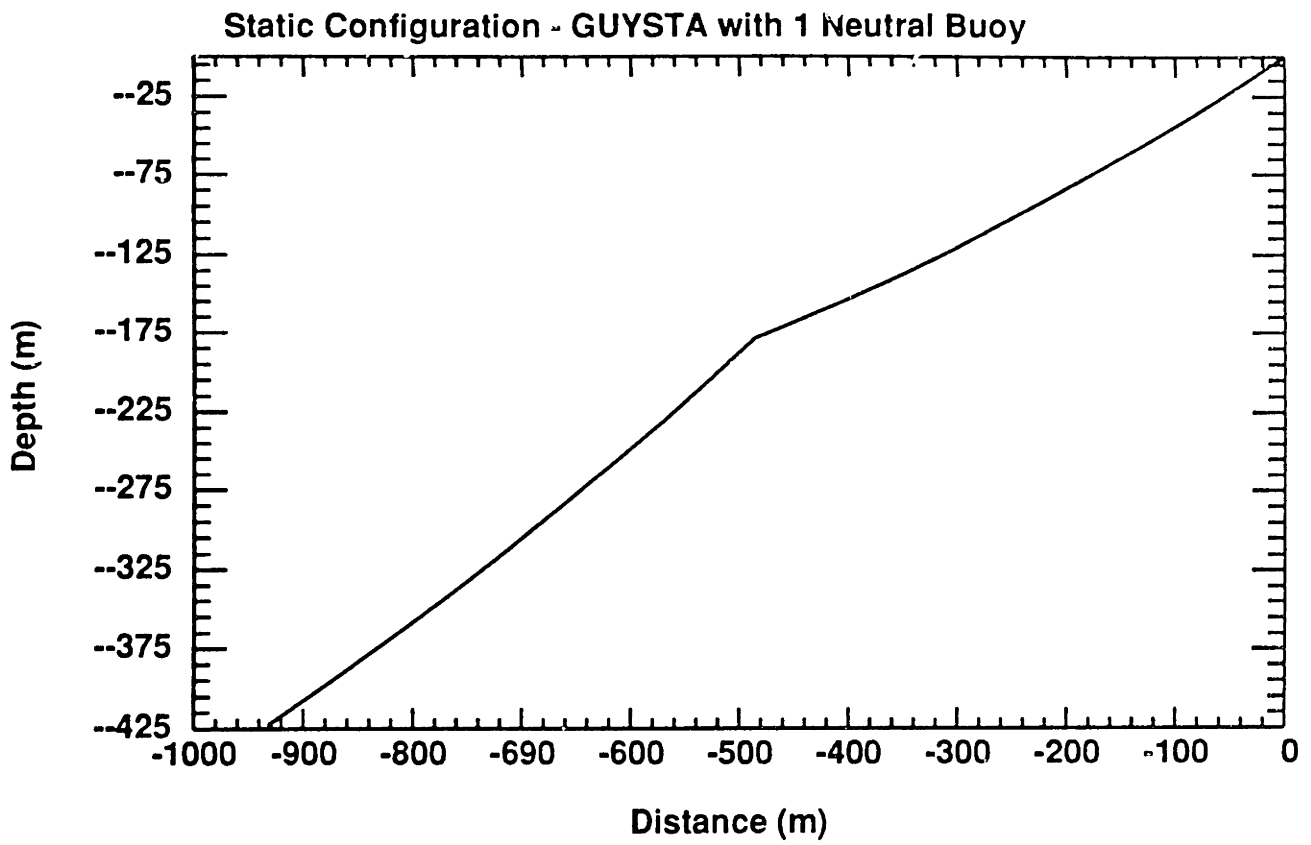


Figure 5-4: Static configuration of the inclined cable with a neutral buoy

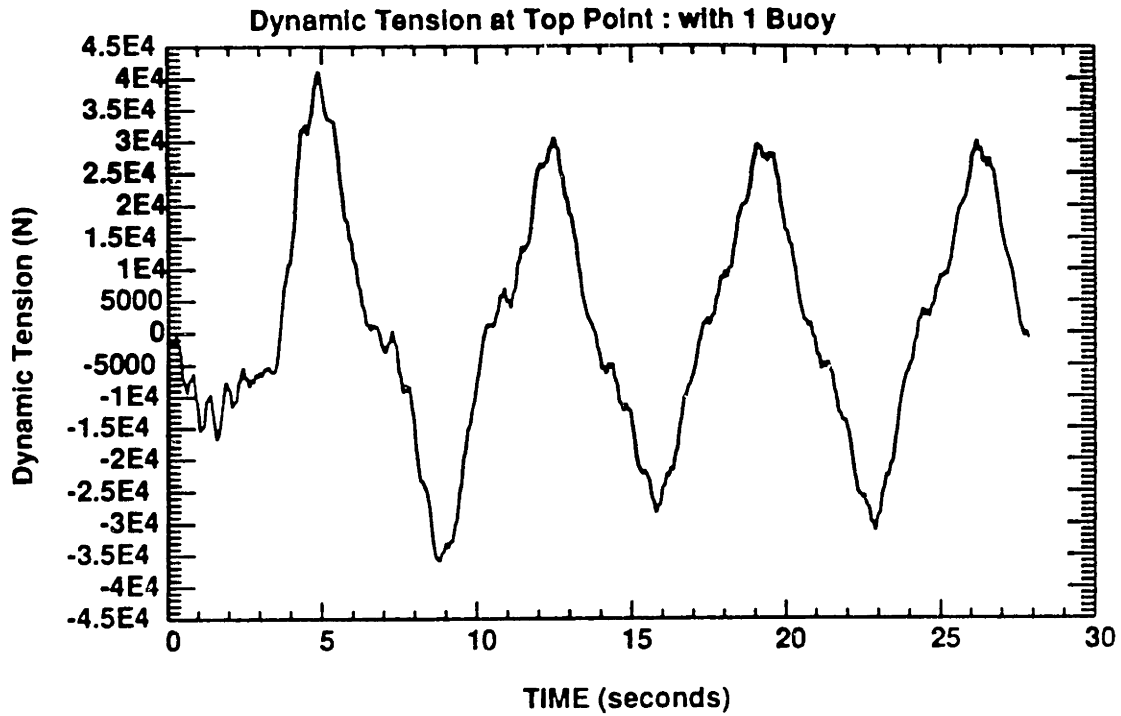


Figure 5-5: Dynamic tension at the top of the cable with a neutral intermediate buoy [10 Dia. 0.9rad/sec, Normal excitation, No window function]

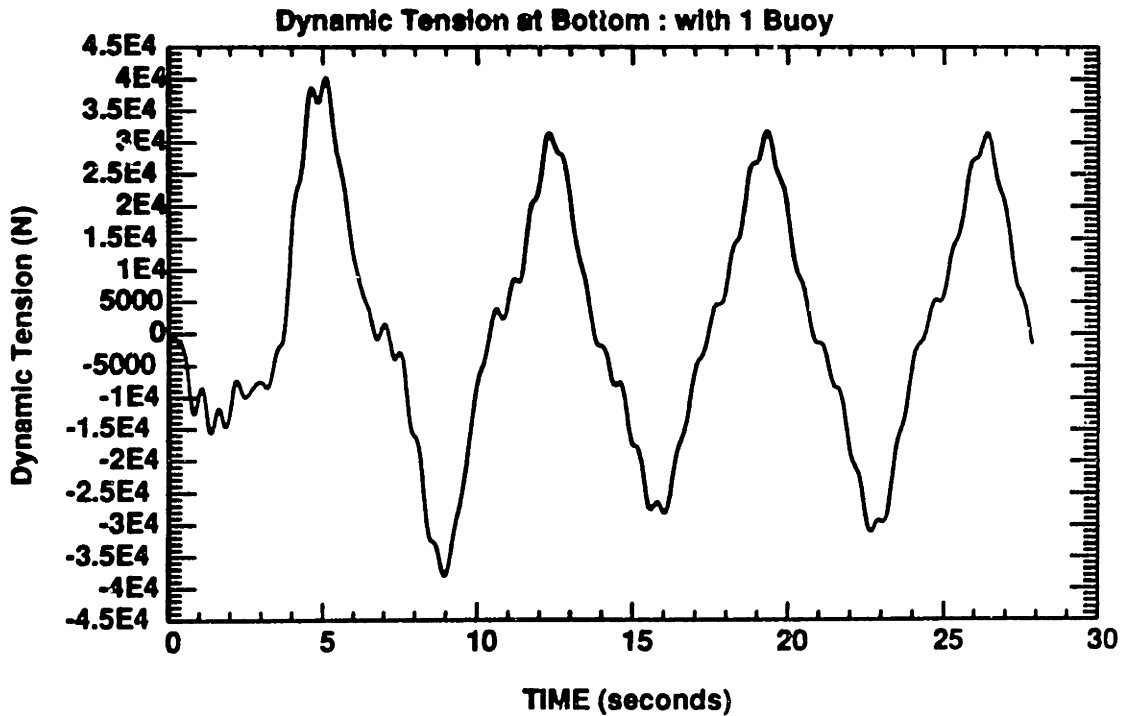


Figure 5-6: Dynamic tension at the bottom of the cable with a buoy [10 Dia. 0.9rad/sec, Normal excitation, No window function]

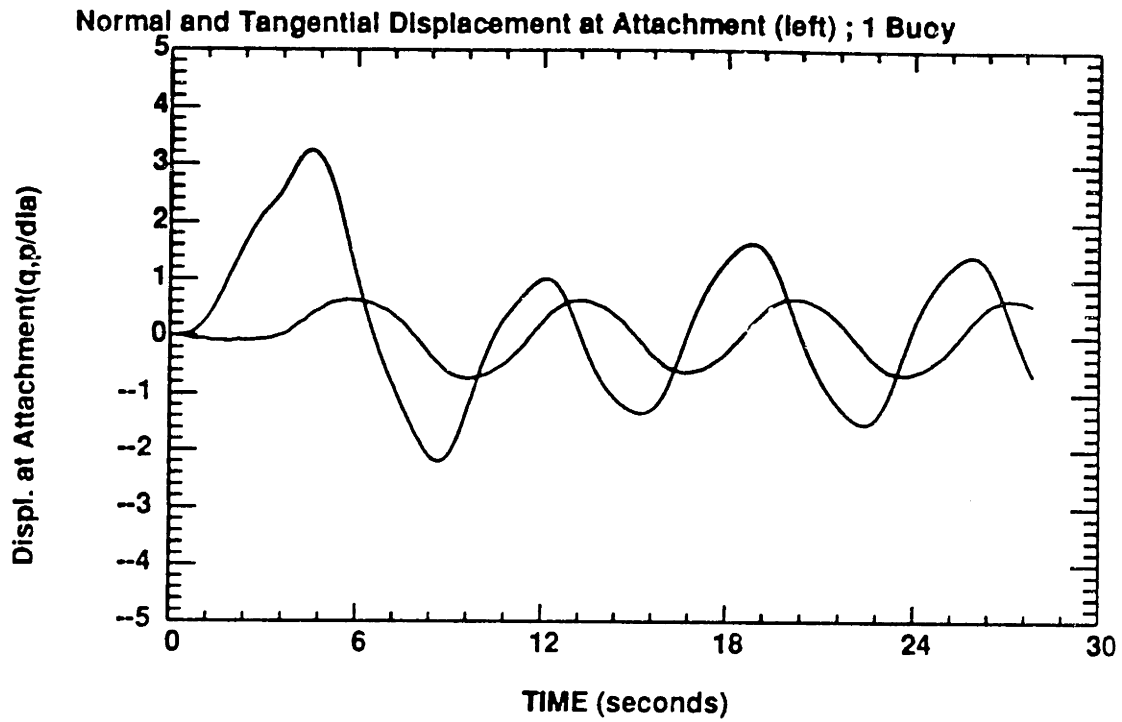


Figure 5-7: Displacement at the attachment of the cable with a buoy [10 Dia. 0.9rad/sec, Normal excitation, No window function, Left side]

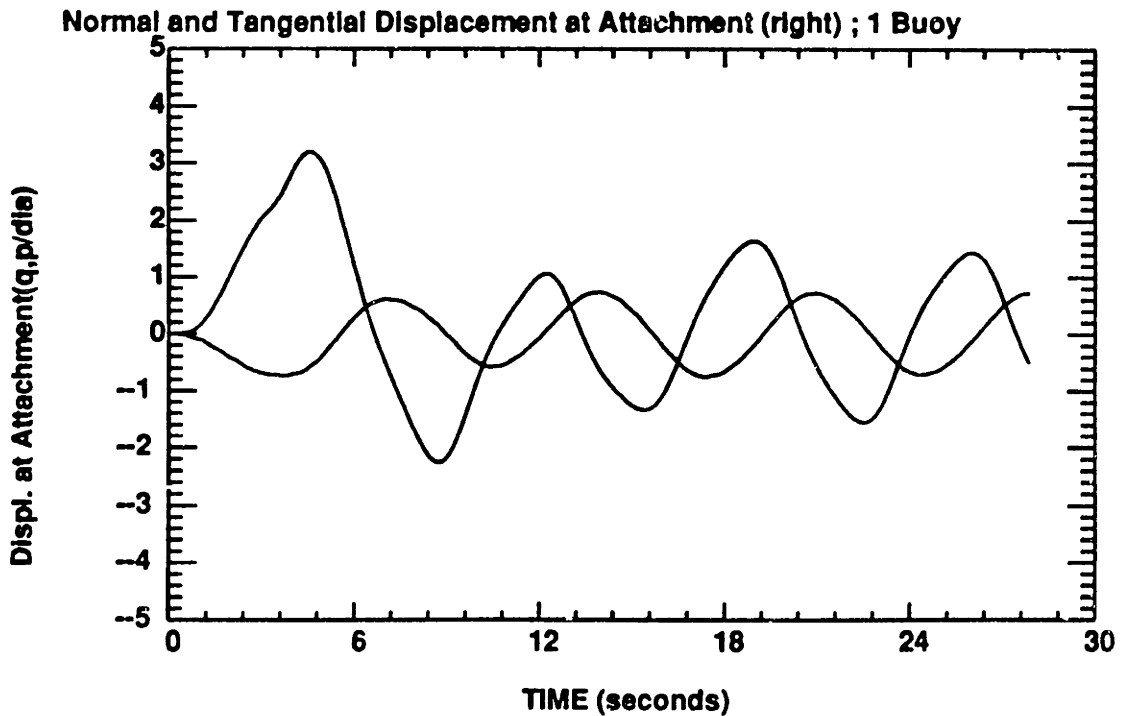


Figure 5-8: Displacement at the attachment of the cable with a buoy [10 Dia. 0.9rad/sec, Normal excitation, No window function, Right side]

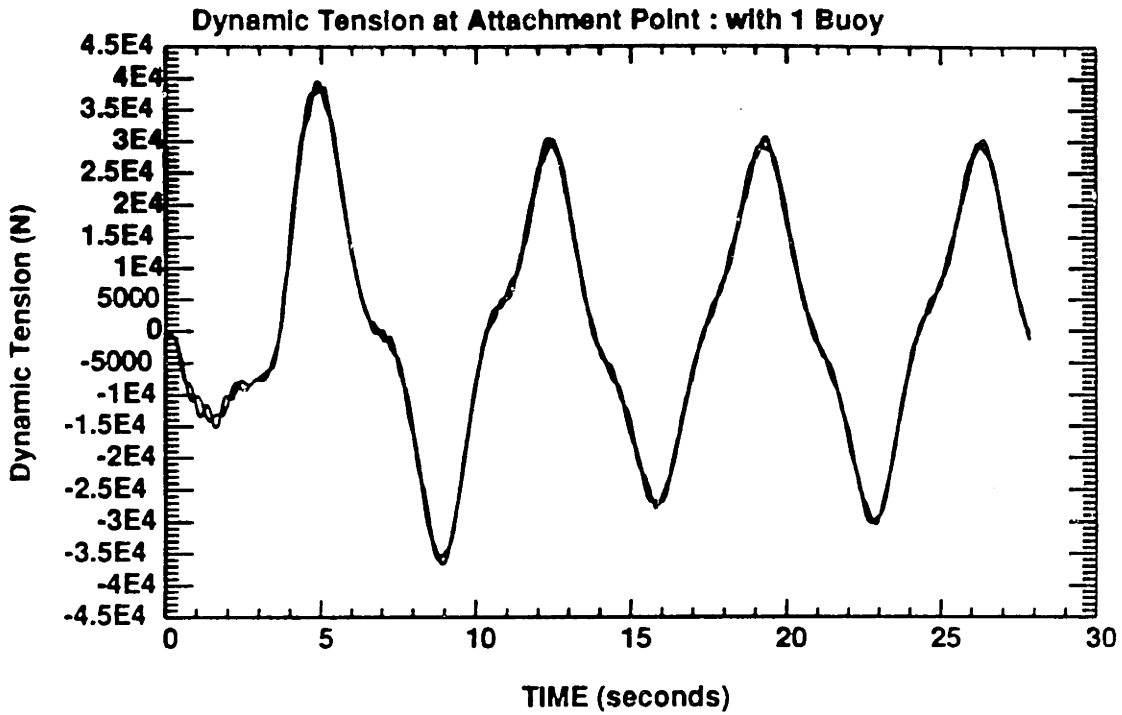


Figure 5-9: Dynamic tension at the attachment of the cable with a buoy [10 Dia. 0.9rad/sec, Normal excitation, No window function]

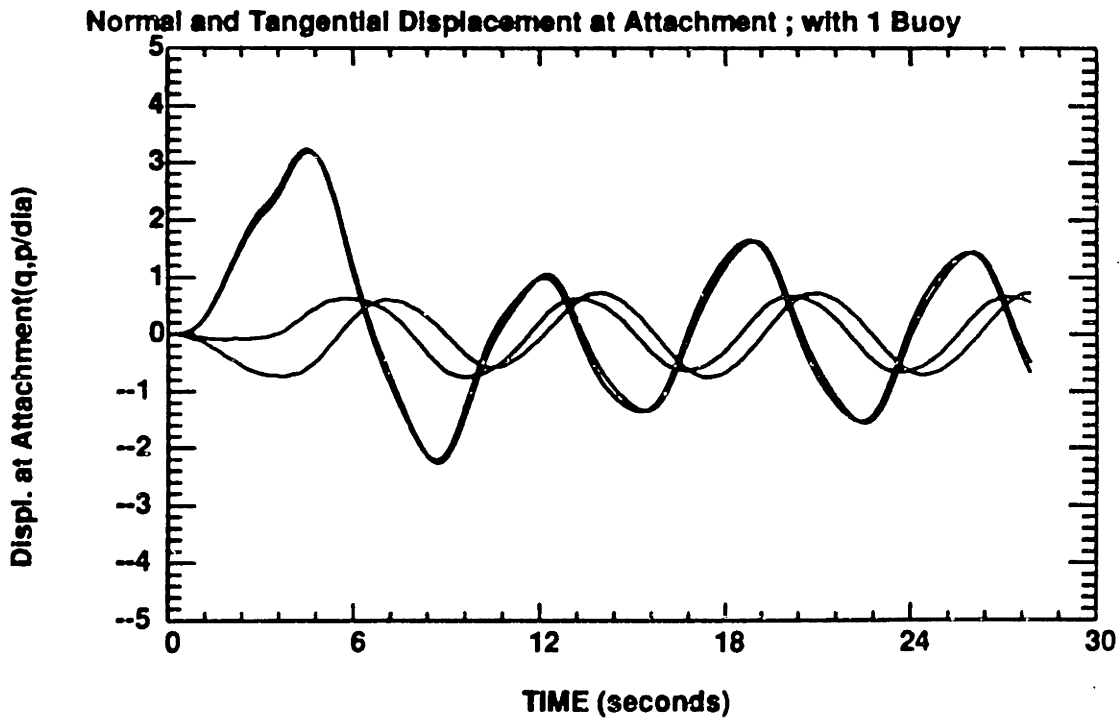


Figure 5-10: Displacement at the attachment of the cable with a buoy [10 Dia. 0.9rad/sec, Normal excitation, No window function]

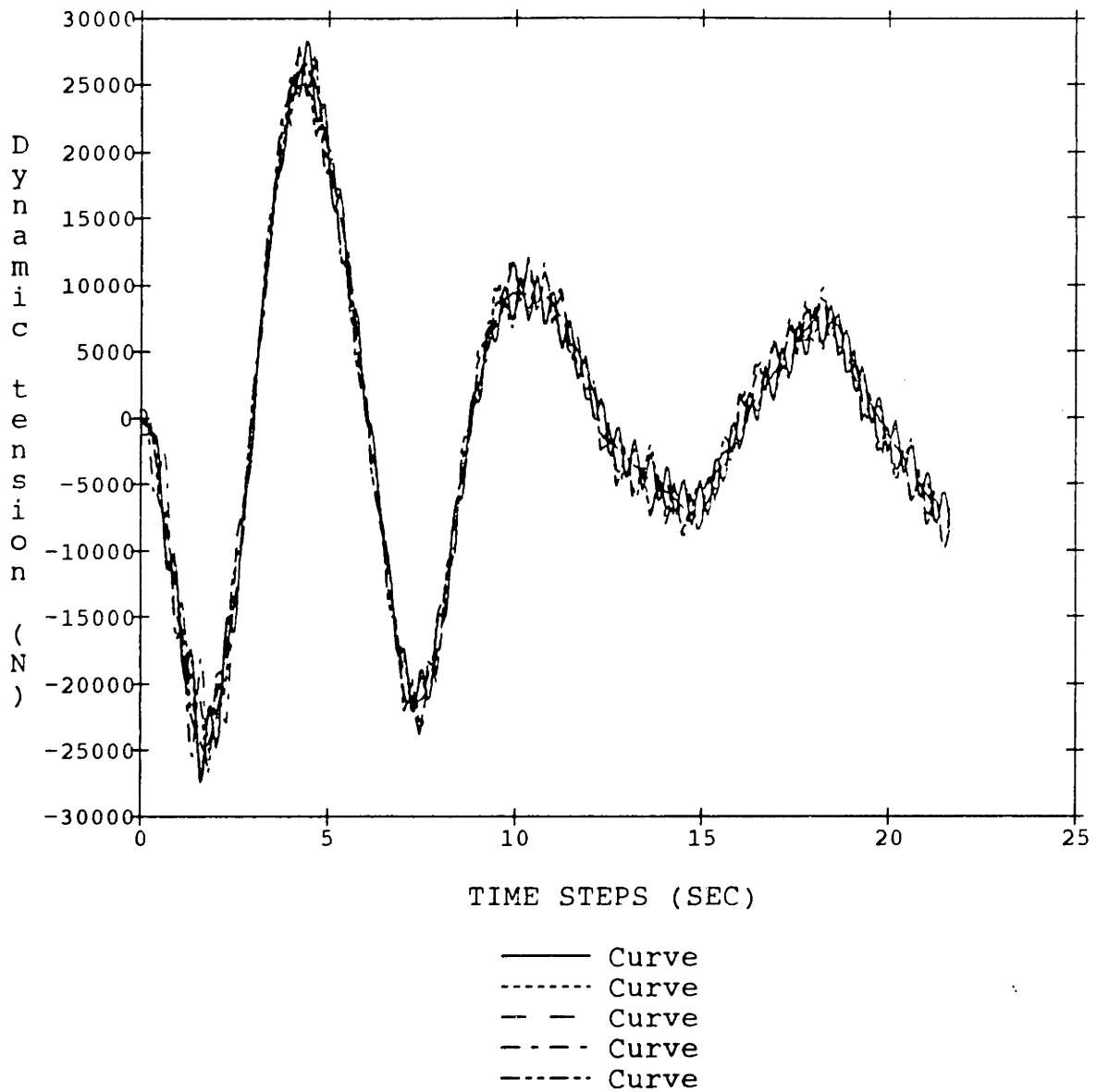


Figure 5-11: Dynamic tensions of a cable with a very small buoy with damping in normal excitation of amplitude equal to 10 diameters at the first natural frequency

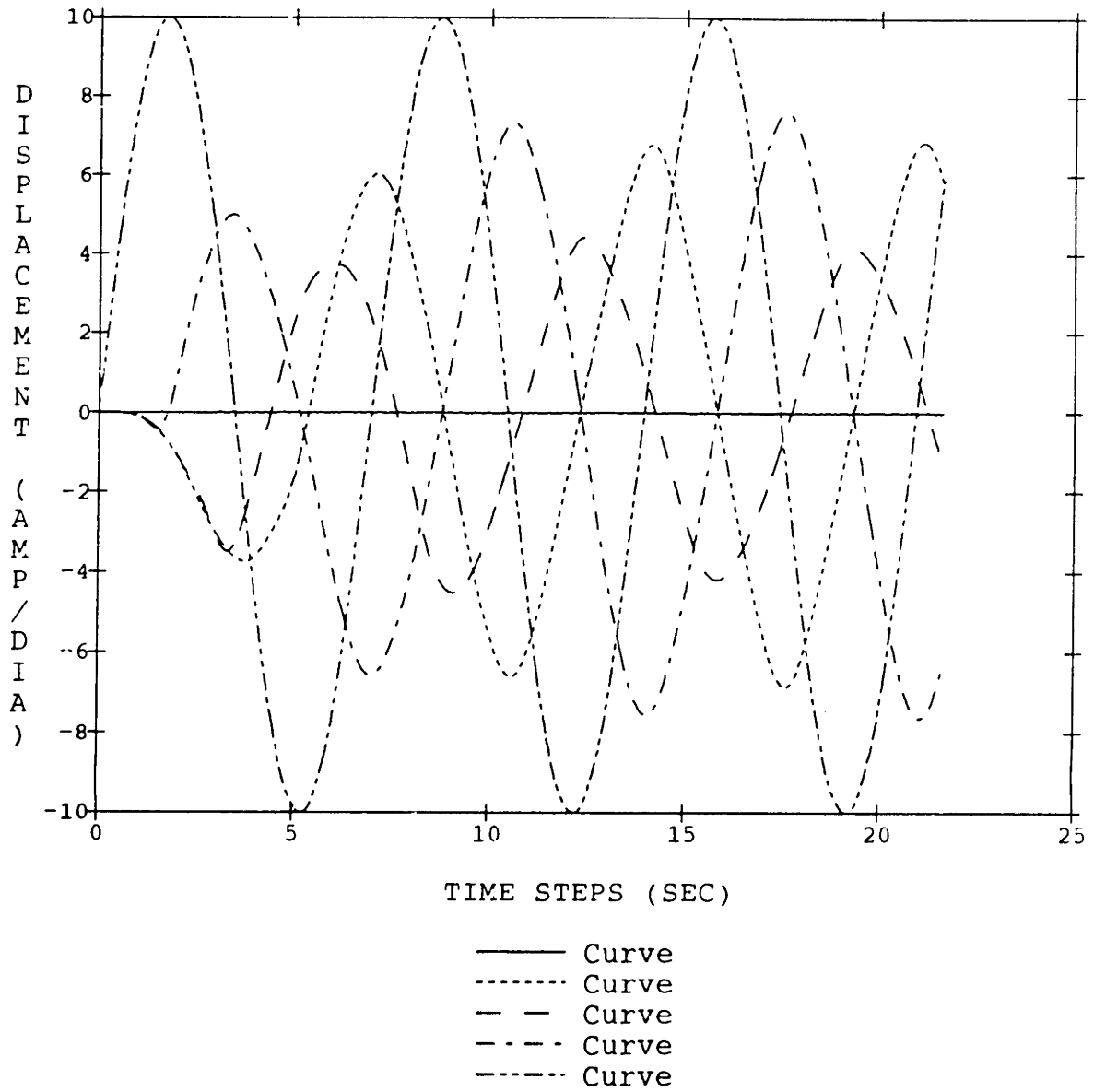


Figure 5-12: Normal displacements of a cable with a very small buoy with damping in normal excitation of amplitude equal to 10 diameters at the first natural frequency

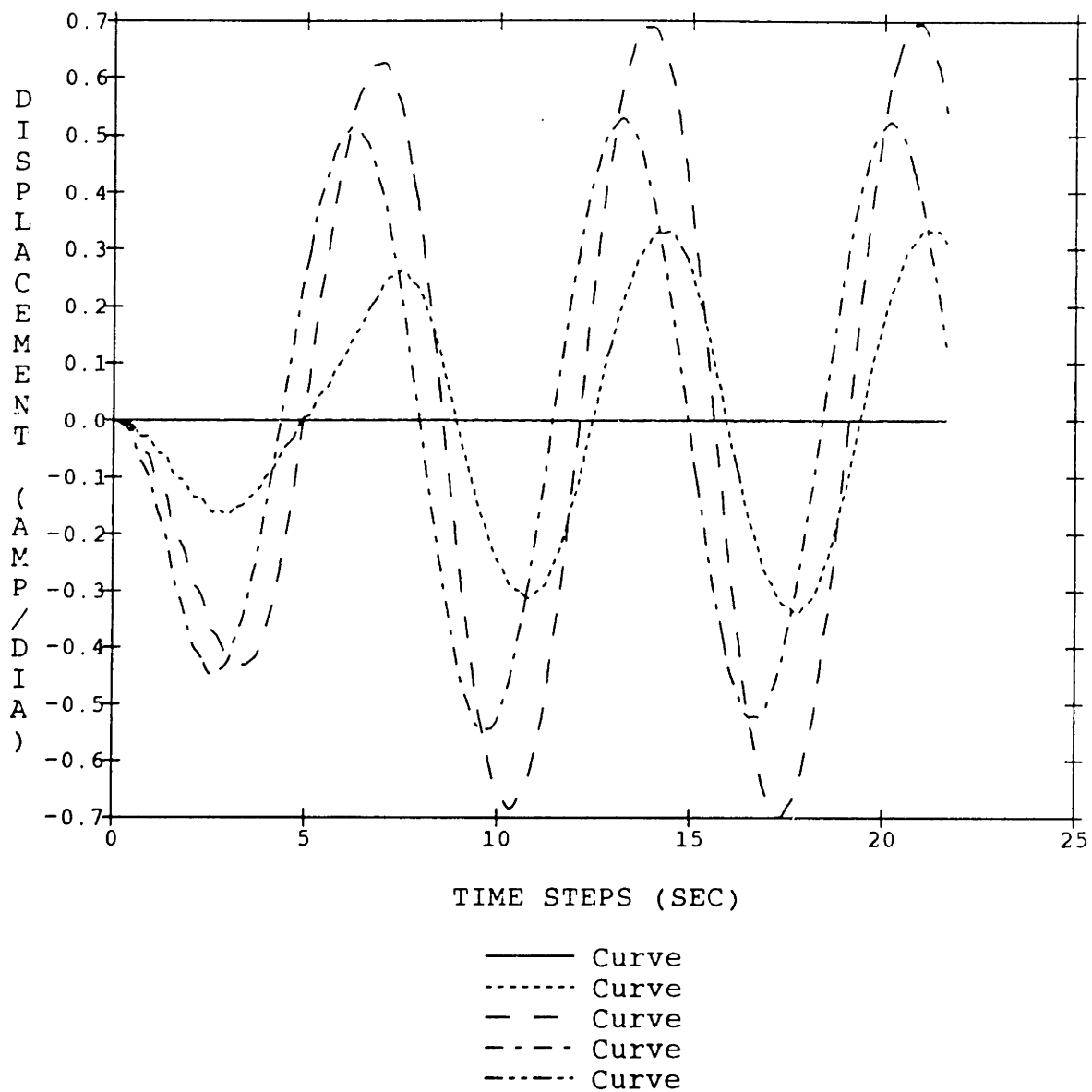


Figure 5-13: Tangential displacements of a cable with a very small buoy with damping in normal excitation of amplitude equal to 10 diameters at the first natural frequency

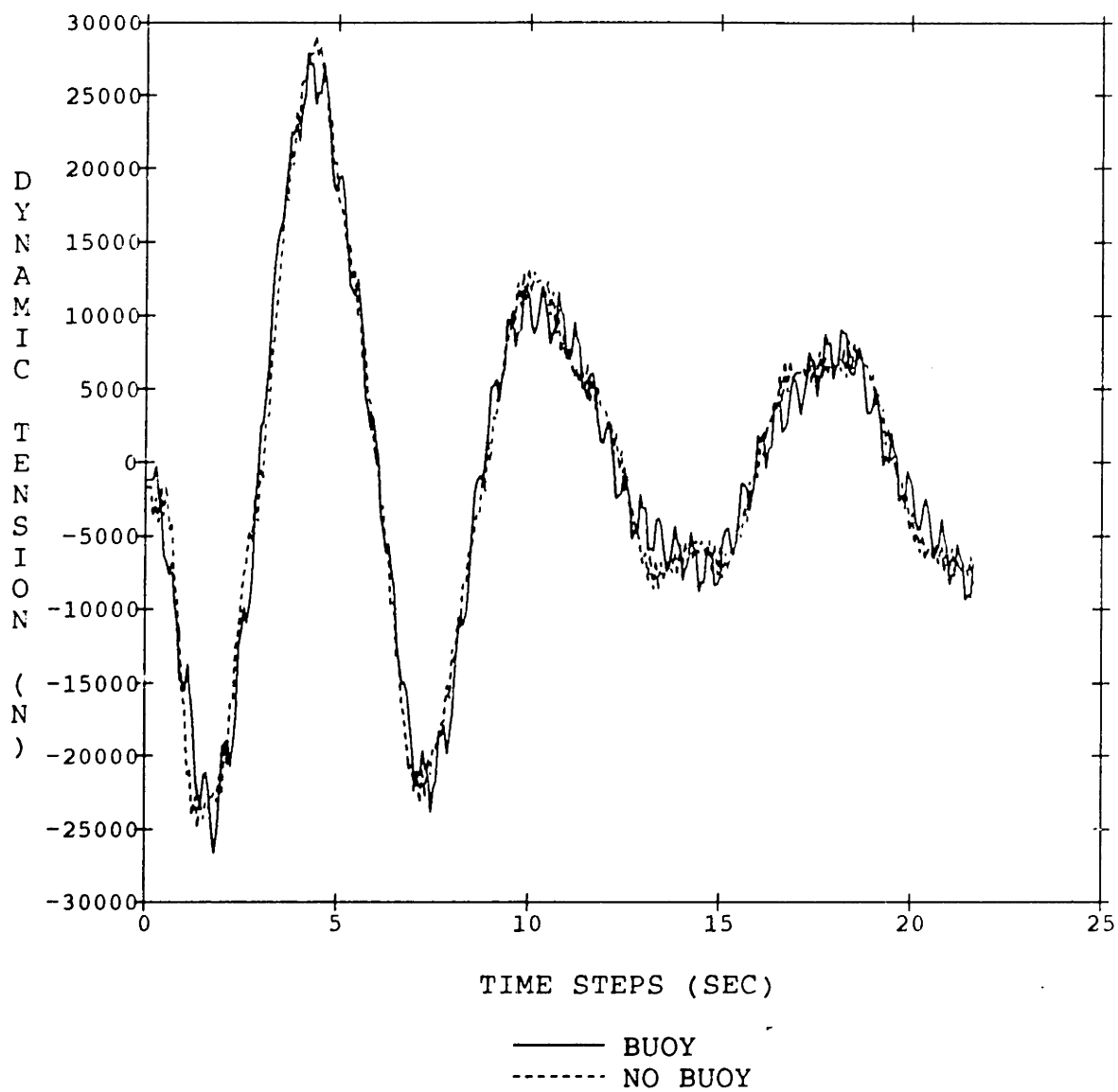


Figure 5-14: Comparison between the dynamic tensions of a cable with a very small buoy and a cable without buoy [excitation of amplitude equal to 10 diameters, at the first natural frequency]

COMPARISON BETWEEN COLLOCATION AND MODAL METHOD
DYNAMIC TENSILE FORCE AT TOP OF CABLE WITH DAMPING ; NORMAL EXCITATION

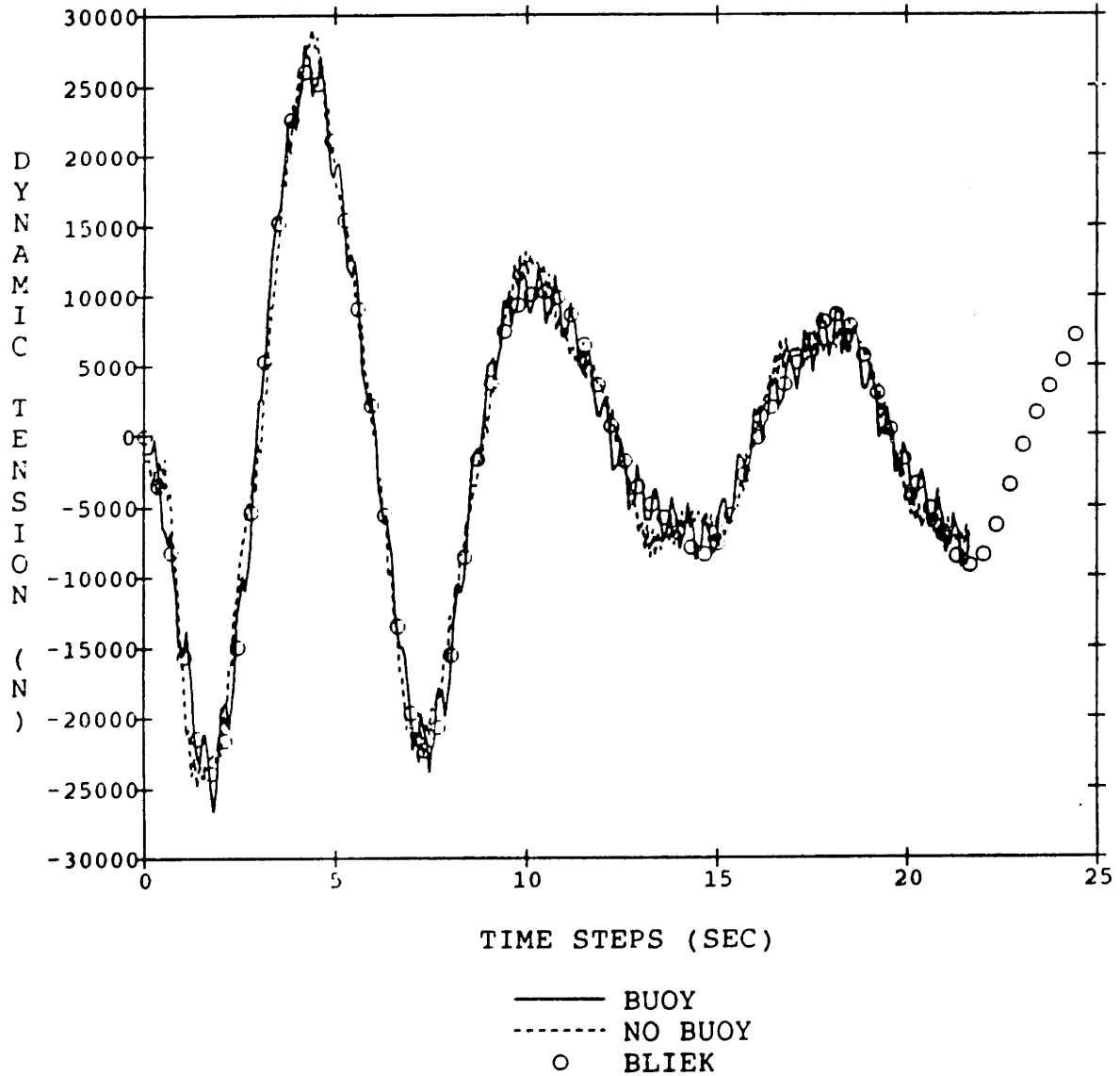


Figure 5-15: Comparison of dynamic tensions at the top of the inclined cable between with a very small buoy and without buoy and Bliiek's results at excitation of amplitude equal to 10 dia. and its first natural frequency

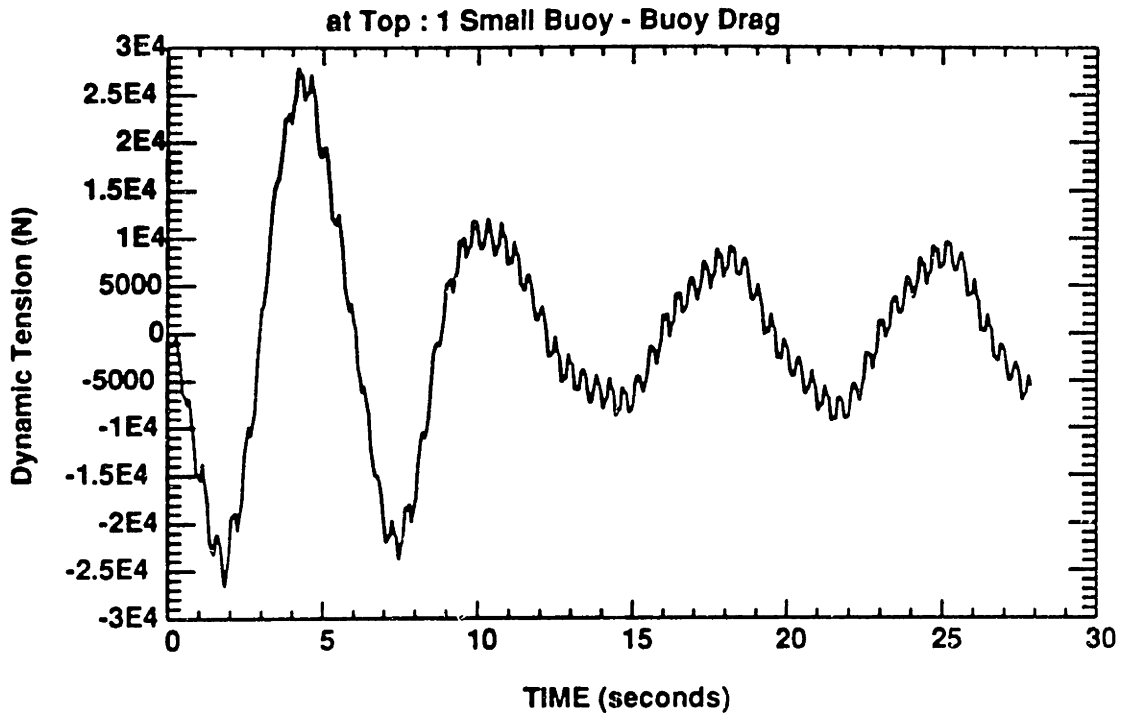


Figure 5-16: Dynamic tension at the top of the cable with a very small buoy [10 Dia. 0.9rad/sec, Normal excitation, No window function]

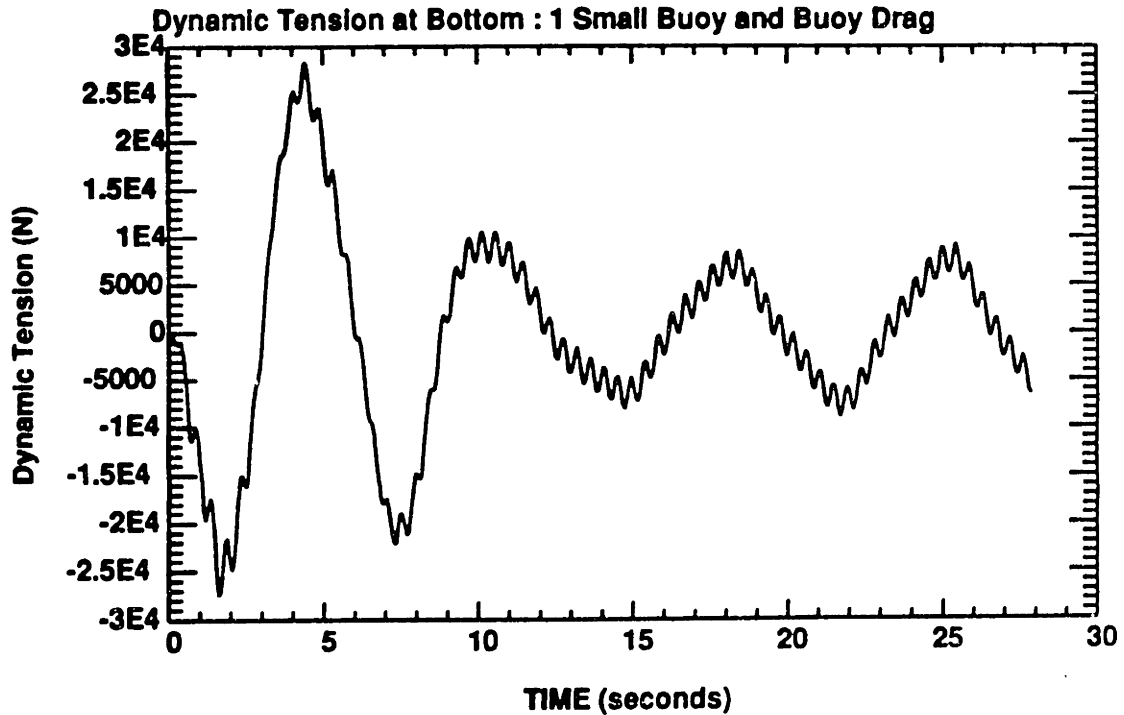


Figure 5-17: Dynamic tension at the bottom of the cable with a very small buoy [10 Dia. 0.9rad/sec, Normal excitation, No window function]

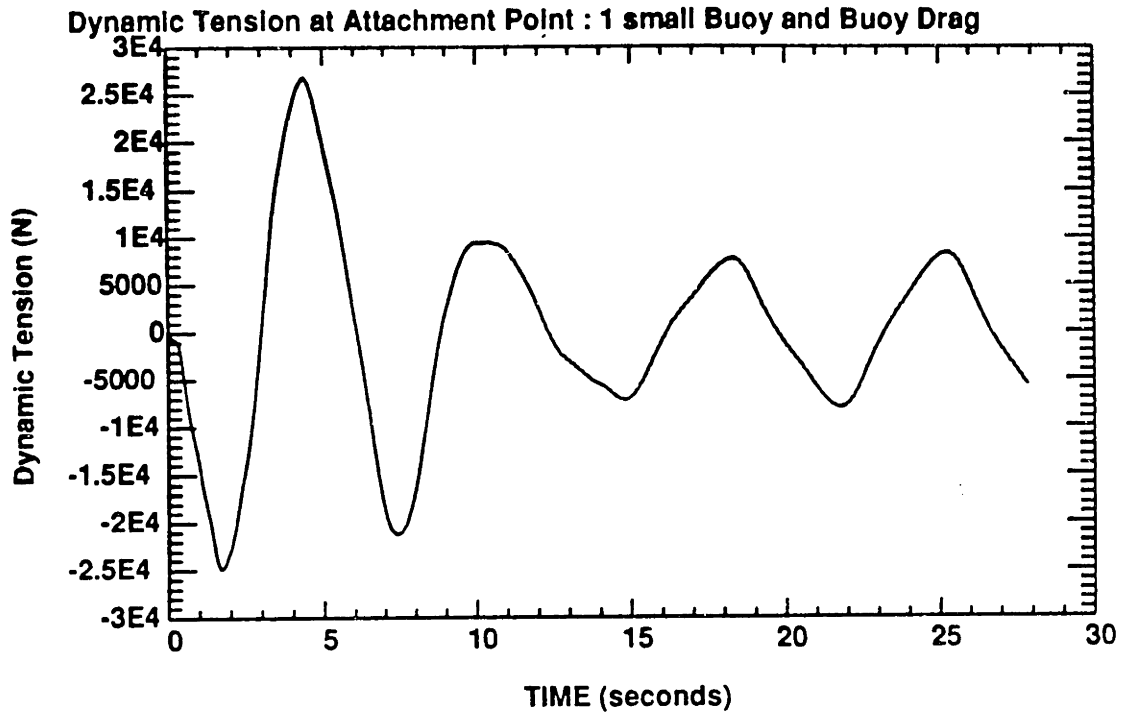


Figure 5-18: Dynamic tension at the attachment of the cable with a very small buoy [10 Dia. 0.9rad/sec, Normal excitation, No window function]

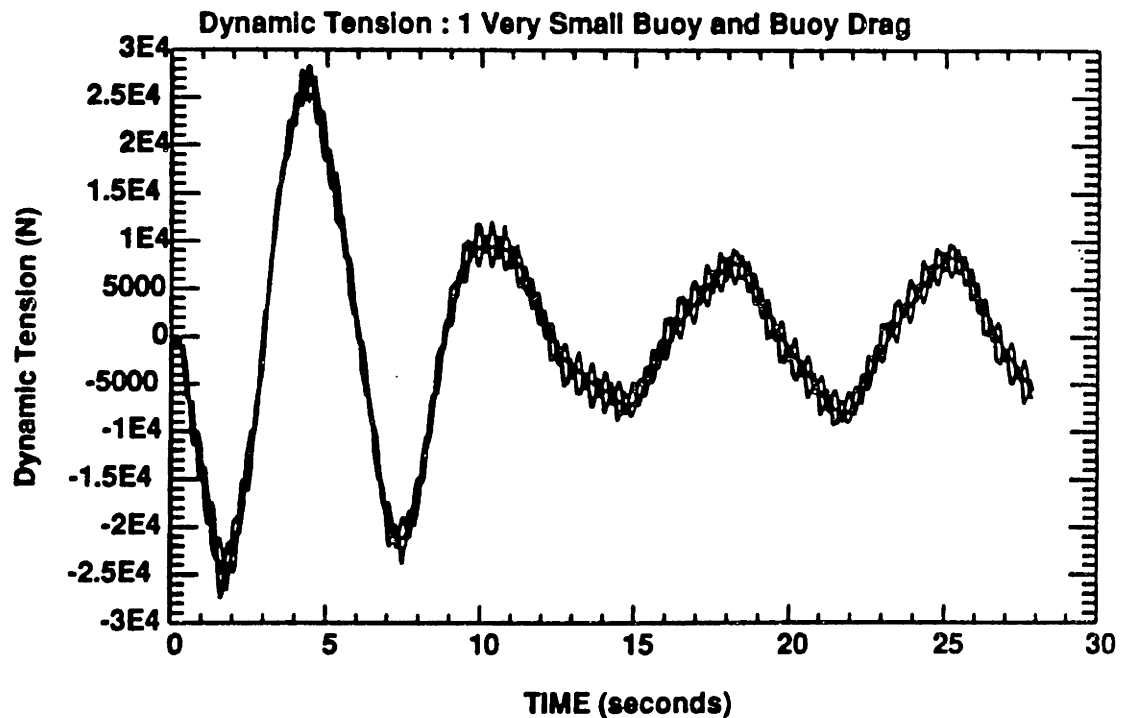


Figure 5-19: Dynamic tensions at several points of the cable with a very small buoy [10 Dia. 0.9rad/sec, Normal excitation, No window function]

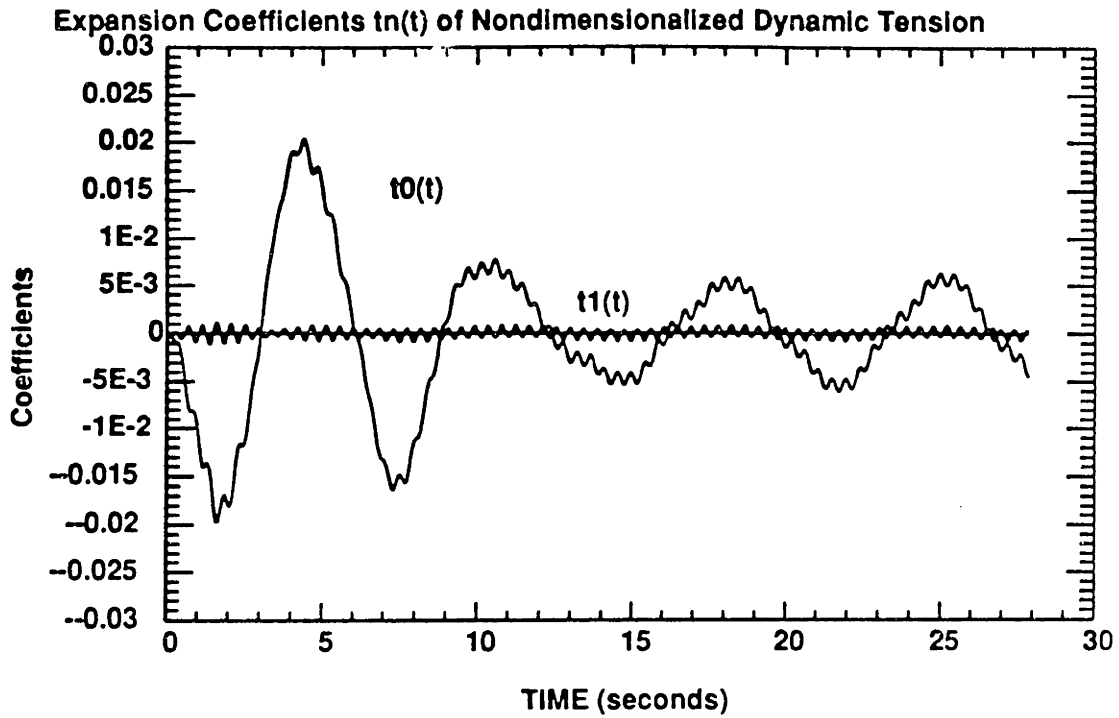


Figure 5-20: First expansion coefficient of nondimensionalized dynamic tension at the lower segment of the cable with a very small buoy [10 Dia. 0.9rad/sec, Normal excitation, No window function]

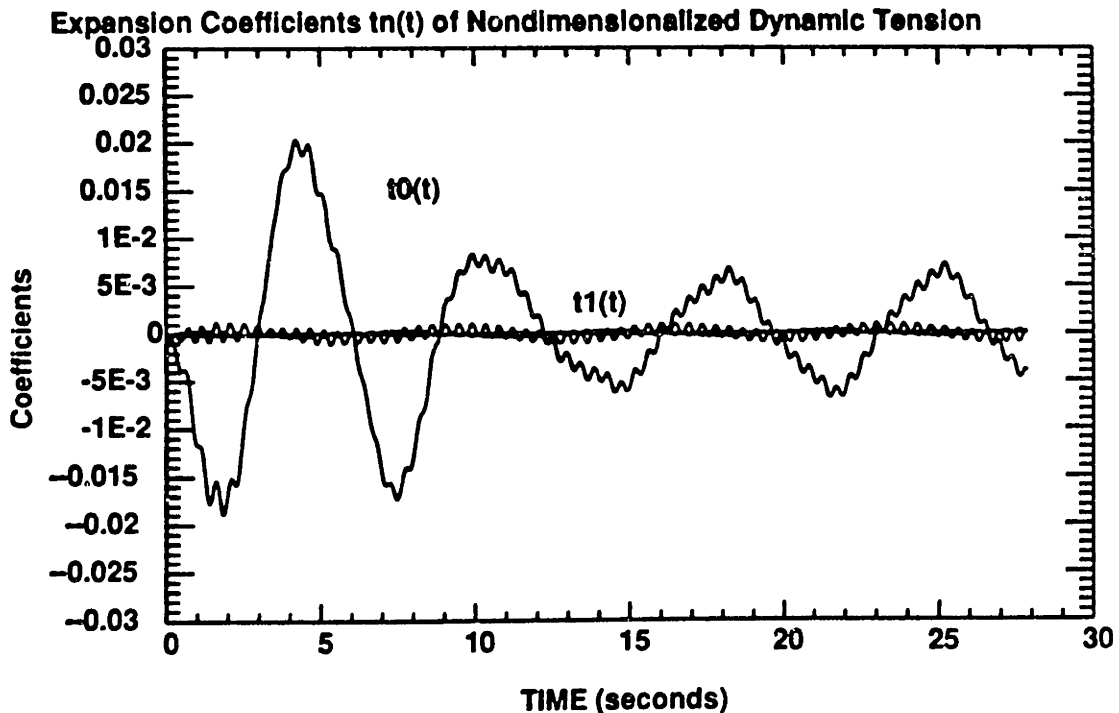


Figure 5-21: First expansion coefficient of nondimensionalized dynamic tension at the upper segment of the cable with a very small buoy [10 Dia. 0.9rad/sec, Normal excitation, No window function]

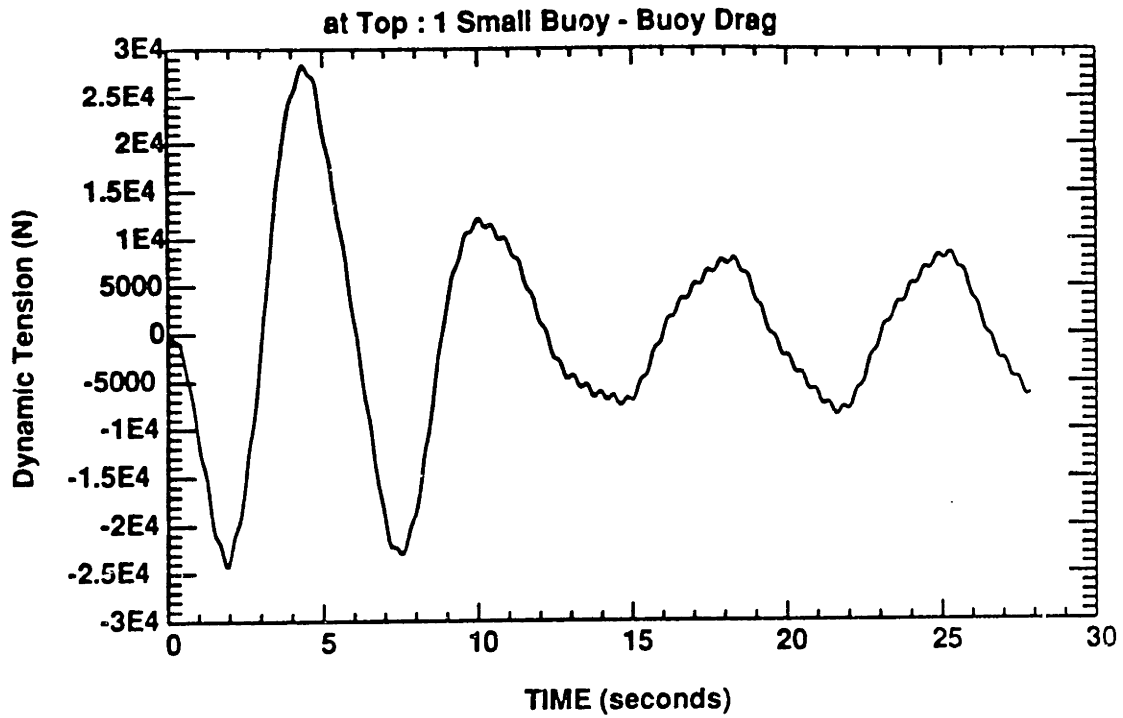


Figure 5-22: Dynamic tension at the top of the cable with a very small buoy [10 Dia. 0.9rad/sec, Normal excitation, Window = 0.5]

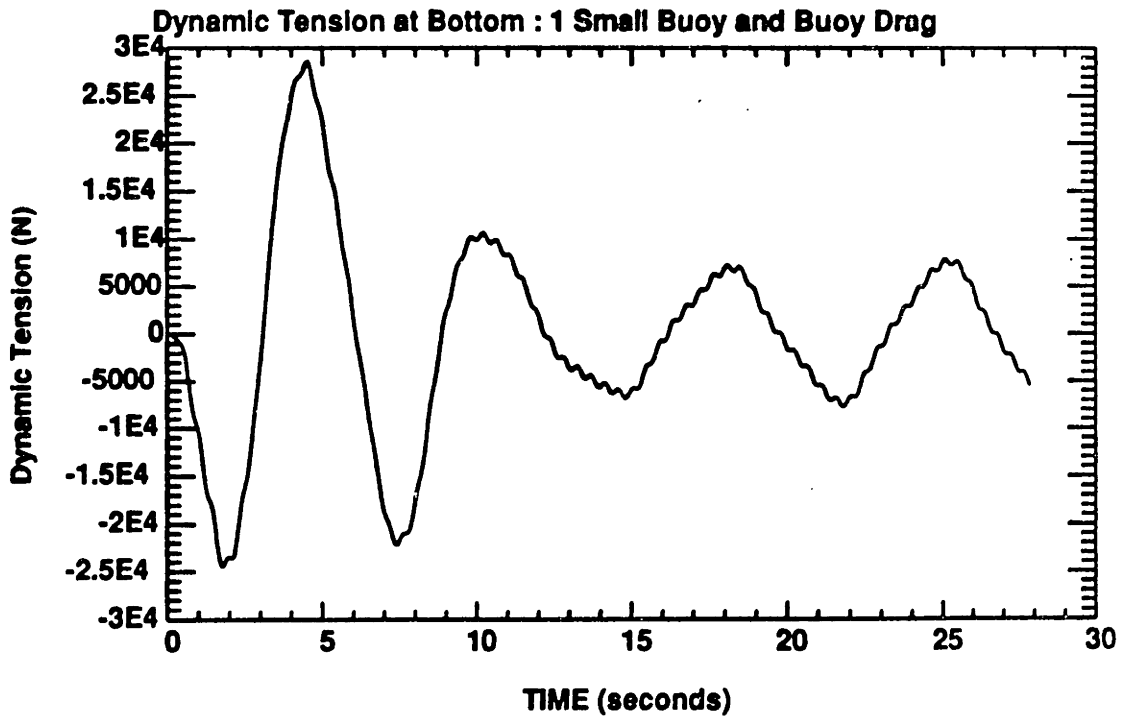


Figure 5-23: Dynamic tension at the bottom of the cable with a very small buoy [10 Dia. 0.9rad/sec, Normal excitation, Window = 0.5]

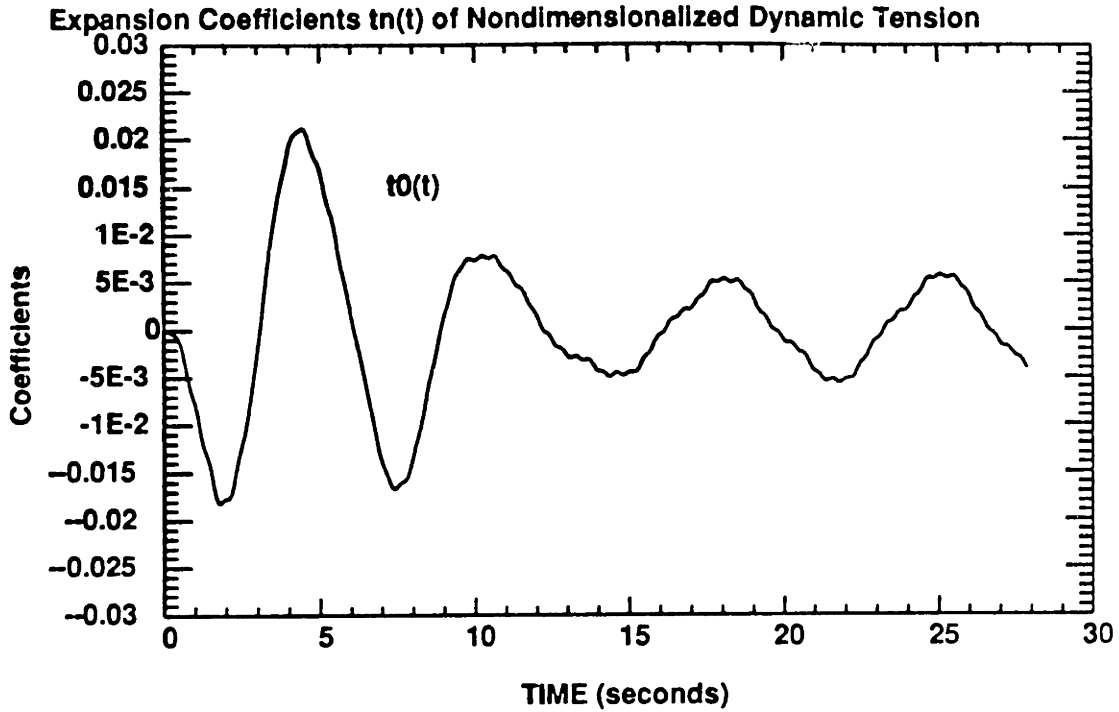


Figure 5-24: First expansion coefficient of nondimensionalized dynamic tension at the lower segment of the cable with a very small buoy [10 Dia. 0.9rad/sec, Normal excitation, Window = 0.5]

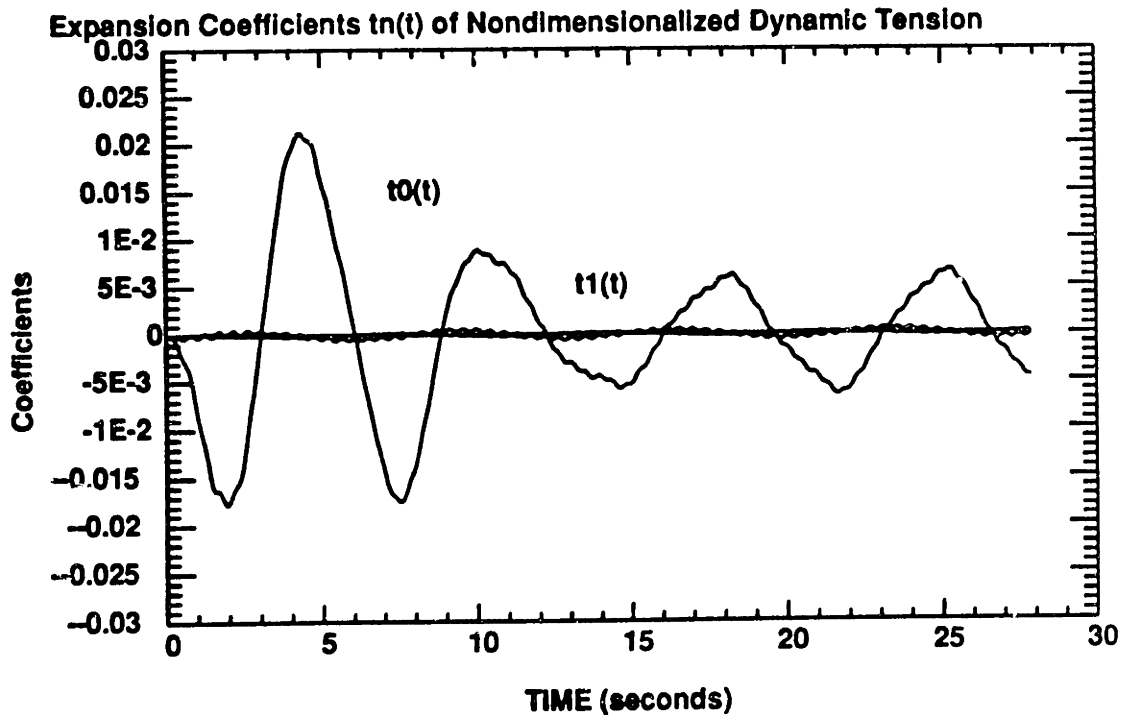


Figure 5-25: First expansion coefficient of nondimensionalized dynamic tension at the upper segment of the cable with a very small buoy [10 Dia. 0.9rad/sec, Normal excitation, Window = 0.5]

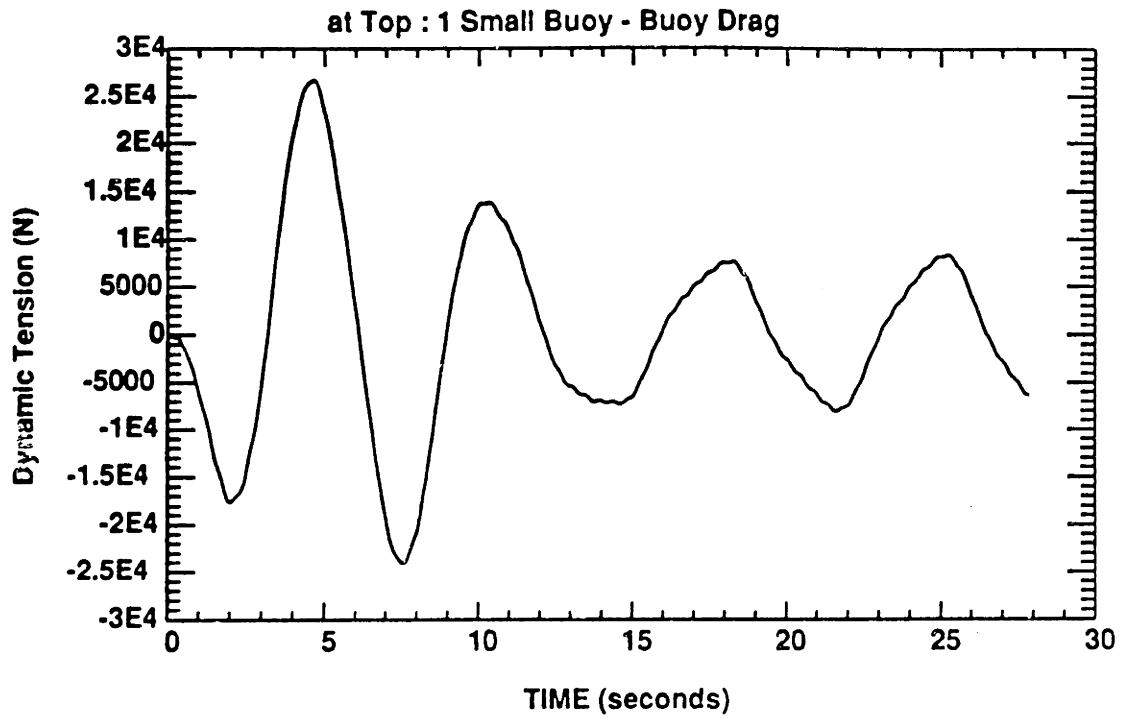


Figure 5-26: Dynamic tension at the top of the cable with a very small buoy [10 Dia. 0.9rad/sec, Normal excitation, Window = 1.5]

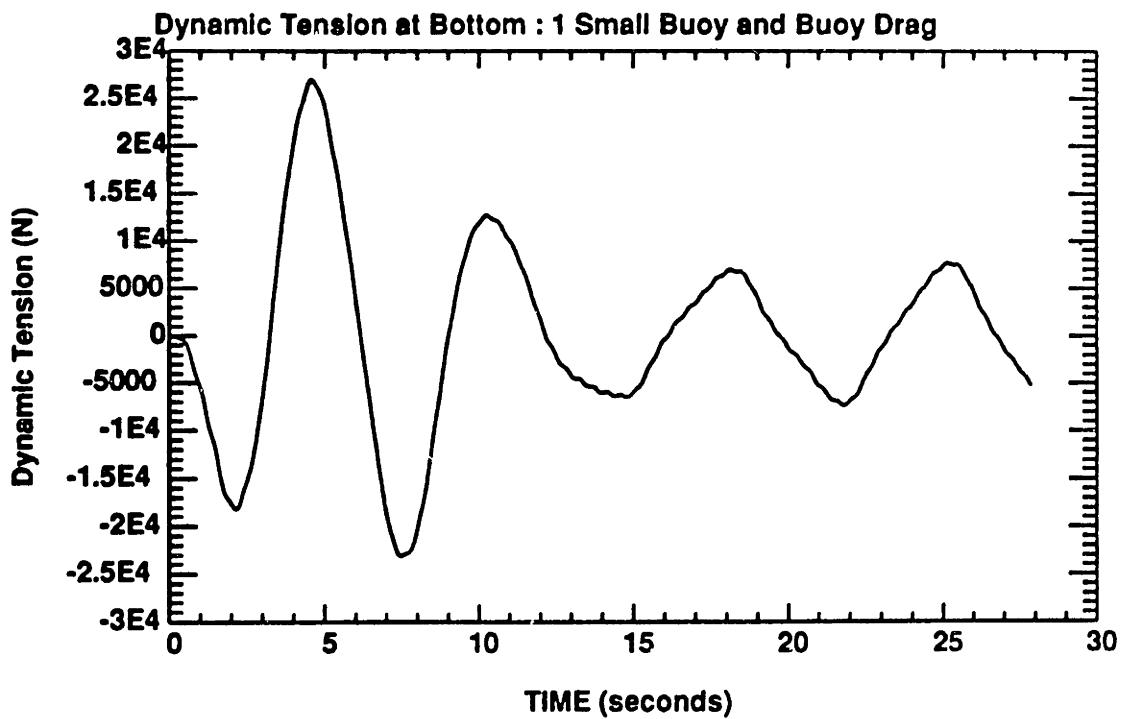


Figure 5-27: Dynamic tension at the bottom of the cable with a very small buoy [10 Dia. 0.9rad/sec, Normal excitation, Window = 1.5]

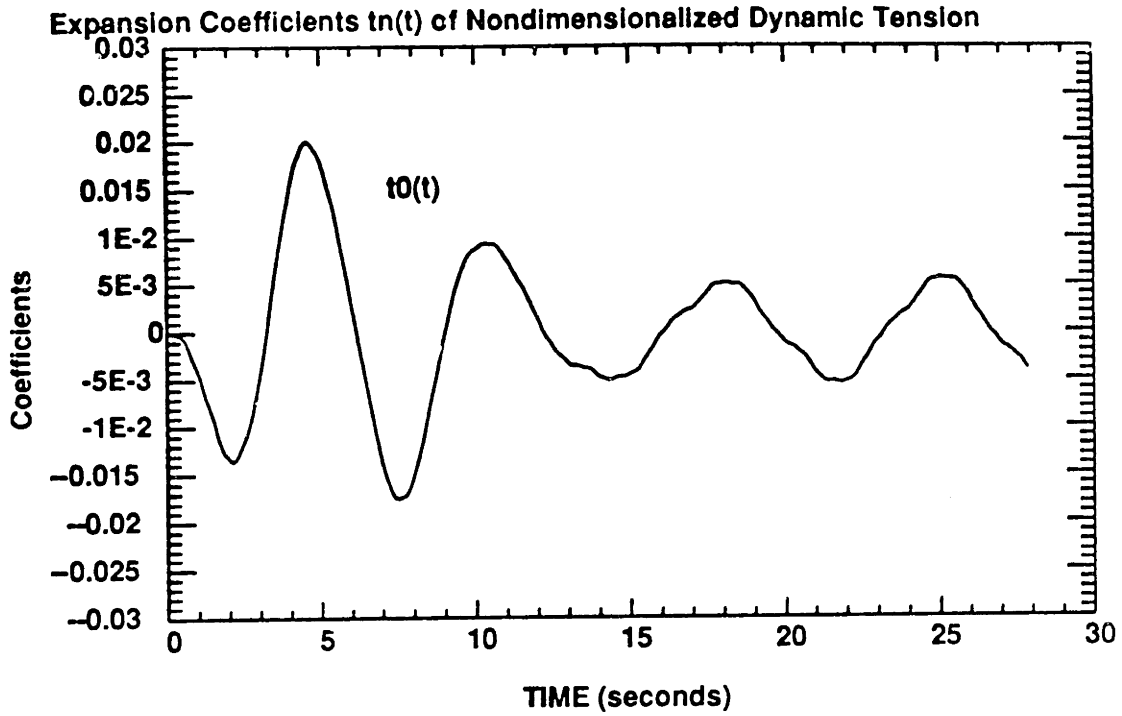


Figure 5-28: First expansion coefficient of nondimensionalized dynamic tension at the lower segment of the cable with a very small buoy [10 Dia. 0.9rad/sec, Normal excitation, Window = 1.5]

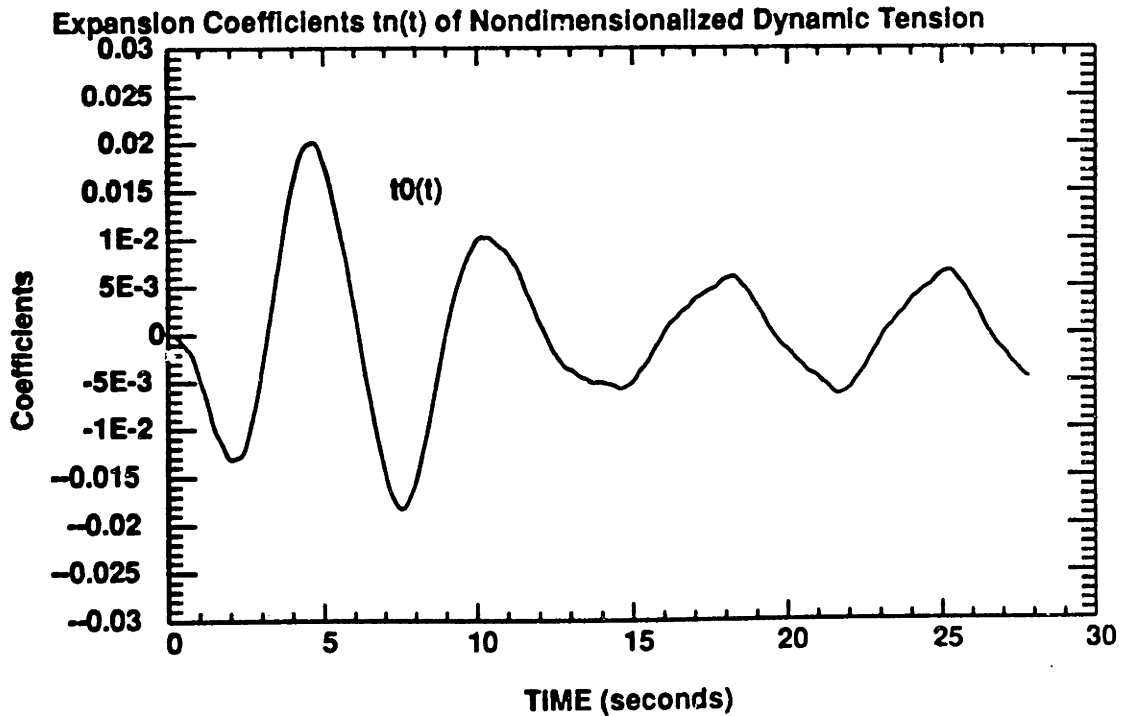


Figure 5-29: First expansion coefficient of nondimensionalized dynamic tension at the upper segment of the cable with a very small buoy [10 Dia. 0.9rad/sec, Normal excitation, Window = 1.5]

Chapter 6

Combined Effects of the Geometric Nonlinearity, Large Tensile Forces and Nonlinear Drag Forces

6.1 Introduction

The fully nonlinear two-dimensional governing equations were derived in Chapter 2, and the simplification of the nonlinear equations was carried out in Chapter 3, in order to use efficient nonlinear numerical schemes.

Bliek, in his thesis, has already pointed out the asymmetry of the time history of displacements due to the geometric nonlinearity [4].

In this chapter, we will study the combined effects of the geometric nonlinearity, large tensile forces, and nonlinear drag forces on the cable dynamic response, with the limitation that the total tension remains at all times positive.

6.2 Nonlinear Governing Equations

The simplified nonlinear governing equations and compatibility relations derived in Chapter 2, are used, which include two important nonlinear mechanisms - geometric nonlinearity and large tensile forces.

$$m \frac{\partial^2 p}{\partial t^2} = \frac{\partial T_1}{\partial s} - T_0 \frac{d\phi_0}{ds} \phi_1 + [F_{dt} - F_{dn} \phi_1] (1 + e)$$

$$- F_{t0} (1 + e_0) + m_a \frac{\partial^2 q}{\partial t^2} \phi_1 \quad \text{from (2.17)}$$

$$(m + m_a) \frac{\partial^2 q}{\partial t^2} = \frac{dT_0}{ds} \phi_1 + T_0 \frac{\partial \phi_1}{\partial s} + T_1 \frac{d\phi_0}{ds} + [F_{dt} \phi_1 + F_{dn}] (1 + e)$$

$$- F_{n0} (1 + e_0) + \frac{\partial T_1}{\partial s} \phi_1 + T_1 \frac{\partial \phi_1}{\partial s} \quad \text{from (2.18)}$$

$$EA \frac{\partial p}{\partial s} - EA q \frac{d\phi_0}{ds} = EA (1 + e) \left(-\frac{\phi_1^2}{2} \right) + EA e_1 \quad \text{from (2.19)}$$

$$EA \frac{\partial q}{\partial s} + EA p \frac{d\phi_0}{ds} = EA (1 + e) \phi_1 \quad \text{from (2.20)}$$

For the numerical scheme, we employ an expansion of the response in terms of Chebyshev polynomials ; a collocation method spatially and Newmark's method for time integration, as already derived in Chapters 3 and 4.

Through the expansion of the residual equations resulting from the trial solutions, $4(N+2)$ simultaneous equations at the N collocation points and the 2 boundary ends are solved (refer to Section 4.4)

6.3 Numerical Application

The inclined cable, used in Chapters 3, 4 and 5, is also used in order to determine the effects on the dynamic response. The principal parameters of the inclined cable is found in Table 4-I.

The excitation is applied at the top point of the inclined cable, in the form of an

imposed motion, whose amplitude is equal to 10 cable diameters and its frequency is equal to the first natural frequency of the cable.

Figures (6-1), (6-2) and (6-3) show the dynamic response of the cable subjected to only the nonlinear drag forces and, in a few periods, the dynamic responses reach steady state. In Fig. (6-3), the high frequency fluctuations result from the strong singularity of the initial velocity, as mentioned earlier in chapter 5.

Figures (6-4), (6-5) and (6-6) show the dynamic response of the cable with geometric nonlinearity and large tensile forces, as well as nonlinear drag forces. The combined effects of both geometric nonlinearity and large tensile forces on the dynamic tension are observed, making small peaks between large peaks of the dynamic tension in Figures (6-4) and (6-6).

Through comparison between the dynamic response of the cable with only nonlinear drag forces and that of the cable with the combined effects of geometric nonlinearity and large tensile forces in Figures (6-7), (6-8), and (6-9), we found that, in steady state, the combined effects increase the maximum dynamic tension (Figures 6-7 and 6-9) and reduce the magnitude of the minimum of the dynamic tension at the middle of the cable (Fig. 6-7). In table 6-, the increase in the maximum dynamic tension at the middle of the cable was 45 % and, the increase at the top 51 %.

This means that, for this particular excitation, we should include the geometric nonlinearity and large tensile forces in order to estimate accurately extreme tensions. For higher frequencies and larger amplitudes of excitation, the contribution to the dynamic tension from large tensile forces, and the geometric nonlinearity is expected to increase. This has serious effects on the fatigue life of the cable, necessitating the use of the present approach if reliable results are to be obtained.

The decrease in the magnitude of the minimum minimum dynamic tension in the middle of the cable is found to be equal to 36 % (Table 6-I). This decrease, together with

Table 6- : Comparison of the dynamic response of GUYSTA with only nonlinear drag forces, with respect to the case of including both geometric nonlinearity and large tensile forces, as well as nonlinear drag forces			
Item	combined effects	nonlinear drag forces only	difference(%)
Maximum dynamic tension in the middle	14138.6 N	9744.02 N	+45 %
Maximum normal displacement in the middle	4.282 (m/dia)	4.10 (m/dia)	+4.44 %
Maximum dynamic tension at the top	12499.5 N	8266.13 N	+51.21 %

Table 6-I: Comparison of the maximum dynamic response of GUYSTA with only nonlinear drag forces, with respect to the case of including both geometric nonlinearity and large tensile forces, as well as nonlinear drag forces

the increase of the maximum dynamic tension (Table 6-), cause the average tension to become higher.

The same phenomena - increase of the maximum and reduction of the magnitude of the minimum - are obtained for both the tangential and normal displacements (Fig. 6-8 and Tables 6- and 6-I).

Table 6-I : Comparison of the dynamic response of GUYSTA with only nonlinear drag forces, with respect to the case of including both geometric nonlinearity and large tensile forces, as well as nonlinear drag forces			
Item	combined effects	nonlinear drag forces only	difference(%)
Minimum dynamic tension in the middle	-6260.96 N	-9779.85 N	-36 %
Minimum normal displacement in the middle	-3.917 (m/dia)	-4.095 (m/dia)	-4.36 %
Minimum dynamic tension at the top	-8820.14 N	-8262.12 N	+6.7 %

Table 6-II: Comparison of minimum dynamic responses of GUYSTA with only nonlinear drag forces with respect to the case of both geometric nonlinearity and large tensile forces, as well as nonlinear drag forces

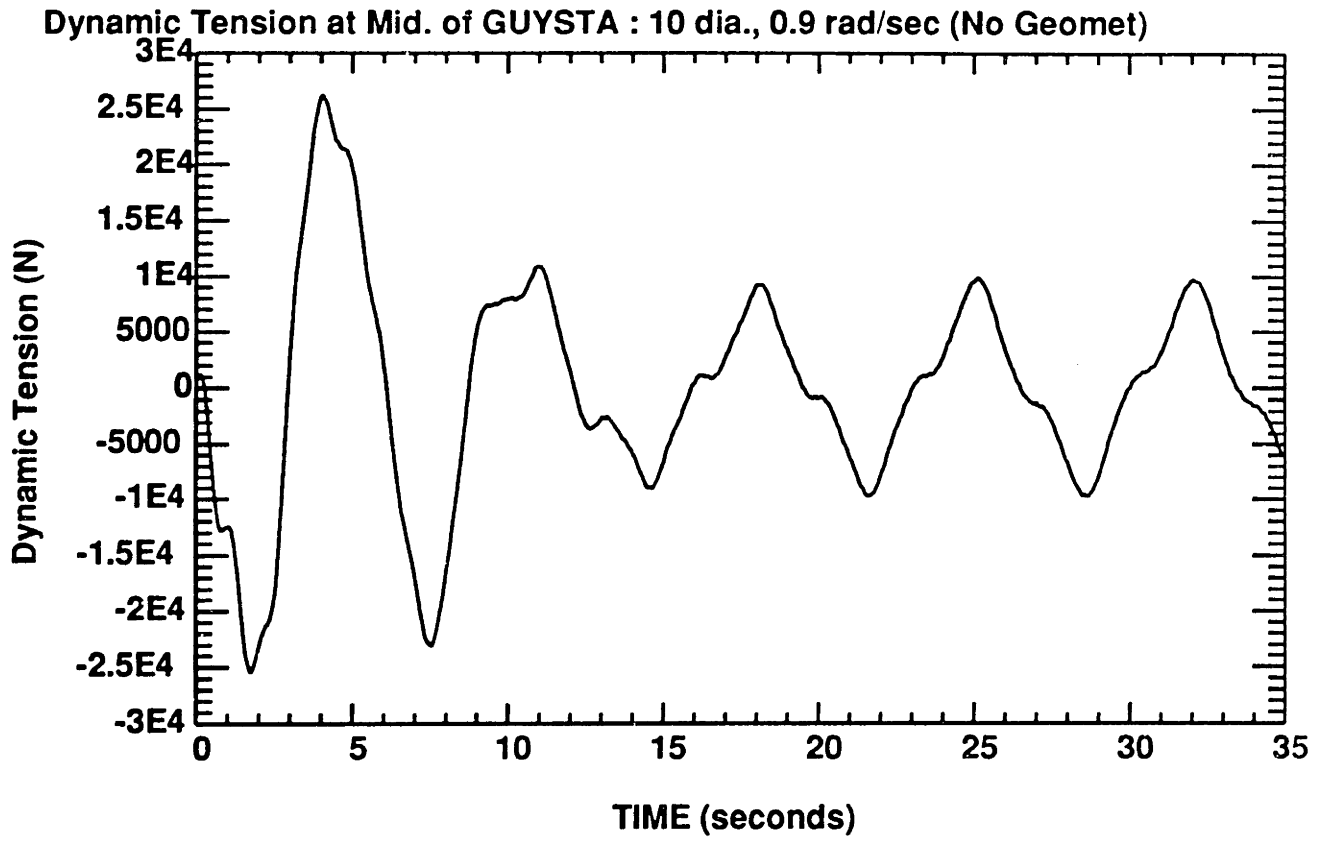


Figure 6-1: Dynamic tension at the middle of GUYSTA, subjected to only nonlinear drag forces [10 diameters, 0.9rad/sec]

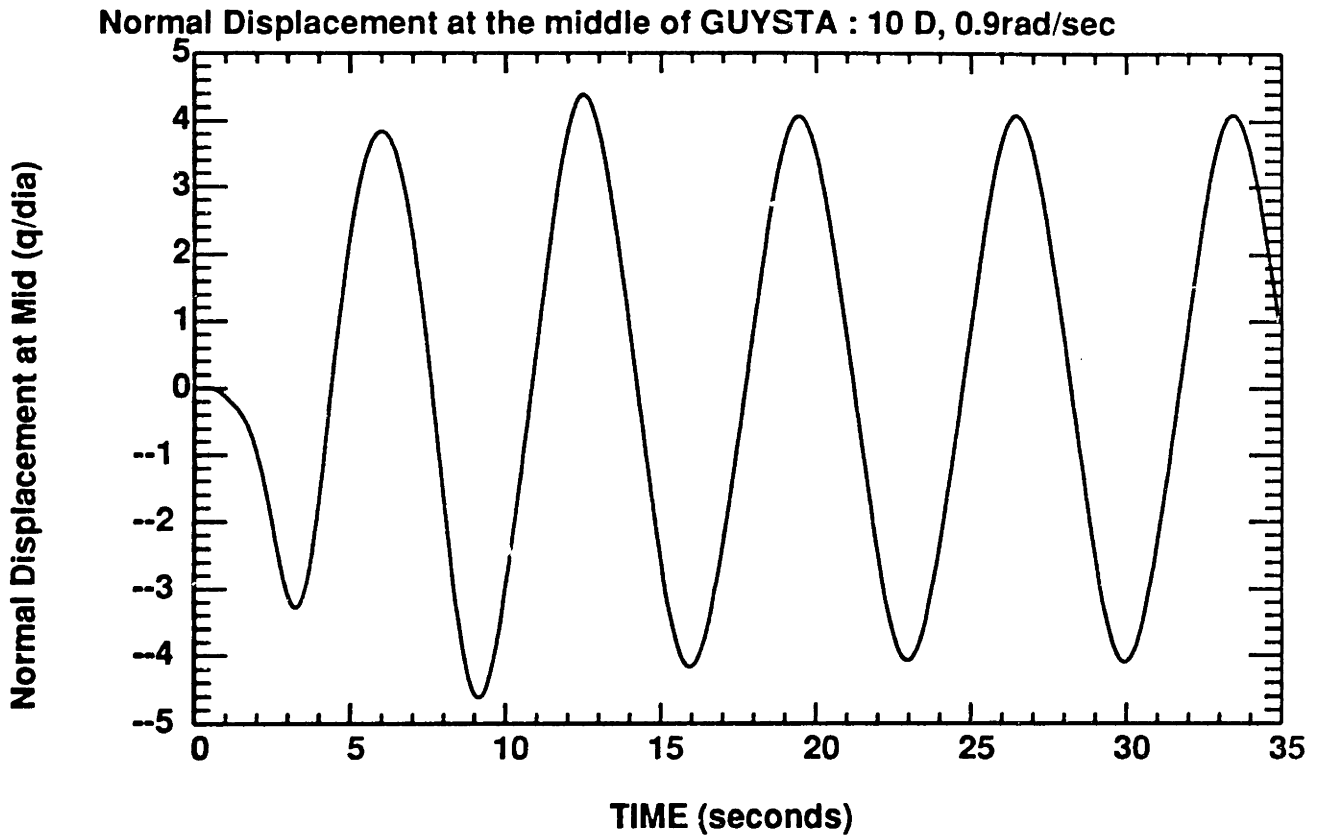


Figure 6-2: Normal displacement at the middle of GUYSTA, subjected to only nonlinear drag forces [10 diameters, 0.9rad/sec]

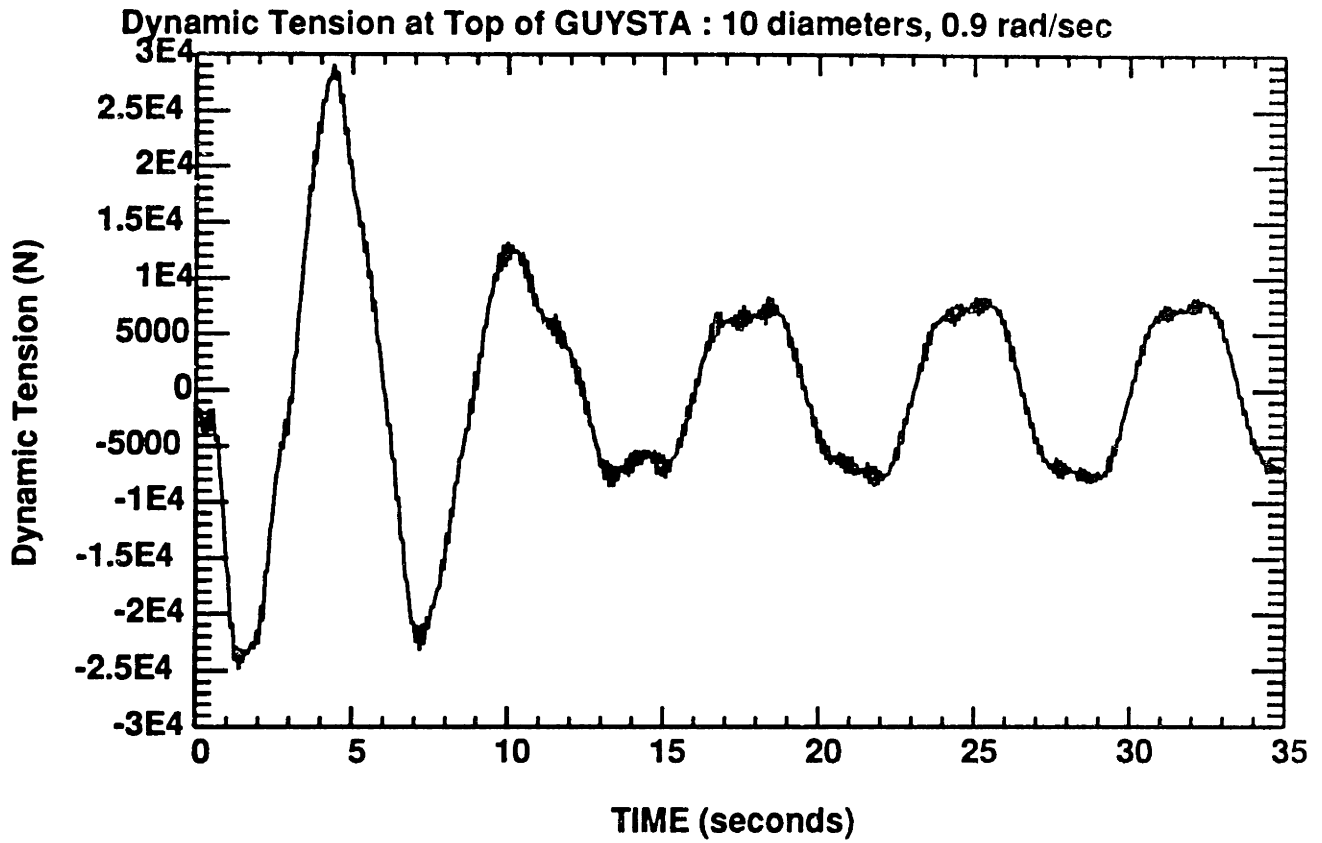


Figure 6-3: Dynamic tension at the top of GUYSTA, subjected to only nonlinear drag forces [10 diameters, 0.9rad/sec]

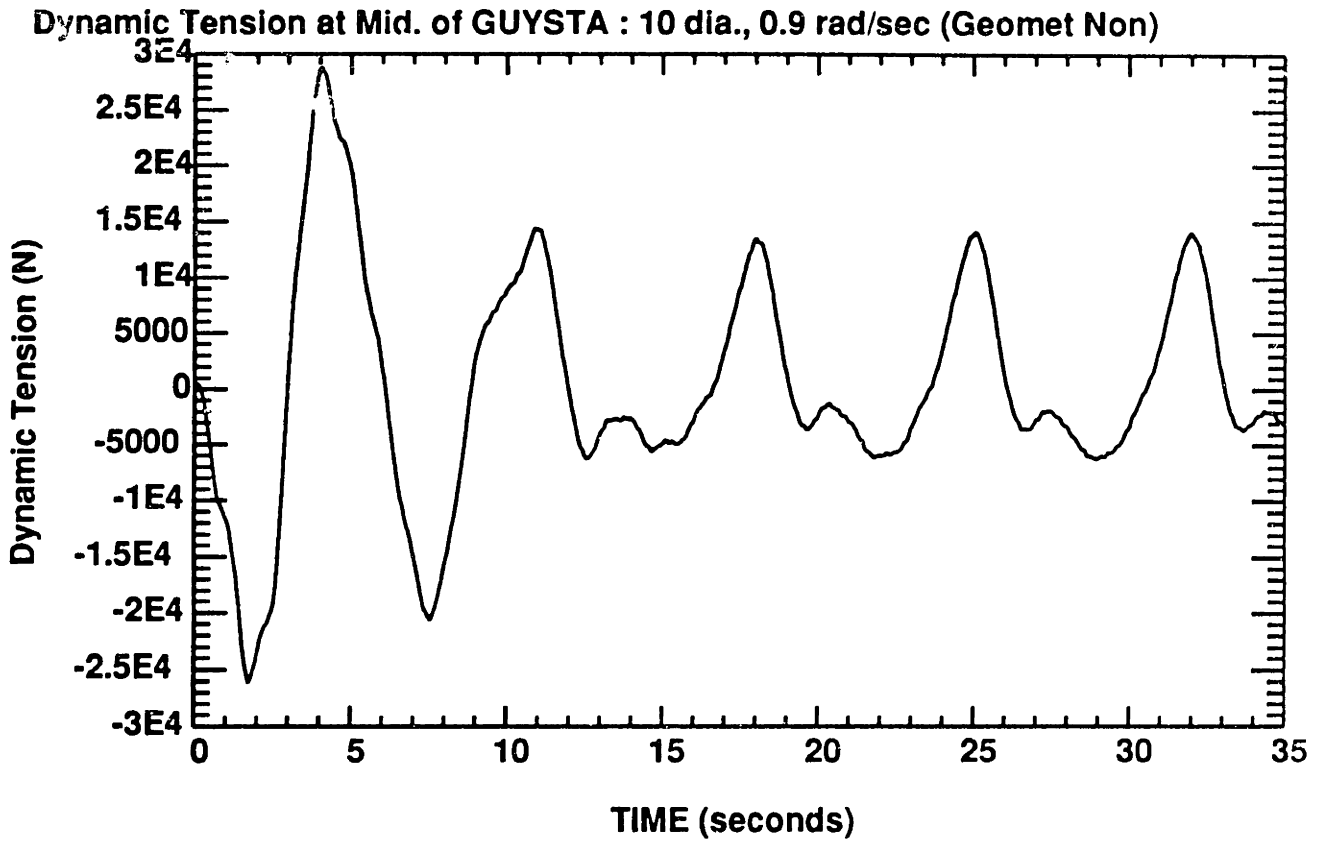


Figure 6-4: Dynamic tension at the middle of GUYSTA, subjected to geometric nonlinearity and large tensile forces as well as nonlinear drag forces [10 diameters, 0.9rad/sec]

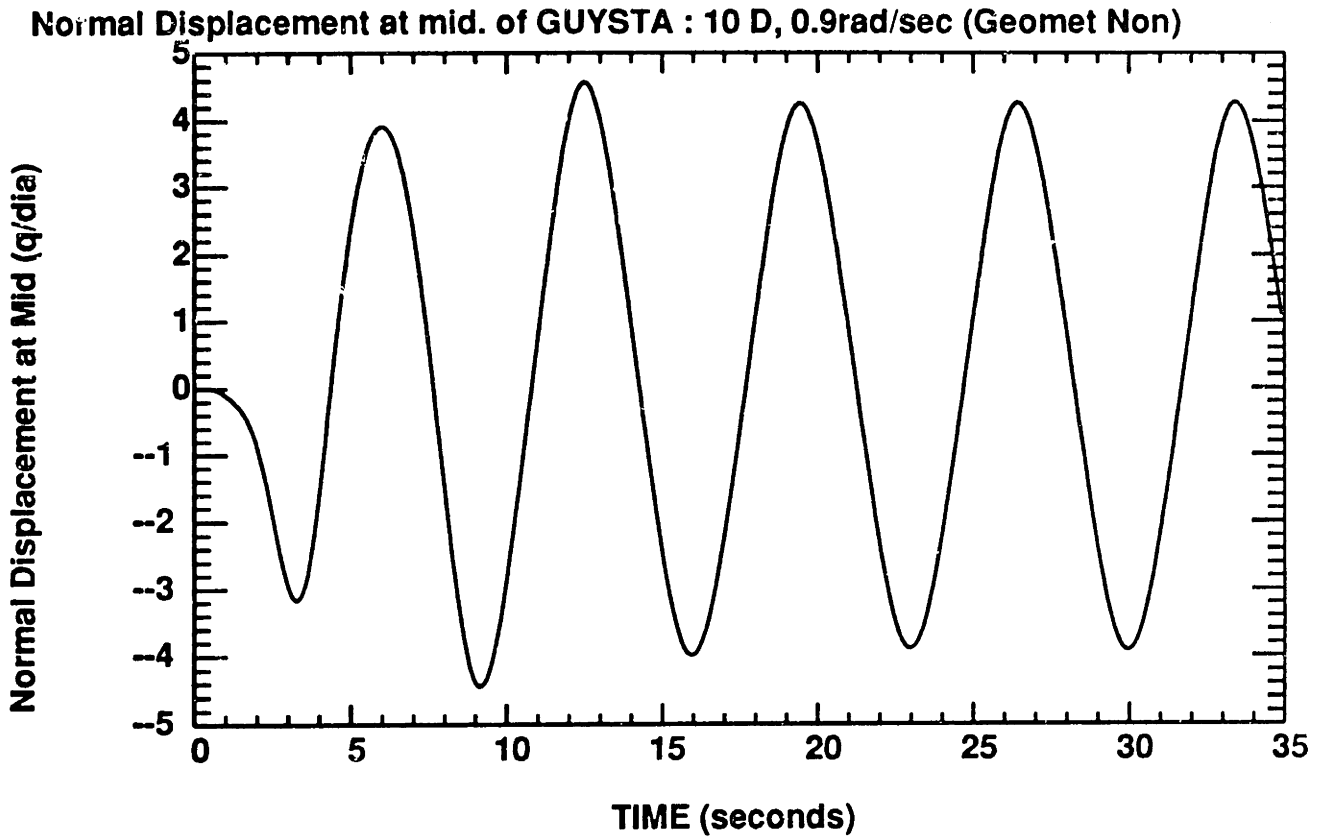


Figure 6-5: Normal displacement at the middle of GUYSTA, subjected to geometric nonlinearity and large tensile forces as well as nonlinear drag forces [10 diameters, 0.9rad/sec]

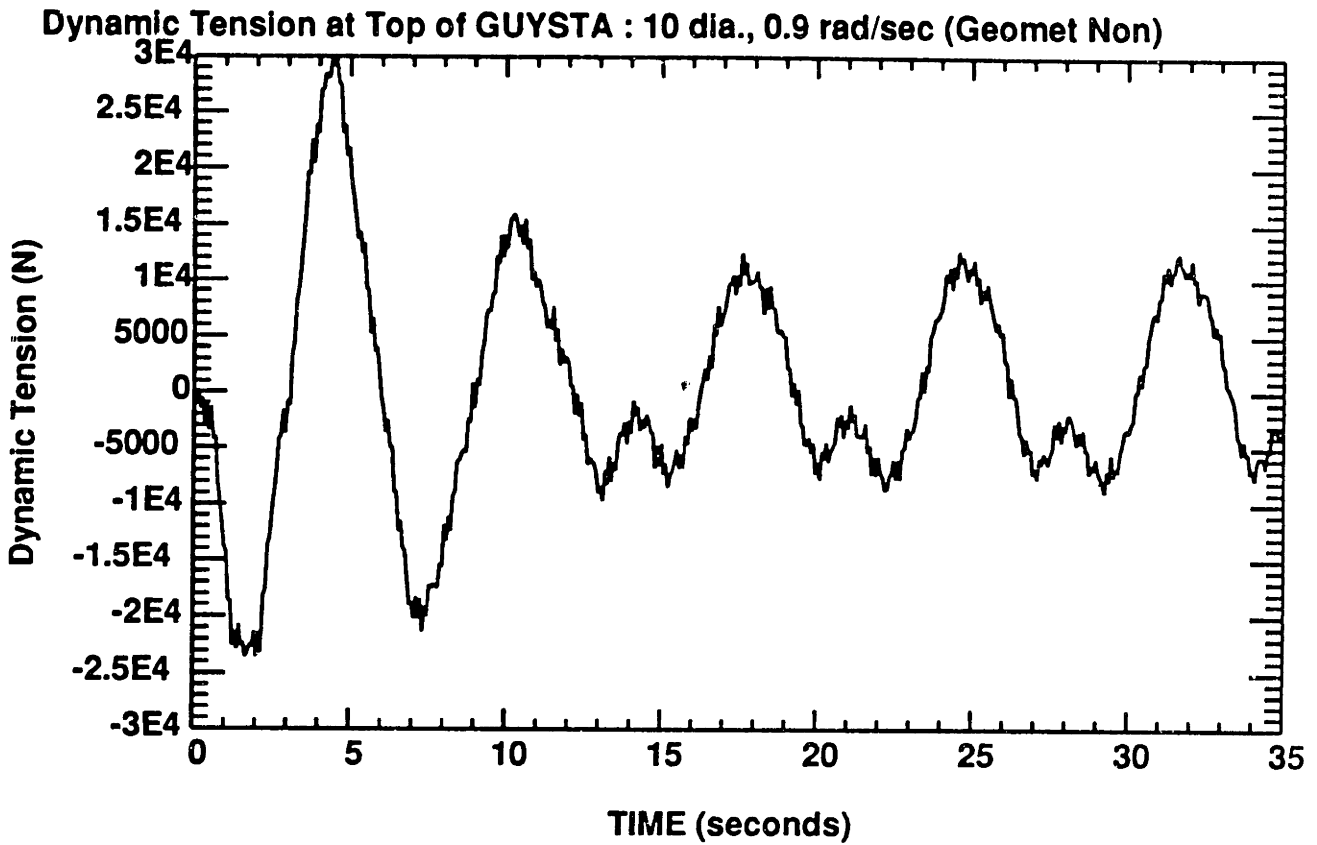


Figure 6-6: Dynamic tension at the top of GUYSTA, subjected to geometric nonlinearity and large tensile forces as well as nonlinear drag forces [10 diameters, 0.9rad/sec]

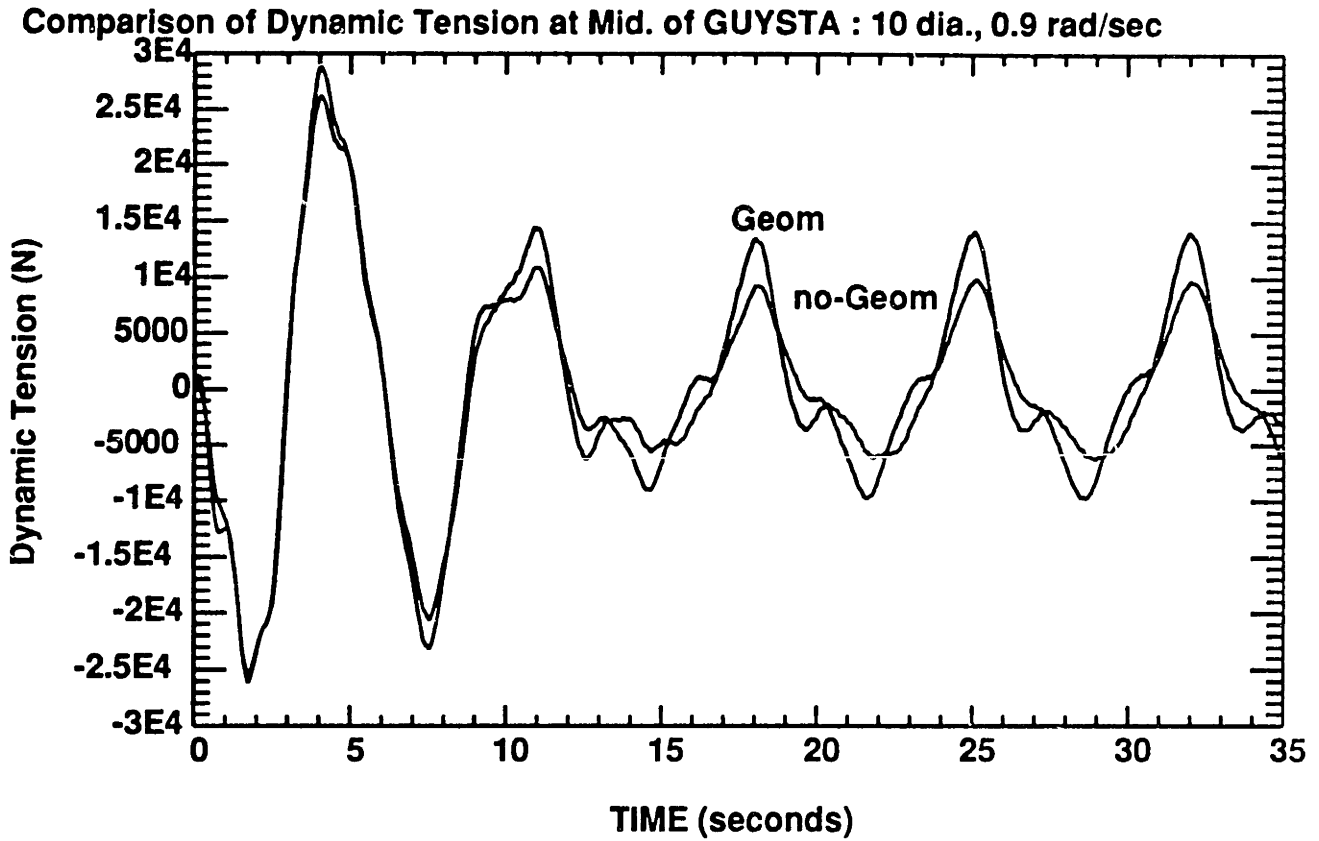


Figure 6-7: Comparison between dynamic tensions at the middle of a cable subjected to nonlinear drag forces and a cable subjected to geometric nonlinearity and large tensile forces, as well as nonlinear drag forces [10 diameters, 0.9rad/sec]

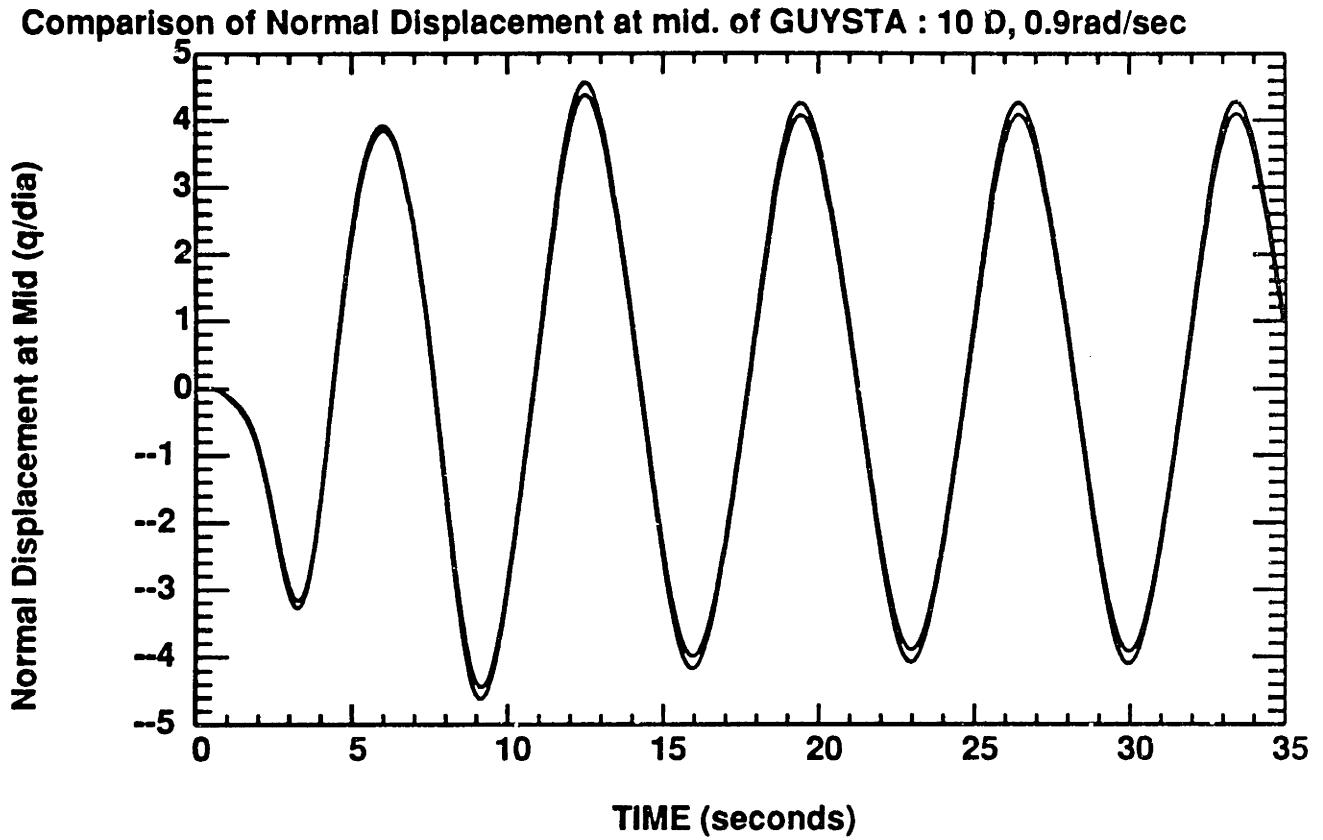


Figure 6-8: Comparison between normal displacements at the middle of a cable subjected to nonlinear drag forces and a cable subjected to geometric nonlinearity and large tensile forces, as well as nonlinear drag forces [10 diameters, 0.9rad/sec]

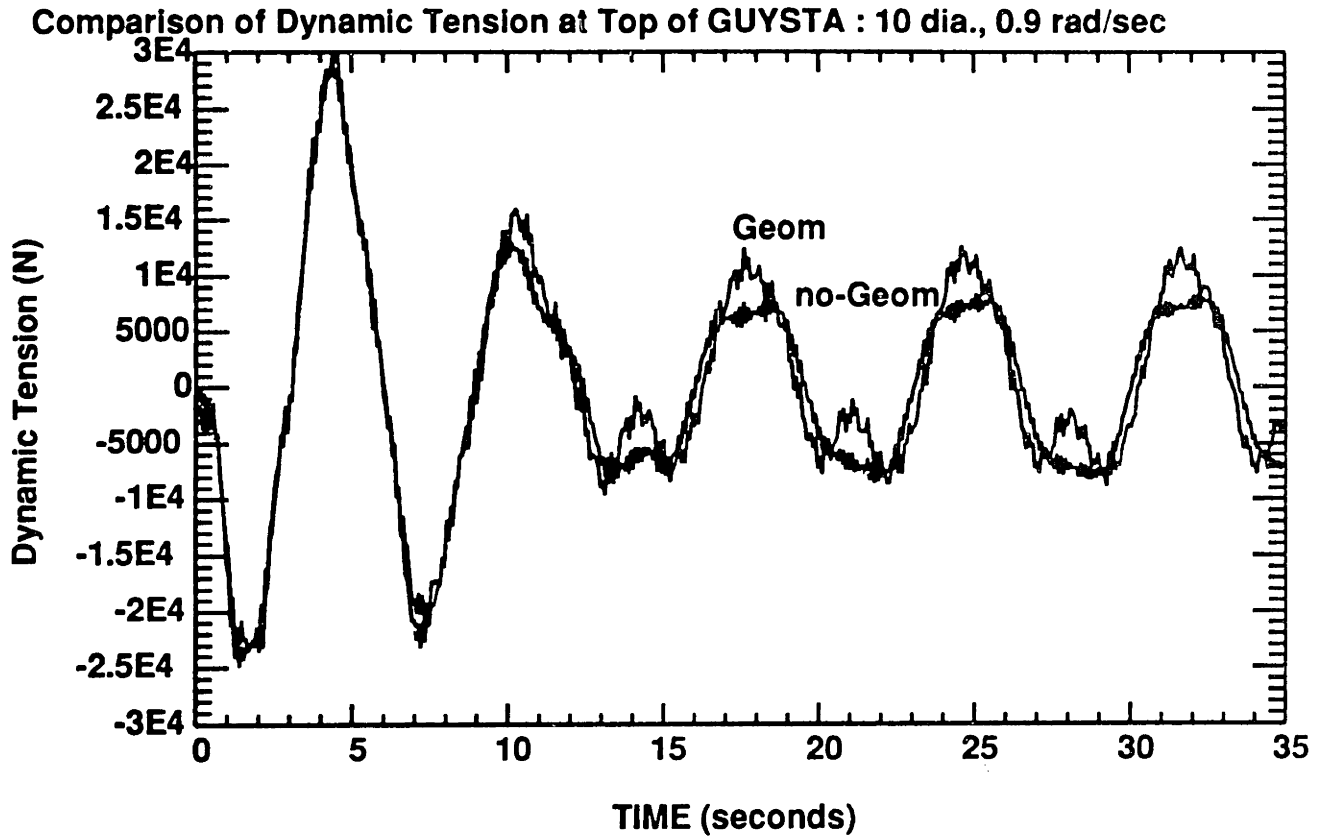


Figure 6-9: Comparison between dynamic tensions at the top of a cable subjected to nonlinear drag forces and a cable subjected to geometric nonlinearity and large tensile forces, as well as nonlinear drag forces [10 diameters, 0.9rad/sec]

Chapter 7

Extreme Tensions in a Snapping Cable

7.1 Introduction

Two offshore applications, deeper water moorings and open sea towing, share a common problem, that of large cable dynamic tension amplification in rough seas. The problem is particularly severe for snapping cables, thus necessitating a detailed analysis. [25], [5] and [11].

Negative overall tensions, caused by large dynamic tension build-up, force the cable to go completely slack. Immediately after the cable goes slack, it is forced to go taut in a rapid motion (snapping of cable). Until now, few papers on extreme tensions of a cable have been presented because of the numerical difficulties involved [11] [17] and [18].

In this chapter we develop a model for a slack-and-snapping cable, which clips off large negative dynamic tensions. The theoretical predictions are then compared with experimental results [11] and [10].

7.2 Behaviour of a Cable subject to Negative Tension

Large dynamic tension build-up in rough seas may cause the total tension to become negative in certain parts of the mooring line. This cannot be sustained by a cable or chain, due to their low bending stiffness, so it is worth exploring what actually happens in a cable under such circumstances.

We start by considering a string (i.e. a cable with zero curvature). The appearance of even a small negative overall tension sets in action a buckling mechanism very quickly, causing the cable to deform in a buckling mode of growing amplitude. This continues until

the increased length causes a positive total tension, when the cable reverts to its normal dynamic behaviour. As a result of this rapid buckling, no large negative tensions can be achieved.

In a cable with finite curvature, on top of the formation of a buckling mode, a different mechanism is set in action : the free-falling of the cable opposed only by the action of the drag force. Since the transition to negative tension is gradual, the cable, under the influence of its own weight, has acquired a certain falling velocity (as the drag force would allow) by the time the cable goes slack. It is reasonable to assume that, for moderately large frequencies, the effect of buckling is restricted to preventing the tension from becoming negative, while kinematically (i.e. in forming the growing buckling mode) and dynamically contributes very little.

In order to get a model of such a slack and then snapping cable, we reformulate the governing equations as follows. As soon as the total tension in an element of the cable reaches a negative value, it is assumed that the buckling mechanism keeps the tension at near zero levels until a positive value is regained, while its dynamic behaviour is governed by the balance of inertia and drag forces.

The following illustrations (Figure 7-1) outline the model used to establish that the tension in the cable remains nonnegative. These illustrations show consecutive total tensions during a short time interval at a certain position s_p .

We can obtain the following relations (7.1), when the sum of the static and dynamic tension is negative :

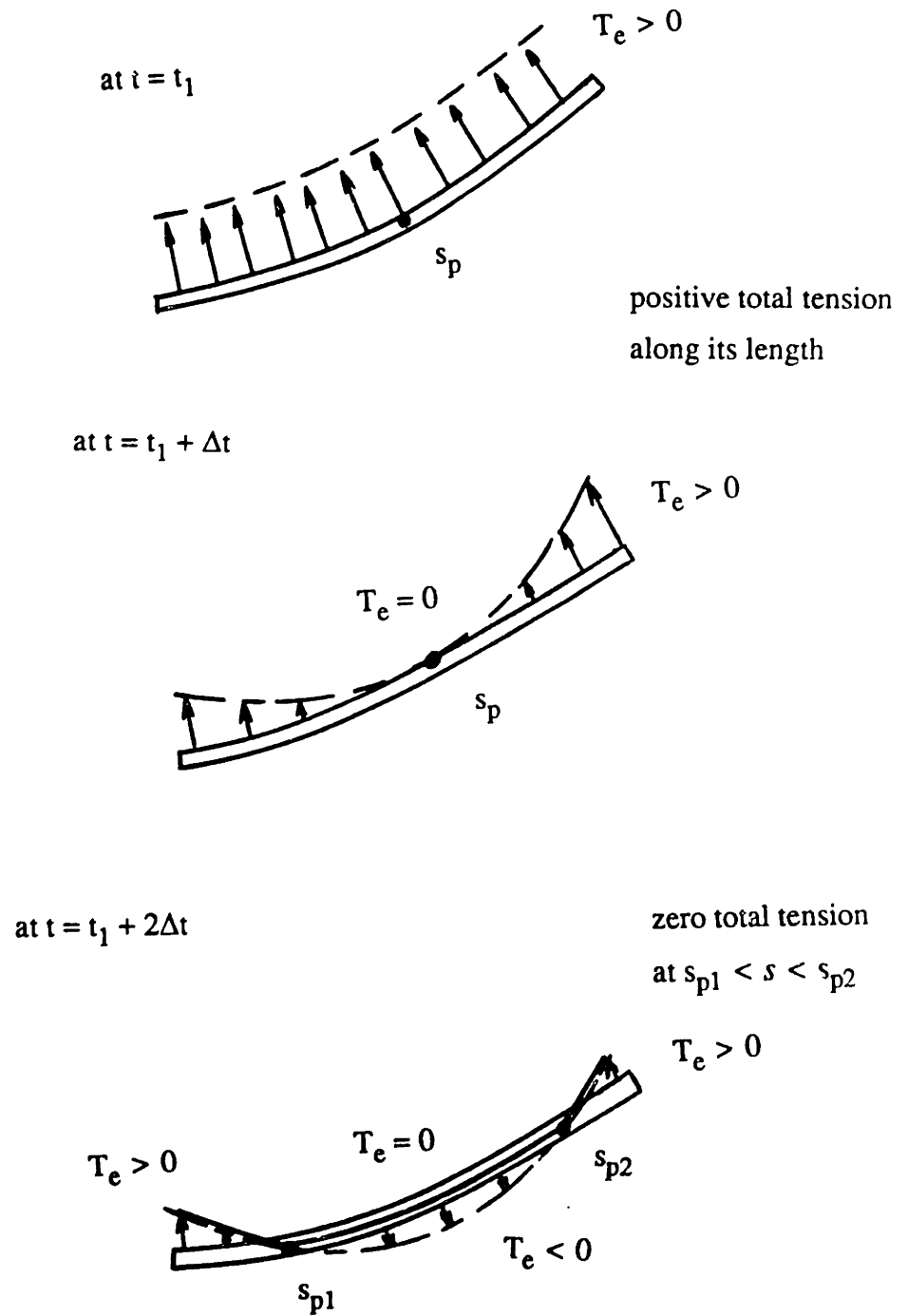


Figure 7-1: Variation of Total Tension during Consecutive Time Steps

$$\frac{\partial T_e}{\partial s} = 0 \quad (\text{or} \quad \frac{dT_0}{ds} = -\frac{\partial T_1}{\partial s})$$

$$e = 0 \quad (\text{or} \quad e_0 = -e_1) \quad (7.1)$$

$$T_e = 0 \quad (\text{or} \quad T_0 = -T_1)$$

where

T_e : total tension ($T_e = T_0 + T_1$)

T_0 : static tension

T_1 : dynamic tension

e : total strain ($e = e_0 + e_1$)

e_0 : static strain

e_1 : dynamic strain

s : Lagrangian coordinate of cable

Here we should make the following distinction : The dynamic tension is related to the dynamic strain, and hence to the cable displacements, provided the total tension is positive. In the absence of bending stiffness, no negative tension can be sustained. Hence, when we calculate a negative dynamic tension that causes the total tension to become negative, it is not a *real* tension, but a mathematical artifact, that helps us decide whether to use the conventional cable equations, or equations (7.1). In the case of equations (7.1) it is clear that the real dynamic tension is simply equal to $-T_0$, and under no circumstances it will become any smaller.

We expect that these equations, which force the clipping-off of the negative dynamic tension, produce spatial discontinuities and, as a result, introduce artificially high frequency excitation, causing numerical convergence problems. In a horizontal cable with small sag, however, as in the case of a towing system, we find out that the dynamic tension is almost uniformly distributed along the cable for frequencies which are not high enough to cause elastic waves [5].

This allows us to simplify the formulation and construct a relatively simple model for a horizontal cable, by assuming that the dynamic tension varies only in time and not along the cable length.

7.3 Clipping-Off Model

By introducing the quasi-static strain assumption, we obtain the following governing equations, which also include a clipping-off model.

Governing Equations :

$$(m+a) \frac{\partial^2 q}{\partial t^2} = (T_0 + T_1) \left(\frac{\partial^2 q}{\partial s^2} + \frac{d\phi_0}{ds} \right) - \frac{1}{2} \rho_w C_{dn} D \frac{\partial q}{\partial t} \left| \frac{\partial q}{\partial t} \right| - T_0 \frac{d\phi_0}{ds}$$

with

(7.2)

$$T_1(t) = \frac{EA}{L} \left[p(L) - \int_0^L q \frac{d\phi_0}{ds} ds + \frac{1}{2} \int_0^L \left(\frac{\partial q}{\partial s} \right)^2 ds \right] \quad \text{if } T_0 + T_1 \geq 0$$

Clipping - Off (if $T_0 + T_1 < 0$, where $T_1(t)$ calculated as in equation (7.2) above) :

$$(m+a) \frac{\partial^2 q}{\partial t^2} = -\frac{1}{2} \rho_w C_{dn} D \frac{\partial q}{\partial t} \left| \frac{\partial q}{\partial t} \right| - T_0 \frac{d\phi_0}{ds} \quad (7.3)$$

and set : $T_1 = -T_0$

where

E : Young's modulus

m : mass per unit length of cable

a : added mass per unit length of cable

D : diameter of cable

A : cross-sectional area of cable

L : unstretched length of cable

s : Lagrangian coordinate of cable

q : displacement of cable in the normal direction

p(L) : tangential component of the excitation amplitude

C_{dn} : tangential drag coefficient

ρ_w : water density

7.4 Effects of Small Cable Bending Stiffness on its Dynamic Behaviour

If the dynamic tension becomes negative and of amplitude equal to, or larger than the value of the static tension, forcing the total tension to become nonpositive, the small bending stiffness of the cable, which can be neglected under less extreme conditions, may become important due to the lack of any other restoring mechanisms. For short span cables, the bending stiffness may cause differences between experimental data and our numerical results. This is due to the delayed onset of zero tension (since the bending stiffness is capable of supporting small negative tensions), relative to our numerical model predictions (Fig. 7-10). In fact, under conditions described in the sequel, a clipped-off total tension at a certain time interval, implies large tension amplification at subsequent times. Our model, therefore, predicts such tension amplification earlier than experimental results from short span cables indicate. Fig. (7-10) shows such a deviation between our results and experimental data from a short cable, 10 m in length.

7.5 Qualitative Analysis of Extreme Tensions in a Snapping Cable

The following figure (7-2) serves to demonstrate the difference between the time history of the normal velocity at a certain point of the cable as predicted by our clipping-off model, relative to the normal velocity without clipping-off. We denote by u_c the former (clipping), and by u_{nc} the latter (non-clipping). We use, for demonstration purposes, the mid-length point of the cable.

As the total tension becomes zero, the major part of the cable span falls under the influence of its own weight, opposed only by drag. Eventually, it acquires a steady velocity u_c^* , which we will call the free-falling velocity. In fact the transition to zero total tension is smooth, so the cable has acquired a steady velocity almost by the time the cable has slack. We distinguish two separate cases, one when $|u_c^*|$ is larger than $|(u_{nc})_{min}|$, and one when

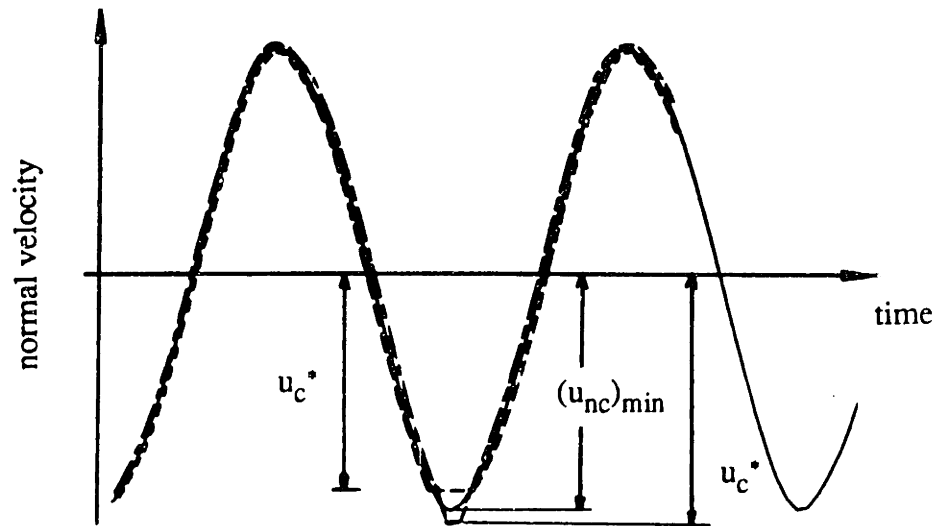


Figure 7-2: Normal velocity at the middle of the cable in the clipping-off region

- the cable with the clip-off model ; $|u_c^*| < |(u_{nc})_{min}|$
- the cable with the clip-off model ; $|u_c^*| > |(u_{nc})_{min}|$
- the cable without the clip-off model

$|u_c^*|$ is smaller than $|(u_{nc})_{min}|$, because they have distinctly different effect on the dynamic tension.

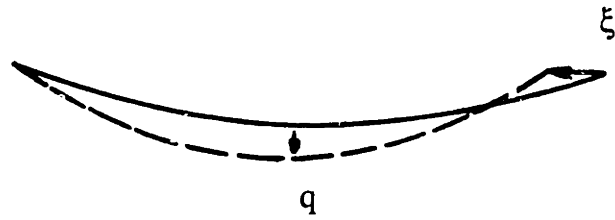


Figure 7-3: Dynamic configuration in slack condition

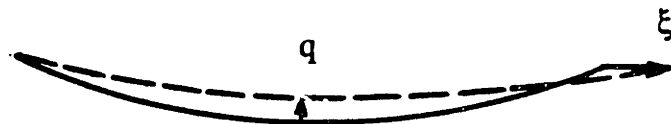


Figure 7-4: Dynamic configuration in snap condition

1. $|(u_{nc})_{\min}| > |u_c^*|$

- If we consider the cable to be in slack condition (Fig. 7-3), $\xi(t)$ is negative and the normal displacement is negative along most of the cable length. In the following relation, therefore,

$$T_1 = \frac{EA}{L} \left[\xi - \int_0^L q \frac{d\phi_0}{ds} ds \right] \quad (7.4)$$

the first term is negative and the second (if we account for the minus sign) positive. Since $|u_{nc}| > |u_c|$ and hence $|q_{nc}| > |q_c|$ (Fig. 7-6), we derive the following inequality (for negative q_{nc}, q_c).

$$-\int_0^L q_{nc} \frac{d\phi_0}{ds} ds > -\int_0^L q_c \frac{d\phi_0}{ds} ds$$

As a result, the dynamic tension is (see Fig. 7-5),

$$|T_{1,nc}| < |T_{1,c}| \quad (7.5)$$

Since the restoring force $T_0 + T_{1,c}$ is smaller than $T_0 + T_{1,nc}$, the rebound of the normal displacement q_c from the minimum happens later, so $q_{nc} > q_c$ at the rebound of the normal displacement q_c (see Fig. 7-6).

- Subsequently, the cable will be taut again (Fig. 7-4). Because the clipping cable remains longer in slack condition, as relation (7.5) indicates, the restoring force remains smaller, and hence the rebound in q_c is slower. This, however, causes a rapid built-up in dynamic tension, once $\xi(t)$ becomes positive as equation (7.4) indicates : for positive $\xi(t)$ and $q(s,t)$, smaller q imply a larger tension T_1 . This triggers an eventual increase in q (Fig. 7-8), which limits finally T_1 . The tension, however, in the clipping case will overshoot above the non-clipping tension (Fig. 7-7).

The large value in the peak of the dynamic tension, relative to the non-

clipping case, and the clipping off in the velocity (due to the free falling velocity) are the causes for the asymmetric form of the time history of the normal displacement at the middle of the cable (Figures 7-18 and 7-21).

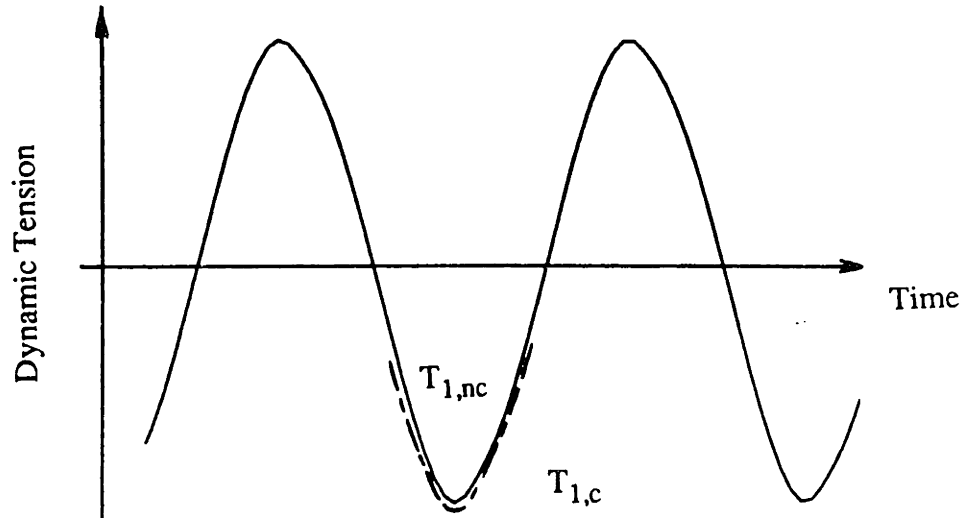


Figure 7-5: Dynamic Tension in the clipping-off area

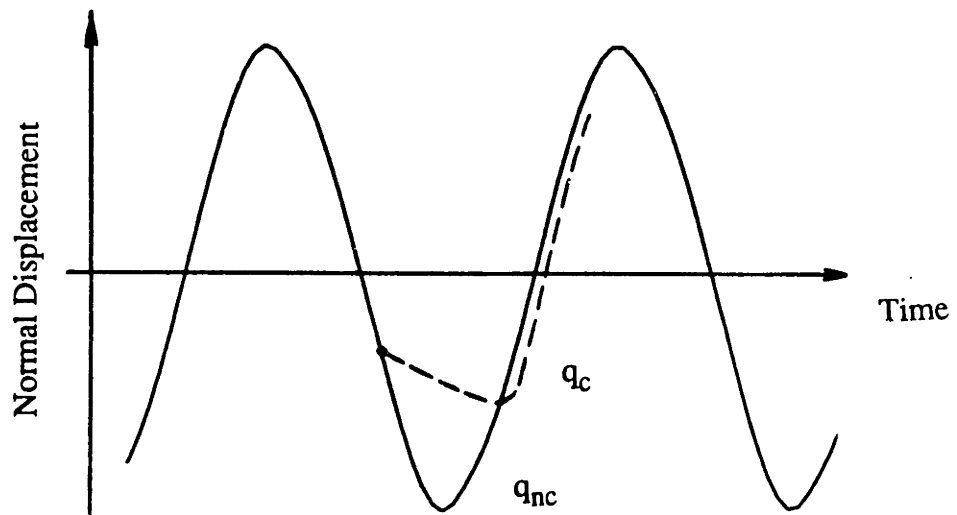


Figure 7-6: Normal displacement in the clipping-off area

• In summary, we point out the following results from having $|(u_{nc})_{\min}| > |u_c^*|$

a. $(T_{1,c})_{\max} > (T_{1,nc})_{\max}$

b. Asymmetry of normal displacement in the time history

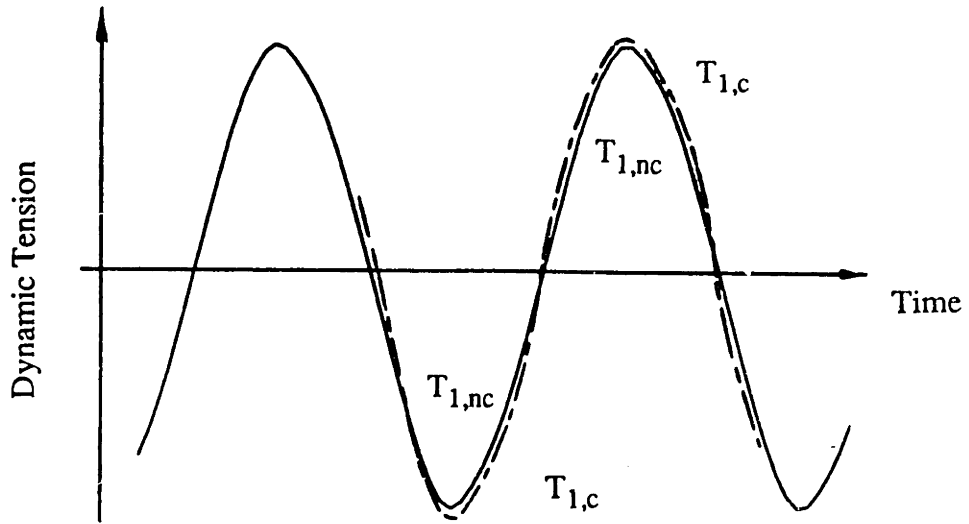


Figure 7-7: Dynamic Tension when $|(u_{nc})_{\min}| > |u_c^*|$

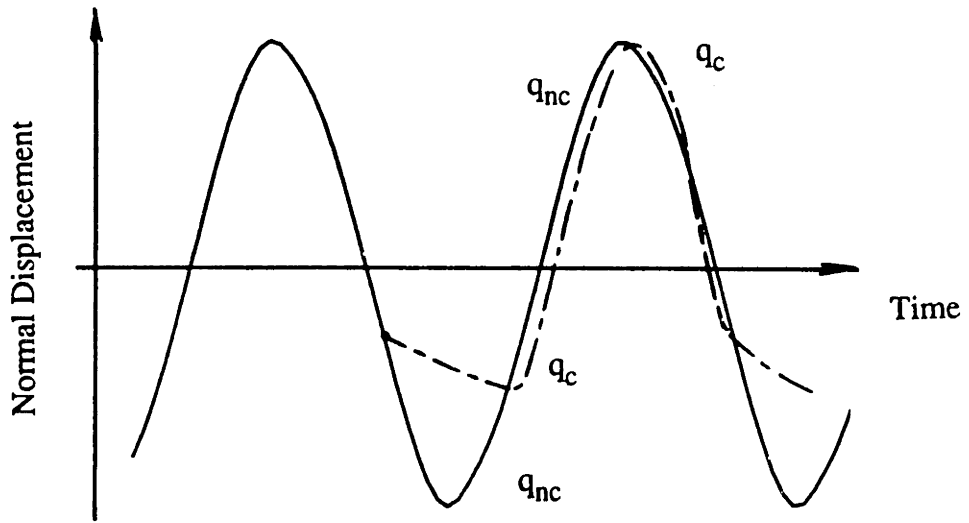


Figure 7-8: Normal displacement when $|(u_{nc})_{\min}| > |u_c^*|$

2. $|(u_{nc})_{\min}| < |u_c^*|$

- All the phenomena described above are reversed and, similarly, the conclusions are reversed.

In summary (Fig. 7-9) :

- $(T_{1,c})_{\max} < (T_{1,nc})_{\max}$
- The normal displacement retains its symmetric time history form

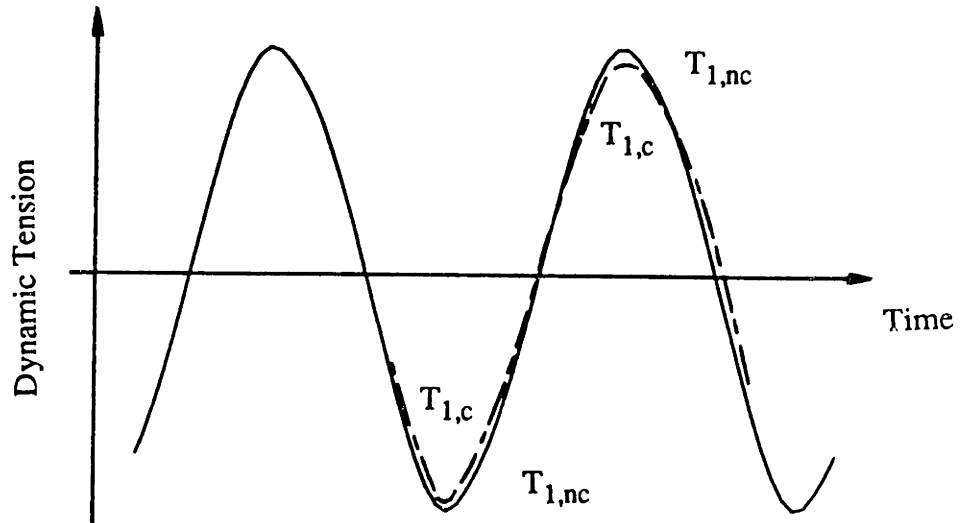


Figure 7-9: Dynamic Tension when $|(u_{nc})_{\min}| < |u_c^*|$

From the considerations above, we can deduce the following rule :

By increasing the free-fall velocity of the cable, we can reduce the peak dynamic tension during snapping. This increase in $|u_c^*|$ can be obtained in several ways, as explained in the sequel.

7.5.1 Principal Parameters to Increase the Free-Falling Velocity $|u_c^*|$

The balance of weight and drag forces during free-falling provides for wires :

$$\frac{1}{2} \rho_w C_d d u^2 = \frac{\pi}{4} d^2 (\rho_c - \rho_w) g$$

From the above balance, we obtain the formula of the free-falling velocity u_c^*

$$u_c^* = \sqrt{\frac{\pi}{2} \left(\frac{\rho_c}{\rho_w} - 1 \right) \frac{d g}{C_d}} \quad (7.6)$$

From this expression, we conclude that in order to increase the free-falling velocity u_c^* we should increase the diameter of the cable d , increase ρ_c , or decrease the drag coefficient C_d .

7.5.2 Other Ways to Reduce the Peak Tension in a Snapping Hawser

It is suggested that inserting a certain length of chain near the middle of a snapping hawser is beneficial for reducing maximum dynamic tensions, because the chain has, as a rule, larger density than commonly used wire, and its ratio of volume to projected area is better than in a cable. Hence, use of chain shots not only deepens the catenary, but alters the free-falling velocity of the line as well, and hence reduces tensions as indicated above.

The suggestion for placing the chain near the middle is based on kinematic considerations, since this is the region which has the maximum kinematic freedom.

Important Parameters for Tension Amplification : MST and TRI

We identify two parameters which cause tension amplification, based on our analysis above :

1. The ratio of the cable free-falling velocity u_c^* to the predicted minimum velocity in a non-clipping condition, $(u_{nc})_{min}$

$$MST = \frac{(u_{nc})_{min}}{u_c^*} \quad (7.7)$$

- If $MST > 1$, the tension will be amplified during cable snapping, so measures to increase the free-falling velocity should be taken.
- If $MST < 1$, we can expect that the tension during snapping will be not be amplified, and in fact it may be smaller than in a non-snapping cable.

2. The ratio of the predicted dynamic tension to the static tension T_0 . As a measure of this ratio we can use the quantity :

$$TRI = \frac{EA}{L} \xi_0 \sqrt{T_0} \quad (7.8)$$

Where ξ_0 = amplitude of imposed end motion.

This ratio represents exactly the ratio of dynamic to static tension for high frequencies, when the response is predominantly elastic.

- If $TRI > 1$, a snap is expected and depending on the value of the first parameter, defined above, large dynamic tensions may occur.

In order to reduce EA/L , we recommend inserting a synthetic line, which has a lower value of Young's modulus E . Or, alternatively, we recommend inserting a piece of chain, whose weight can increase the static tension. Similar results can be achieved by using a weight in the middle (sinker), whose properties, however, (mass, free-falling velocity) may alter the dynamics substantially, so a separate analysis is needed.

7.6 Applications and Comparisons with Experimental Data

7.6.1 NSFI Experiment

The principal parameters of the horizontal cable used in the experiment of the Ship Research Institute of Norway are found in Table (7-IV). The comparisons between experimental data and numerical predictions of the cable show good agreement at lower frequencies, while the effect of the bending stiffness is apparent at higher frequencies, causing the theoretical dynamic tensions to be higher than the experimentally measured tensions.

For higher frequencies, and after clipping-off sets in, numerical difficulties arise in the form of high frequency oscillations, that eventually lead to divergence (Fig. 7-13). Also, smaller time steps must be used to ensure numerical accuracy. Let us consider the particular case of excitation at a frequency of 1.5hz and with an amplitude equal to 5 cable diameters. The sensitivity of the magnitude of the total tension to the number of time steps per period is shown in (Table 7-I). Convergence has been achieved after using 200 steps or more.

Table 7-I : Sensitivity of the maximum total tension to the number of time steps per period [Chebyshev terms=11, Cd=1.5]			
Item	steps=100	steps=200	steps=300
maximum total tension	287.793 N	242.261 N	242.828 N

Table 7-I: Sensitivity of the maximum total tension
to the number of time steps per period [$C_d=1.5$, Chebyshev terms=11]

Next, we checked the sensitivity of the total tension on the number of Chebyshev polynomials, using 200 time steps per period (Table 7-II). The difference between using 7 Chebyshev polynomials, and using 11 Chebyshev polynomials (which is the standard for our calculations) was 3.5%. This means we can safely reduce somewhat the number of polynomials without significant effect on the accuracy.

Table 7-II : Sensitivity of the maximum total tension to the number of Chebyshev polynomials [time steps=200, Cd=1.5]		
Item	terms=7	terms=11
maximum total tension	250.923 N	242.261 N

Table 7-II: Sensitivity of the maximum total tension to the number of Chebyshev polynomials [$C_d=1.5$, time steps per period=200]

Finally we checked the effect of the drag coefficient C_d (Table 7-III). It is found that no tension clipping occurs for $C_d=1.0$, while clipping is found for $C_d=1.5$.

This sensitivity investigation was repeated for an excitation at 1.8hz and with amplitude of 5 diameters : 500 time steps per period were required for sufficient accuracy. For higher frequencies even smaller steps were required, while eventually instability set in, establishing a limitation for the applicability of the present numerical code.

Table 7-III : Effect of the drag coefficient on the extreme total tension [time steps=200, Chebyshev terms=11]		
Item	$C_d=1.0$	$C_d=1.5$
maximum total tension	220.354 N	242.261 N
minimum total tension	1.854 N	0 N

Table 7-III: Effect of the drag coefficient on the maximum total tension
[time steps per period=200, Chebyshev terms=11]

$$T_0 = 88 \text{ N}$$

$$M = 0.666 \text{ kg/m}$$

$$w = 5.05 \text{ N/m}$$

$$EA = 7,854,000 \text{ N}$$

$$L = 10.9774 \text{ m}$$

$$D = 0.01 \text{ m}$$

$$C_{Dn} = 1.5$$

Table 7-IV: Cable used in the experiment of the Ship Research Institute of Norway [11].

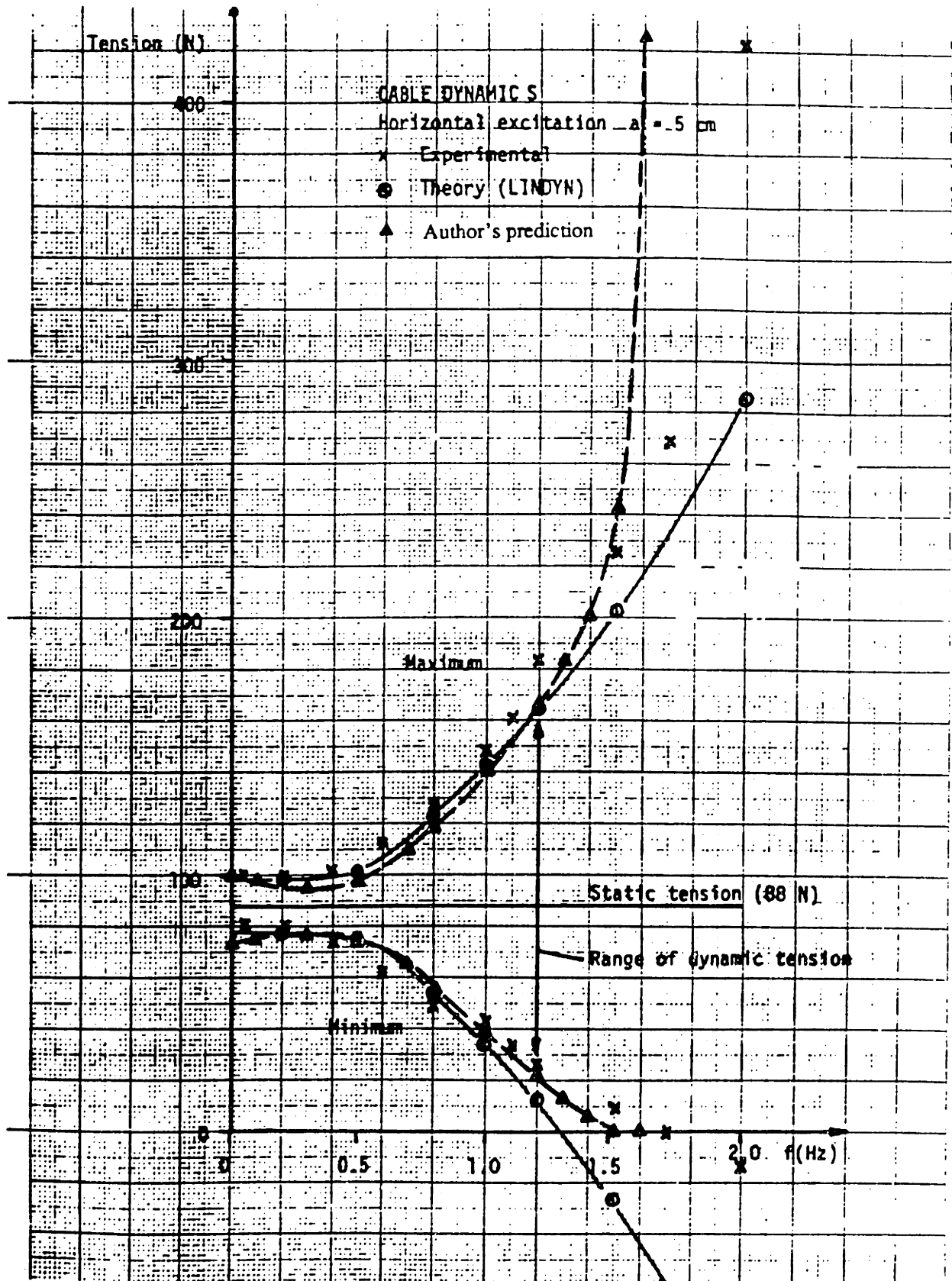


Figure 7-10: Comparison of extreme tensions : NSFI-5d

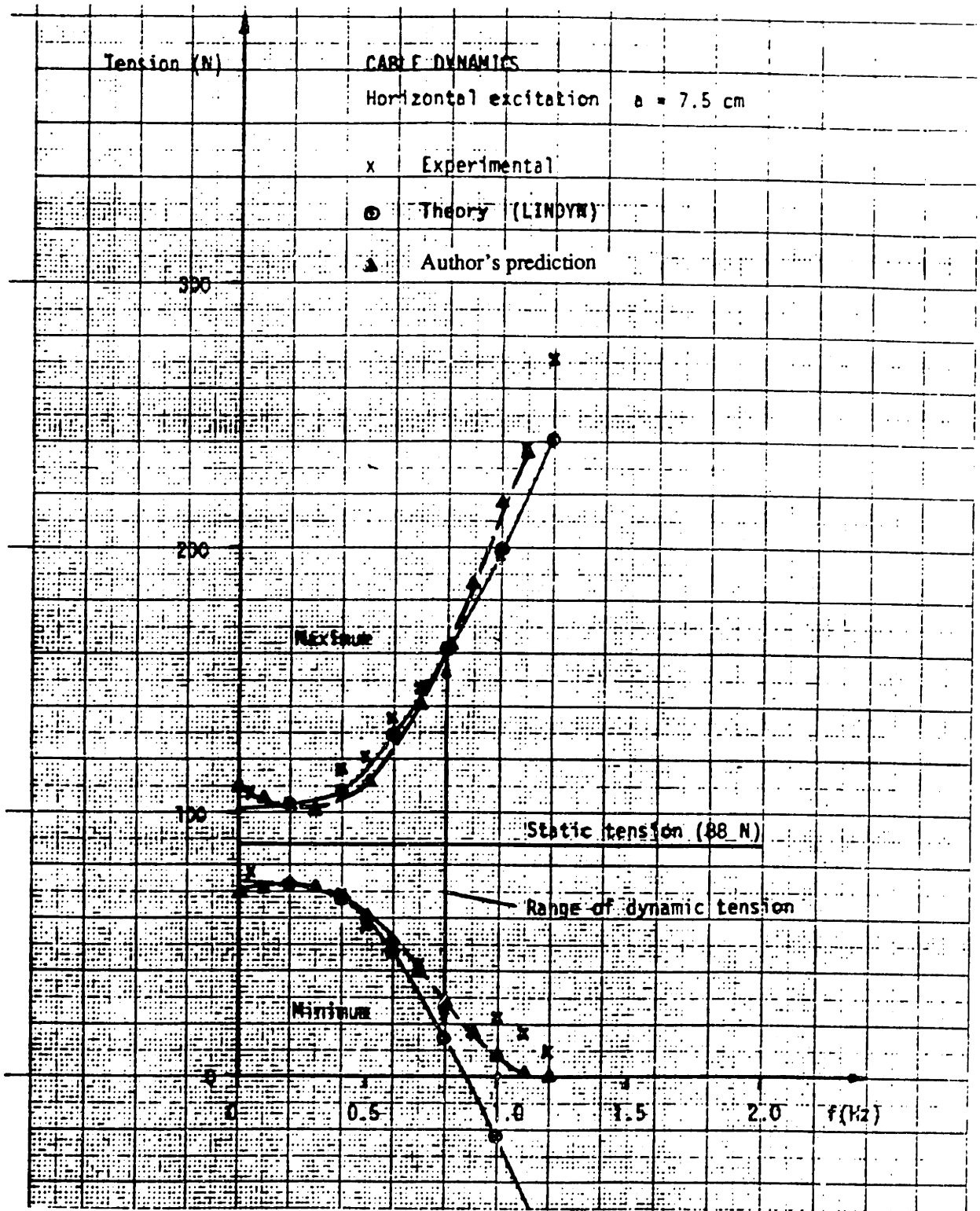


Figure 7-11: Comparison of extreme tensions : NSFI-7.5d

CABLE DYNAMIC S

Horizontal excitation $a = 10$ cm

x Experimental

○ Theory (LINDYN)

▲ Author's prediction

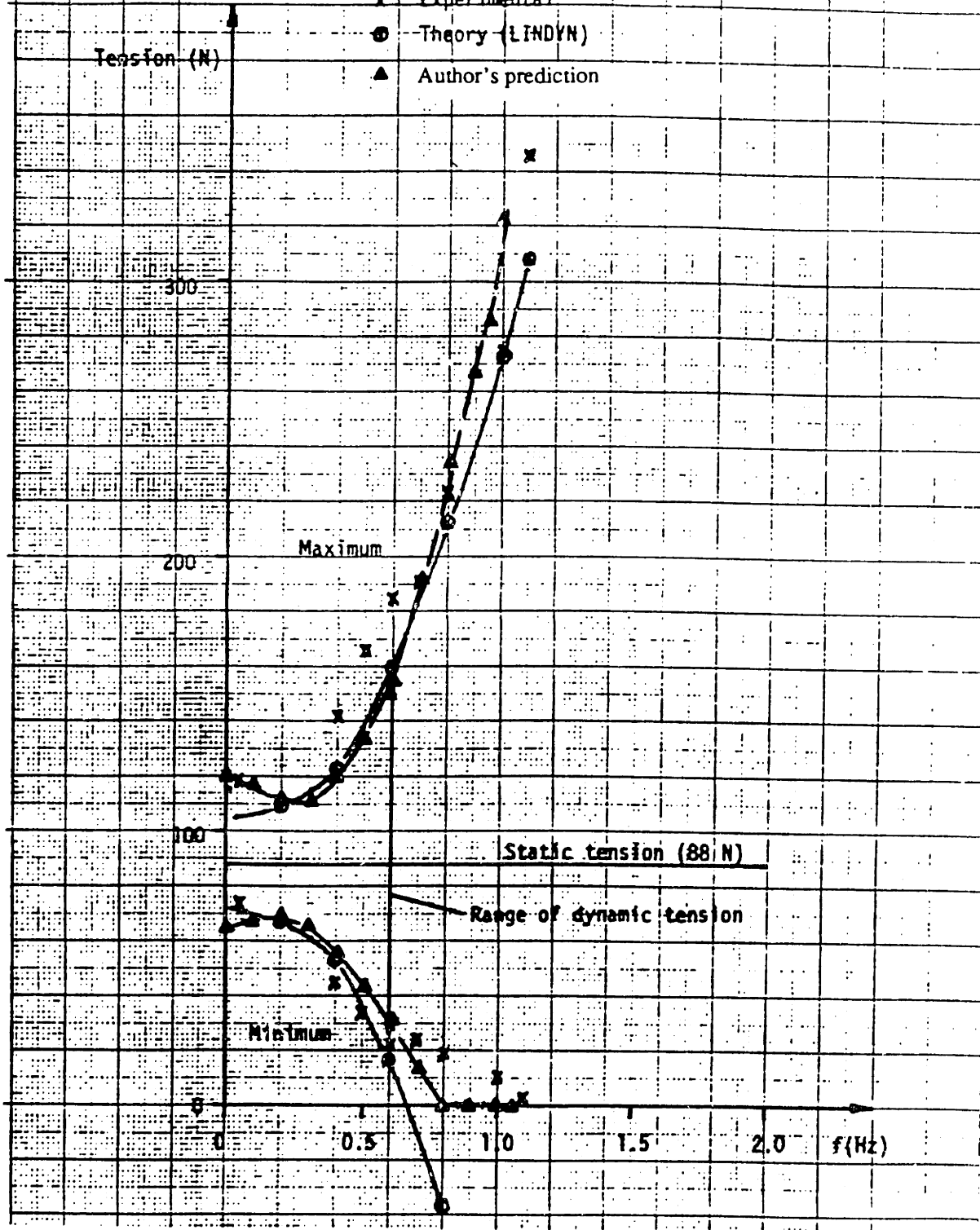


Figure 7-12: Comparison of extreme tensions : NSFI-10d

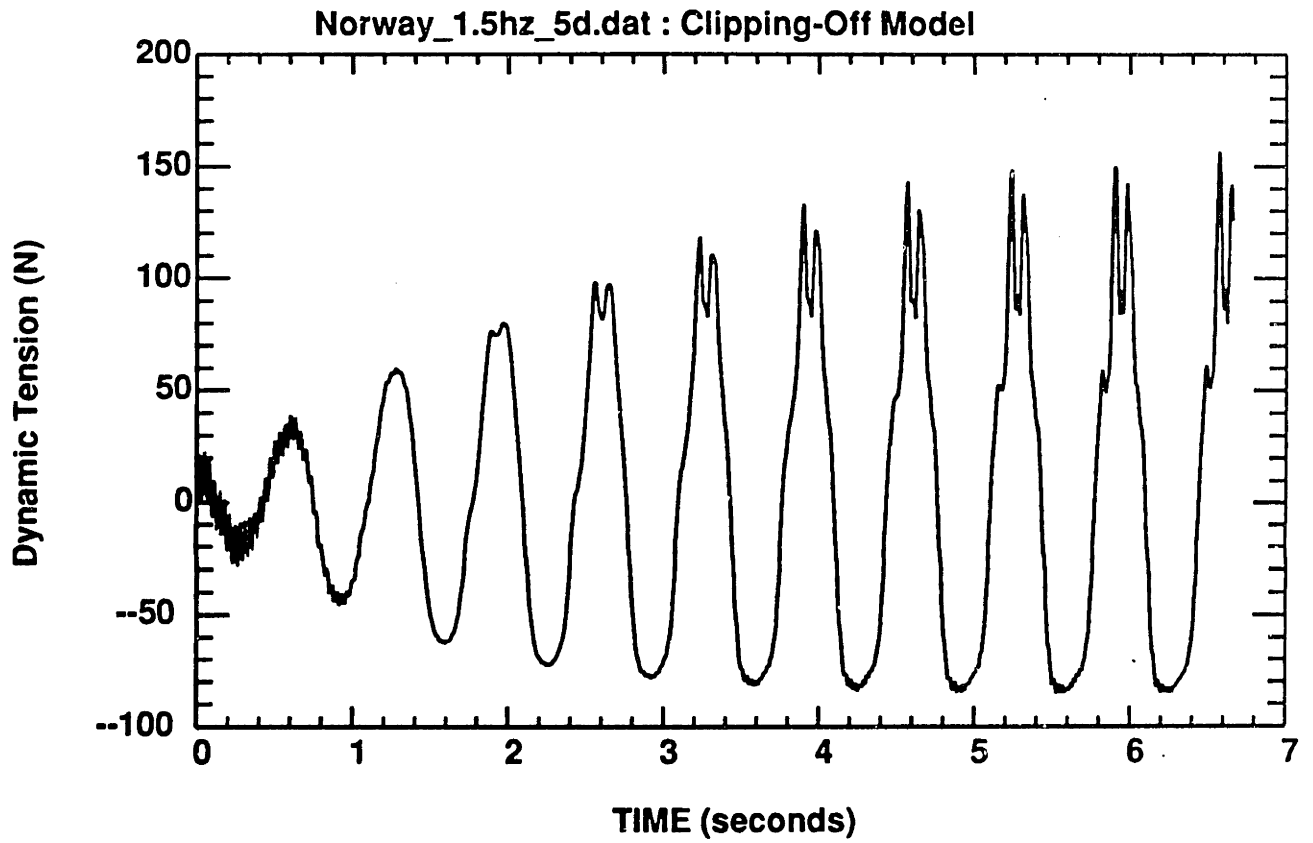


Figure 7-13: Time history of predicted dynamic tension ; 1.5hz_5d_1.0Cd

7.6.2 MIT Experiment

The principal parameters of the cable used in the MIT experiment are found in Table (7-XII).

Cable with a Spring Attached at one End

A spring was connected to one end of the cable to reduce significantly the effective value of EA. Mounting the spring in the model scales accurately the elastic stiffness of the cable relative to the full scale mooring line. The equivalent EA for the combined system of the cable and the spring is calculated using the following formula [24].

$$\frac{1}{(EA)_{eq}} = \frac{1}{kL} + \frac{1}{EA} \quad (7.9)$$

where : EA = 3423688 N

k = 8240 N/m

L = 67.67 m from Table (7-XII)

(EA)_{eq} = 479468 N

Tables (7-V) and (7-VI) provide a comparison between our predictions and experimental results. The difference between our numeric results and the experimental data was 11.8%, on the average, for a low frequency excitation at 0.1hz and for a high frequency excitation at 1hz.

The time history of the dynamic tension of the combined cable-spring system is shown in Figures (7-14) and (7-16). Also Figure (7-17) shows the asymmetry of the normal displacemnt due to the clipping-off model.

Table 7-V : Comparison of the Dynamic Tension of the cable with a spring [0.1hz, 25d]			
Item	experiment	numeric	difference(%)
maximum dynamic tension	210 N	184 N	12.4 %

Table 7-V: Comparison of the dynamic tension of the cable with a spring [0.1hz, 25d]

Table 7-VI : Comparison of the Dynamic Tension of the cable with a spring [1hz, 25d]			
Item	experiment	numeric	difference(%)
maximum dynamic tension	1356 N	1510 N	11.3 %

Table 7-VI: Comparison of the dynamic tension of the cable with a spring [1hz, 25d]

Cable without a Spring

Several comparisons were also made at low and high frequencies for the cable without the spring. Differences were found between numerical predictions and the experimental data as follows (Table 7-VII).

Table 7-VII : Comparison of Dynamic Tensions in the cable without spring between the predicted results and MIT experimental data		
Item	0.1 hz, 25 d	1 hz, 12.5 d
Experiment	300 N	2000 N
Numeric	204 N	2731 N
difference(%)	32 %	33 %

Table 7-VII: Comparison between numerical results and experimental data for the dynamic tension in the cable without spring

For horizontal excitation at frequency 0.1hz and with amplitude equal to 25 cable diameters, the difference was 32%. To account for this difference we tried to investigate the effect of the principal parameters. We started by varying the drag coefficient C_d (Table 7-VIII).

Table 7-VIII : Effect of the drag coefficient on the dynamic tension and comparison with experimental data			
Item	$C_d = 0.5$	$C_d = 1.0$	$C_d = 1.2$
Experiment	2000 N	2000 N	2000 N
Numeric	2596 N	2731 N	2765 N
difference(%)	29.8 %	36.5 %	38.3 %

Table 7-VIII: Effect of the drag coefficient on the dynamic tension and comparison with experimental data

We found that the cable was not sensitive to the value of C_d (Fig. 7-19). Also we found that the free-falling velocity of the cable was a function of the square root of the C_d in agreement with equation (7.6) for a wire (See Fig. 7-21). Figure (7-20) showed the asymmetry of the normal displacement at the middle due to clipping-off.

Table 7-VIII : Comparison of the Methodologies used in M.S. Triantafyllou's Analysis and in Author's Analysis	
M. T.	Author
clipping	clipping
constant static quantities	variable static quantities
constant dynamic strain	constant dynamic strain
Galerkin' method	collocation method

Table 7-IX: Comparison of the methodologies used in M. S. Triantafyllou's Analysis and in author's Analysis

Here, we compare our predictions with M.S. Triantafyllou's result [26]. Differences between two numerical analyses are found in Table 7-VIII.

The comparison between our predictions, M.S. Triantafyllou's results and experimental data for the particular case derived in Table 7-VII, is shown in Tables 7-IX and 7-X.

From the comparisons above, we conclude that experimental results represent

Table 7-IX : Comparison of Dynamic Tensions of the cable without spring (Static Tension = 577.9 N) between M.S. Triantafyllou's result, author's prediction and MIT experiment data [0.1hz 25d]		
experiment	M. T.	author
300 N	230 N	204 N

Table 7-X: Comparison between M.S. Triantafyllou's result, Author's prediction and experimental data [0.1hz, 25d]

Table 7-X : Comparison of Dynamic Tensions of the cable without spring (Static Tension = 577.9 N) between M.S. Triantafyllou's result, author's prediction and MIT experiment data [1hz 12.5d]		
experiment	M. T.	author
2000 N	2913 N	2731 N

Table 7-XI: Comparison between M.S. Triantafyllou's result, Author's prediction and experimental data [1hz, 12.5d]

adequately the qualitative behaviour of a full scale cable only if they are long enough and of sufficient diameter, so that the dynamic tension is not overly amplified.

$$T_0 = 577.899 \text{ N}$$

$$M = 0.5046 \text{ kg/m}$$

$$w_{\text{water}} = 3.62 \text{ N/m}$$

$$w_{\text{air}} = 4.2294 \text{ N/m}$$

$$EA = 3423688 \text{ N}$$

$$L = 67.6656 \text{ m}$$

$$l_1 = 3.3833 \text{ m}$$

$$l_2 = 63.6057 \text{ m}$$

$$l_3 = 4.0599 \text{ m}$$

$$D = 0.009525 \text{ m}$$

$$C_{Dn} = 1.0$$

Table 7-XII: Cable used in MIT experiment [10].

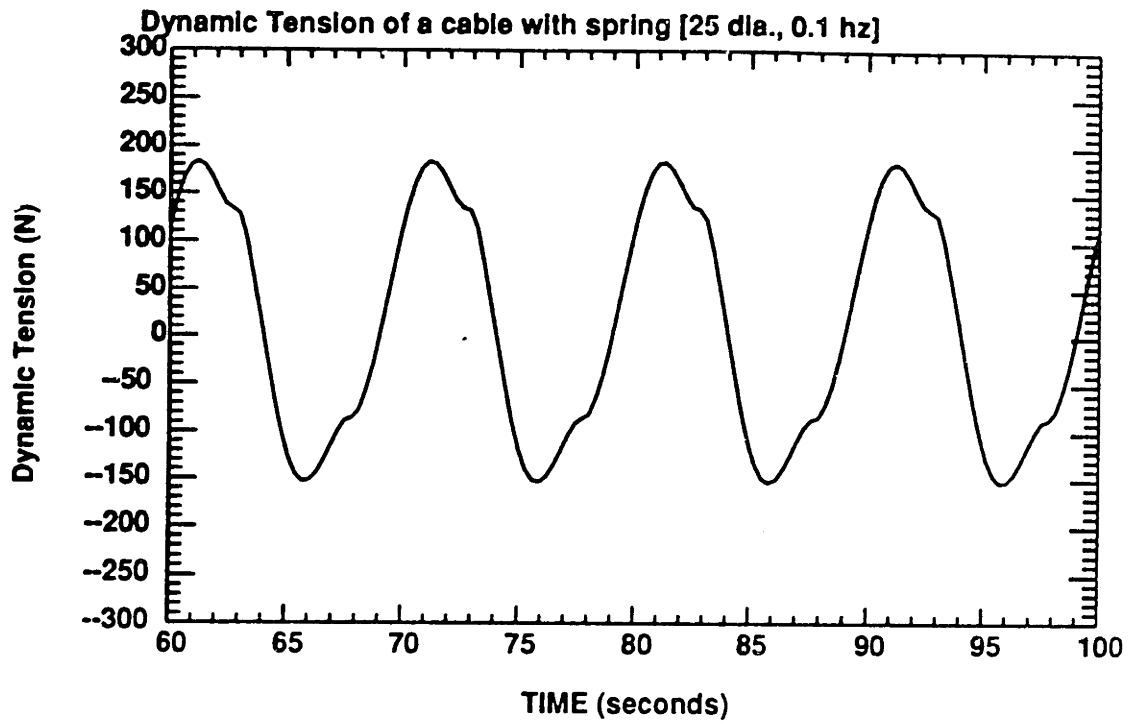


Figure 7-15: Time history of predicted dynamic tension ; cable with spring [0.1hz, 25d]

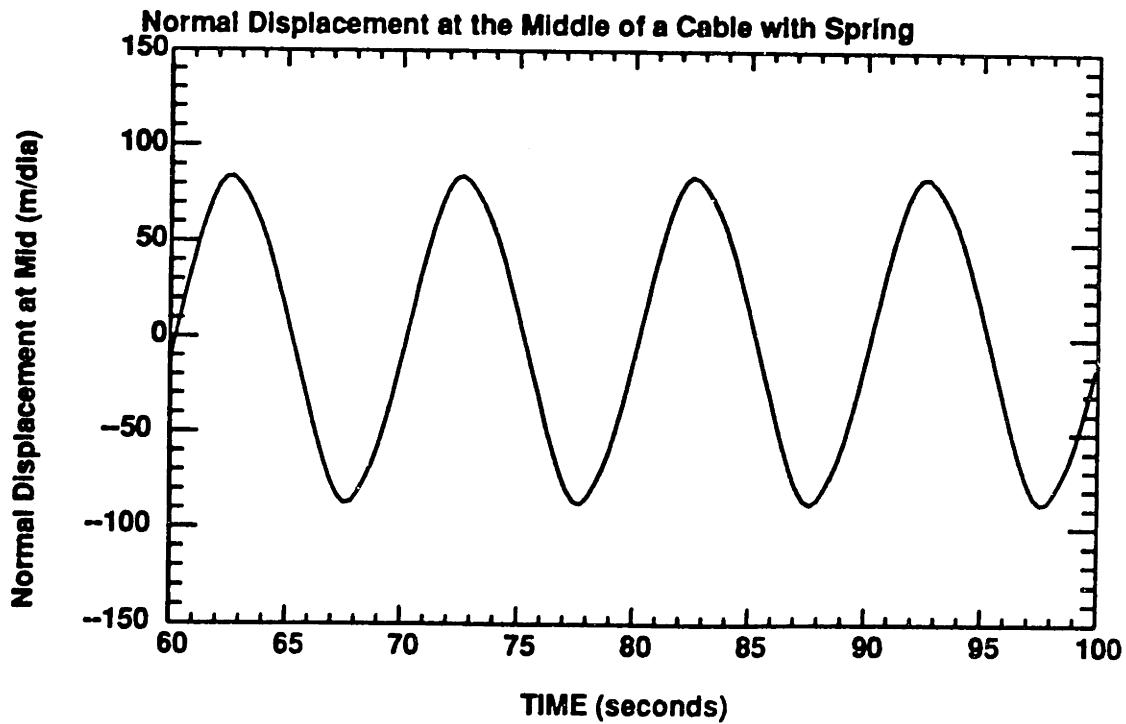


Figure 7-16: Time history of predicted normal displacement at the middle ; cable with spring [0.1hz, 25d]

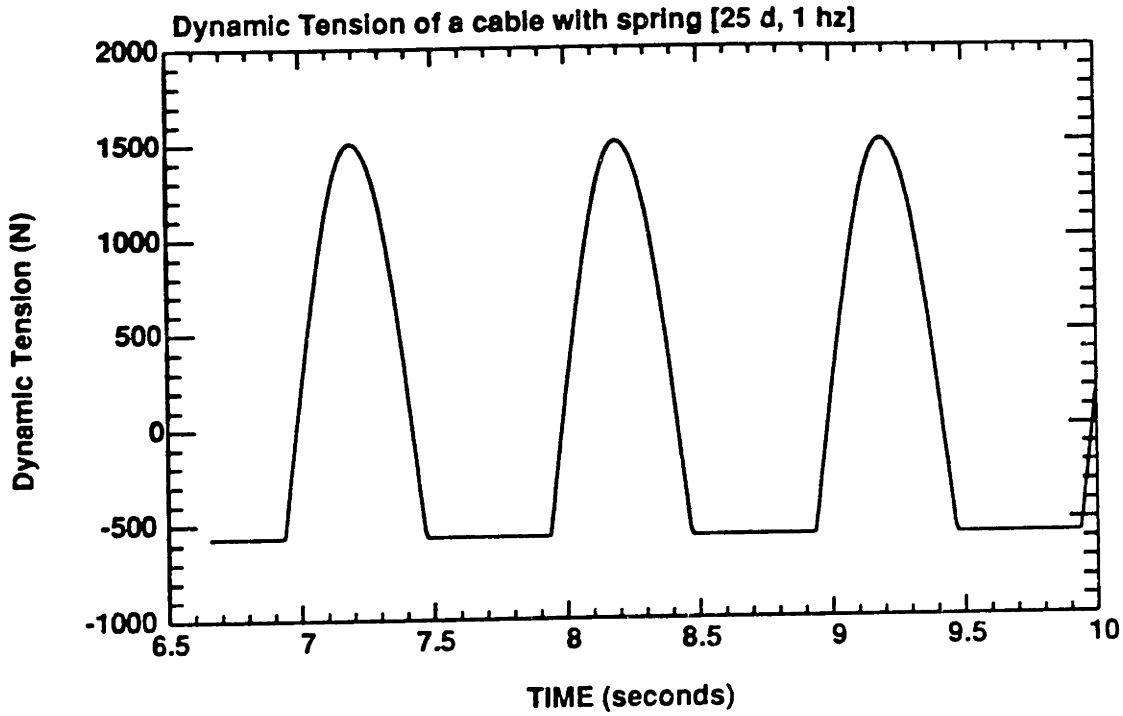


Figure 7-17: Time history of predicted dynamic tension ; cable with spring [1hz, 25d]

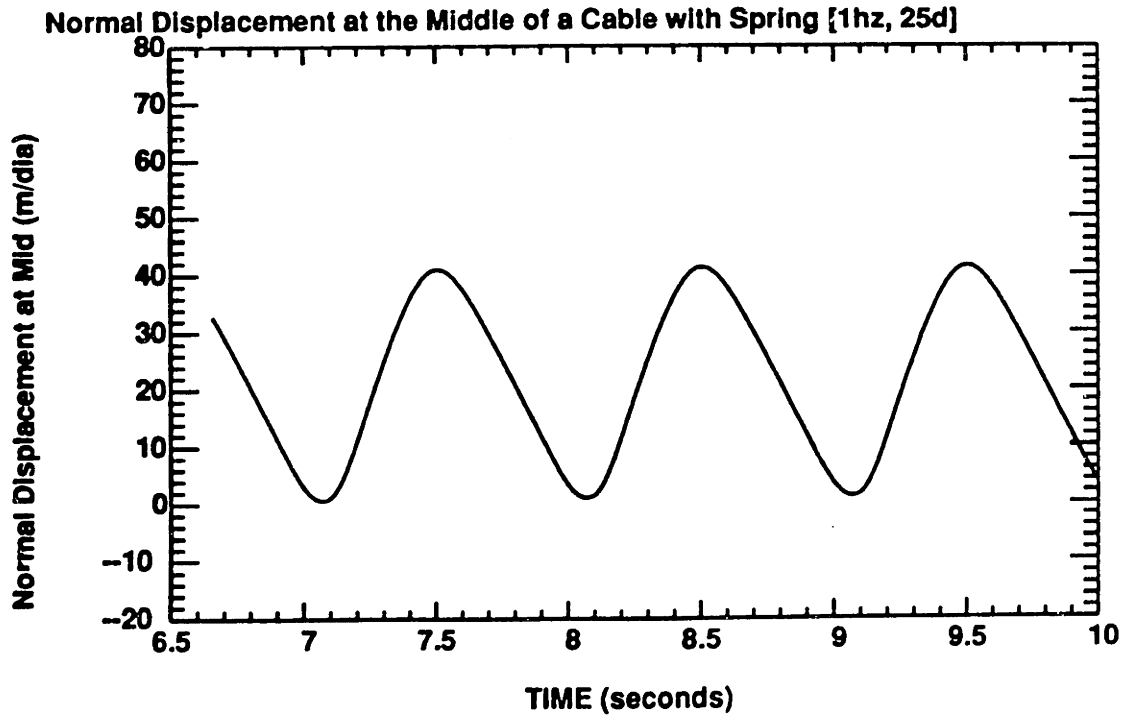


Figure 7-18: Time history of predicted normal displacement at the middle ; cable with spring [1hz, 25d]

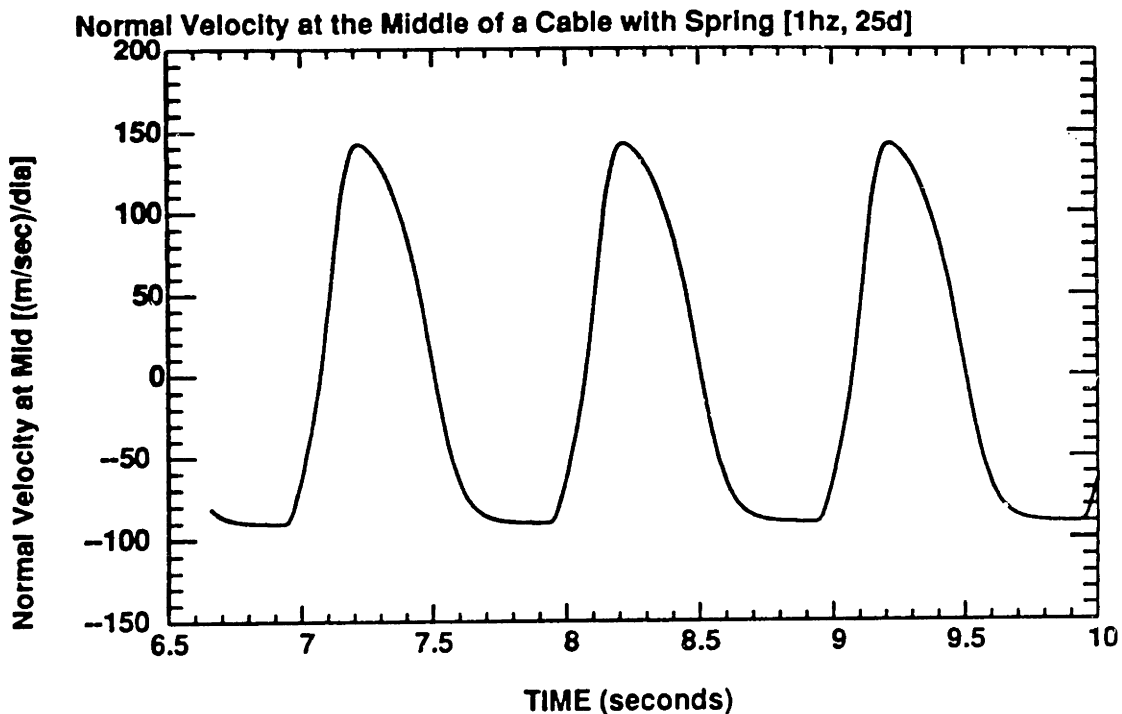


Figure 7-19: Time history of predicted normal velocity at the middle ; cable with spring [1hz, 25d]

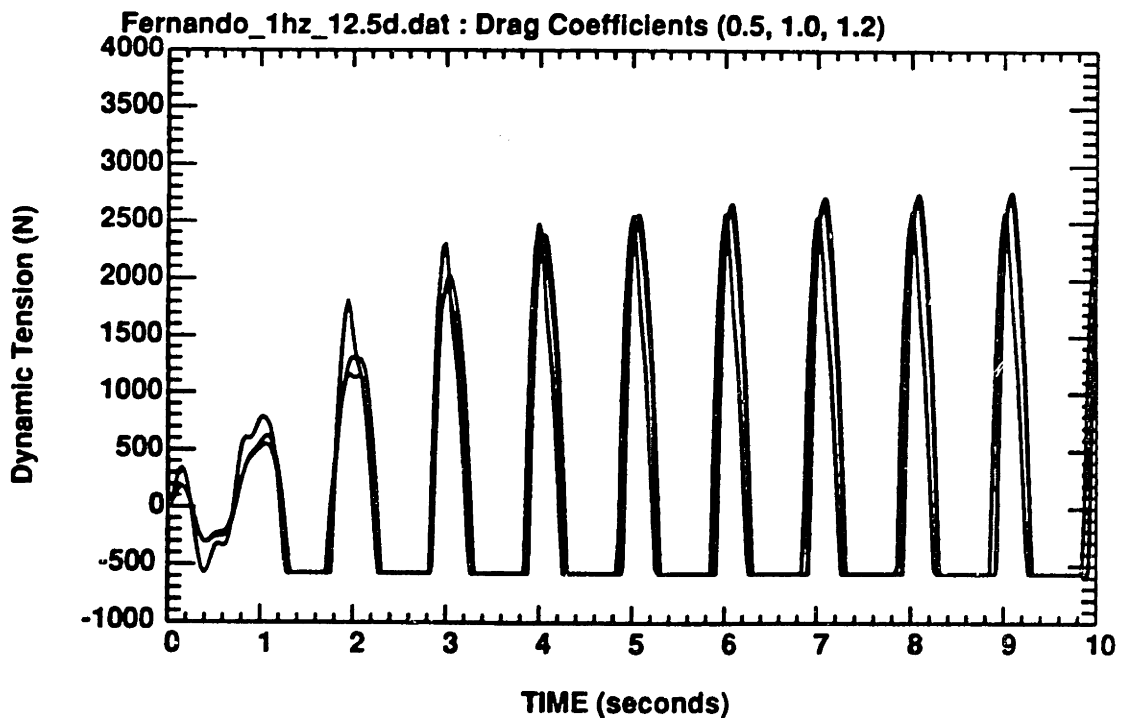


Figure 7-20: Effect of the drag coefficient on predicted dynamic tensions

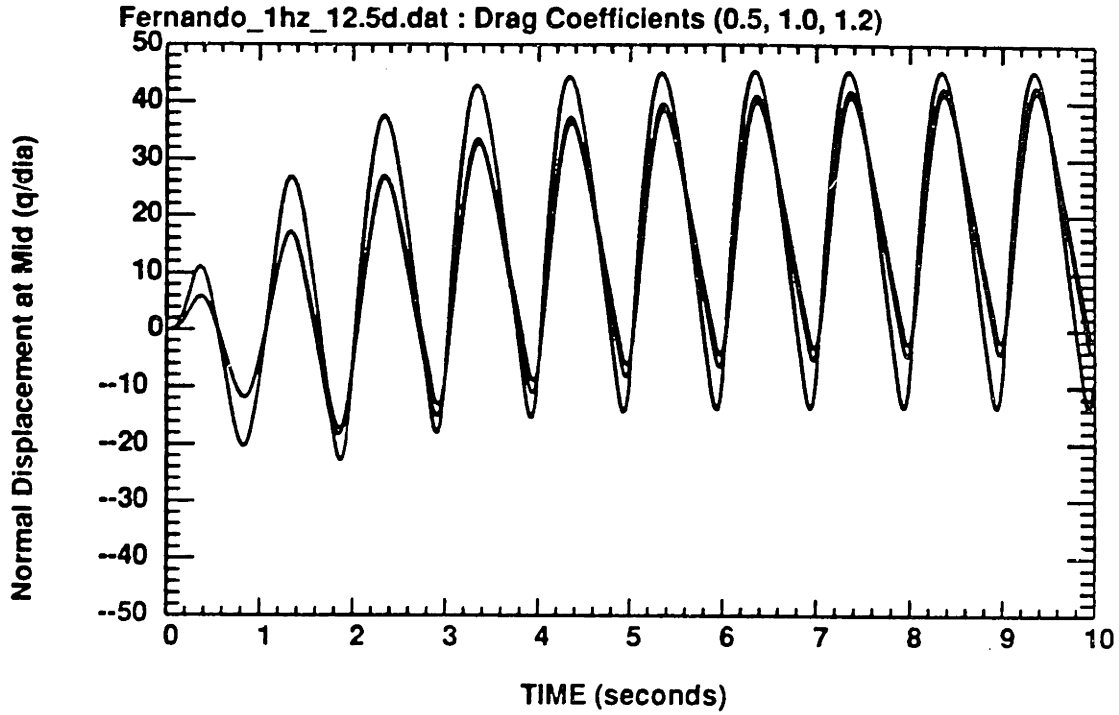


Figure 7-21: Effect of the drag coefficient on predicted normal displacement at the middle

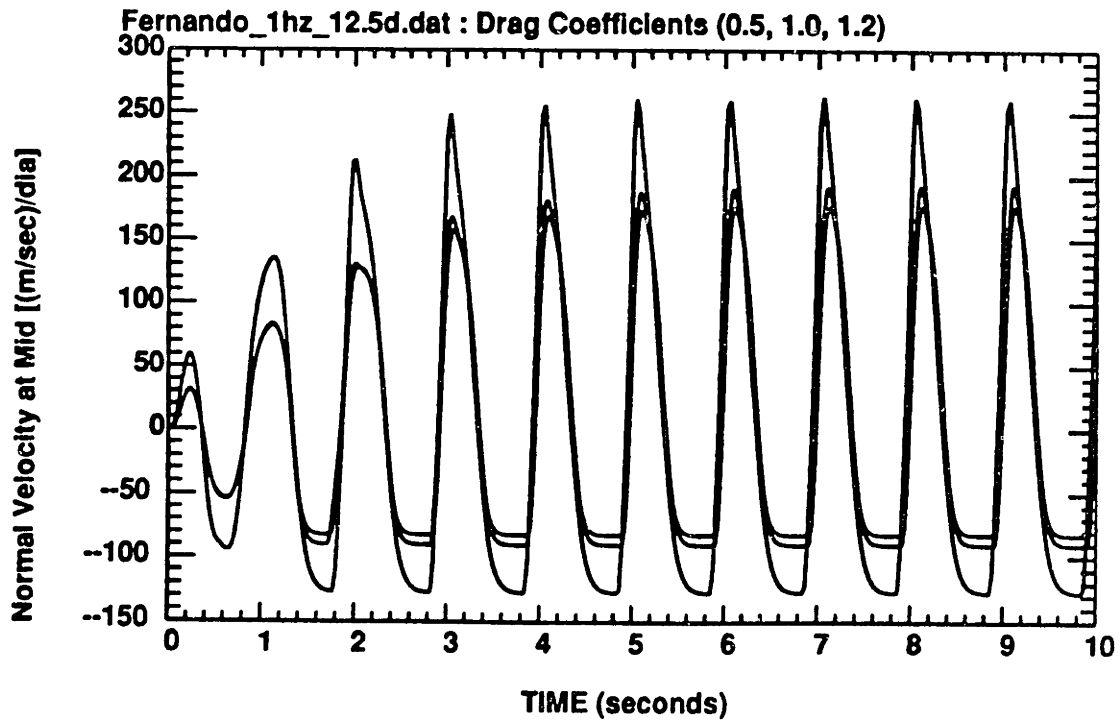


Figure 7-22: Effect of the drag coefficient on predicted normal velocity at the middle

Conclusion

In chapter 1, we derived the fully nonlinear two-dimensional dynamic equations of a mooring line; in chapter 2, we simplified the equations, while retaining all the important nonlinear terms, so as to implement efficient numerical schemes. In order to do this, we first used the relations between the two different coordinate systems, employed in deriving the fully nonlinear dynamic equations - one is fixed on the static configuration of the cable, and the other is fixed on its dynamic configuration. This transformation allows the identification of nonlinear terms, which have not been found in previous derivations (See section 1.6). Subsequently, a comparison using order of magnitude arguments, enabled us to simplify the fully nonlinear equations.

In chapter 3, we dealt with the problem of a taut string, as a first step in developing our numerical schemes and checking their validity. Because of the geometric simplicity of the string with respect to a cable, we used Galerkin's method spatially instead of the collocation method, and Newmark's method for the time integration, employing Chebyshev polynomials in expanding the dynamic responses of the string. The comparison between our predicted results and analytical results using sine series, showed very good agreement (Fig. 3.7).

For the problem of a string hitting against an object, we found that there is a basic difficulty in obtaining fast convergence, and we used a variable size time integration step. A parametric variation of the values of the spring constant k and damping coefficient c , which are used to model the given object, produced several interesting dynamic responses of the string. Large values of k and c simulated the dynamic responses of the string, hitting a very hard soil (Fig. 3.17). This formulation of the string-obstacle problem may be extended and then used to study the dynamic behaviour of a cable which lies partly on the sea bottom.

Through systematic numerical applications and comparisons with experimental data, we investigated basic nonlinear mechanism of cable dynamic response (chapters 4 through 7).

The dynamic response of a cable excited at its first natural frequency, 0.9 rad/sec, with an amplitude equal to 10 cable diameters, shows that the fluid drag force serves as a damper preventing the amplitude of vibration from growing without bound (Figures 4.4 through 4.9), as expected from classical vibration theory (Chapter 4). At the same time, fluid drag forces the cable to use the elastic stiffness more than the catenary stiffness, this altering fundamentally the character of cable response, relative to a cable vibrating in air.

From the investigation into the combined effects of geometric nonlinearity, large tensile forces and nonlinear drag forces, we found that the maximum value of the dynamic tension response increased by about 50 % for the particular case studied (Table 6-1) and the magnitude of minimum dynamic tension response decreased slightly or remained constant. This, in turn, causes the average tension in the cable to increase.

In chapter 5, the study of a cable with buoys attached along its length, which is proposed for deeper water mooring applications, allowed us to quantify the dynamic effect of the buoys on the cable responses. In one case, the increase in maximum dynamic tension was more than 300 % (Figures 5.18 and 5.9). Attention should be paid, therefore, when designing a cable-buoy system for a particular offshore purpose, otherwise the dynamic performance may deteriorate significantly. Our numerical scheme may serve as a first tool for the preliminary design of such a system.

In chapter 7, we studied the effect of zero total tension on the dynamic behaviour of a cable. This is the first step in our effort to model properly and understand the principal mechanisms of a snapping cable.

We found that the values of two important nondimensionalized parameters MST and TRI, determine whether snapping will occur, and if it occurs, whether large tension amplification should be expected. If snapping occurs, the free falling velocity of the cable (approximated by formula 7.6 - for wires) is the determining factor for tension amplification. The prediction of extreme tensions for the cable used in experiments conducted by the Ship Research Institute of Norway, showed good agreement up to a certain frequency, while comparison with experimental data conducted by MIT, showed a difference of about 30 % for a very stiff cable, and good agreement for a softer cable, when the elastic stiffness dominates the response of the cable. A systematic effort to interpret the differences provided plausible explanations, and the agreement we obtained overall is encouraging, given the complexity of the problem.

Appendix A

Classical Wave Equation

1. Eigenvalue Problem

- Governing Equation :

$$\frac{\partial^2 u}{\partial t^2} = \frac{\partial^2 u}{\partial x^2} \quad (0 \leq x \leq l) \quad (A.1)$$

- Boundary Conditions :

$$u(0,t) = 0$$

$$u(l,t) = 0$$

- Initial Conditions :

$$u(x,0) = \phi(x)$$

$$u_t(x,0) = \psi(x)$$

- Eigenvalues :

$$\lambda = \frac{n\pi}{l} \quad (A.2)$$

- Eigenfunctions :

$$x_n = \sin \frac{n\pi}{l} x \quad (A.3)$$

- General Solution :

$$u(x,t) = \sum_{n=1}^{\infty} \sin \frac{n\pi}{l} x \left[C_n \cos \frac{n\pi}{l} t + D_n \sin \frac{n\pi}{l} t \right]$$

(A.4)

where $\phi(x) = \sum_{n=1}^{\infty} C_n \sin \frac{n\pi}{l} x$

$$\psi(x) = \sum_{n=1}^{\infty} \frac{n\pi}{l} D_n \sin \frac{n\pi}{l} x$$

2. Forced Motion

- Governing Equation :

$$\frac{\partial^2 u}{\partial t^2} = \frac{\partial^2 u}{\partial x^2} + Q(x,t) \quad (A.5)$$

- We expand $Q(x,t)$ in terms of eigenfunctions (A.3)

$$Q(x,t) = \sum_{n=1}^{\infty} [Q_n(t) \sin \frac{n\pi}{l} x] \quad (A.6)$$

$$\text{with } Q_n(t) = \frac{2}{l} \int_0^l Q(x,t) \sin \frac{n\pi}{l} x \, dx \quad (A.7)$$

- Solution :

$$u(x,t) = \sum_{n=1}^{\infty} [q_n(t) \sin \frac{n\pi}{l} x] \quad (A.8)$$

with

$$q_n(t) = \frac{1}{n\pi/l} \int_0^t Q_n(t') \sin \frac{n\pi}{l} (t-t') \, dt' + a_n \frac{\cos n\pi t}{l} + b_n \frac{\sin n\pi t}{l} \quad (A.9)$$

where a_n and b_n are determined from the initial conditions

3. Forced Vibrations

- Governing Equation :

$$\frac{\partial^2 u}{\partial t^2} = \frac{\partial^2 u}{\partial x^2} + Q(x,t)$$

$$\text{with } Q(x,t) = f(x)\cos\omega t \quad (\text{A.10})$$

- Expansion Coefficients $Q_n(t)$ of $Q(x,t)$:

$$Q_n(t) = \frac{2}{l} \cos\omega t \int_0^l f(x) \sin \frac{n\pi}{l} x \, dx \quad (\text{A.11})$$

- Solution :

$$u(x,t) = -\cos\omega t \sum_{n=1}^{\infty} \frac{C_n}{\omega^2 - (n\pi/l)^2} \sin \frac{n\pi}{l} x \quad (\text{A.12})$$

$$+ \sum_{n=1}^{\infty} \left(A_n \cos \frac{n\pi}{l} t + b_n \sin \frac{n\pi}{l} t \right) \sin \frac{n\pi}{l} x$$

$$\text{with } C_n = \frac{2}{l} \int_0^l f(x) \sin \frac{n\pi}{l} x \, dx \quad (\text{A.13})$$

- When initial conditions are as follows :

$$u(x,0) = 0$$

$$u_t(x,0) = 0 \quad (\text{A.14})$$

The above unknown coefficients are obtained as :

$$A_n = \frac{C_n}{\omega^2 - (n\pi/l)^2}, \quad b_n = 0$$

- Exact Series Solution :

$$u(x,t) = -\sum_{n=1}^{\infty} \frac{C_n}{\omega^2 - (n\pi/l)^2} \left[\cos \omega t - \cos \frac{n\pi}{l} t \right] \sin \frac{n\pi}{l} x$$

$$\text{with } C_n = \frac{2}{l} \int_0^l f(x) \sin \frac{n\pi}{l} x \, dx \quad (\text{A.15})$$

4. Time Differential Equation Governing the Expansion Coefficients $q_n(t)$ of $u(x,t)$

- From equations (A.5), (A.6), (A.8) and (A.10), we obtain the following differential equation.

$$\frac{d^2 q_n}{dt^2} = -\left(\frac{n\pi}{l}\right)^2 q_n(t) + C_n \cos \omega t \quad (\text{A.16})$$

- By using the Newmark method as the time integration scheme, we can calculate $q_n(t)$ numerically in the same way as employed for equations (3.13) and (3.14) in section 3.5.

References

- [1] Bathe K.J.
Finite Element Procedures in Engineering Analysis.
Prentice Hall, Englewood Cliffs N.J., 1982.
- [2] Bender, C.M. and Orszag S.A.
Advanced Mathematical Methods for Scientists and Engineers.
McGraw-Hill Book Company, New York, 1978.
- [3] Berteaux H.O.
Buoy Engineering.
John Wiley & Sons, New York, 1976.
- [4] Blied, A.
Dynamic Analysis of Single Span Cables.
PhD thesis, MIT, 1984.
- [5] Burgess, J.J.
Natural Modes and Impulsive Motions of a Horizontal Shallow Sag Cable.
PhD thesis, Massachusetts Institute of Technology, 1985.
- [6] Cannon, T. C. and Genin, J.
Three Dimensional Dynamical Behaviour of a Flexible Towed Cable.
Aeronautical Quarterly 25:201-210, August, 1972.
- [7] Crandall, S.H.
Dynamics of Mechanical and Electromechanical Systems.
Robert E. Krieger Publishing Company, Malabar, Florida, 1982.
- [8] Crandall, S.H.
Engineering Analysis - A Survey of Numerical Procedures.
Robert E. Krieger Publishing Company, Malabar, Florida, 1983.
- [9] Critescu, N.
Dynamic Plasticity.
North Holland Publishing Company, Amsterdam, Holland, 1967.
- [10] Frimm, F.C.
PhD thesis, MIT,
1987.
- [11] Fylling, I.J. and Wold, P.T.
Cable Dynamics - Comparison of Experiments and Analytical results.
Technical Report R-89.79, The Ship Research Institute of Norway, 1979.
- [12] Gottlieb, D. and Orszag S.A.
Regional Conference Series in Applied Mathematics: Numerical Analysis of Spectral Methods, Theory and Applications.
Society for Industrial and Applied Mathematics, Philadelphia, 1977.

- [13] Graff, K.F.
Wave Motion in Elastic Solids.
Ohio State University Press, 1975.
- [14] Hildebrand, F.B.
Advanced Calculus for Applications.
Prentice Hall, Englewood Cliffs N.J., 1949.
- [15] Lanczos, Cornelius.
Applied Analysis.
Prentice Hall, INC, Englewood Cliffs, N.J., 1956.
- [16] Lenskii, E. V.
Motion of Flexible Strings in an Ideal Liquid.
Vestnik Moskovskogo Universiteta Mekhanika 33(1):116-127, 1978.
In Russian, translation Allerton Press 1978.
- [17] Liu, F.C.
Snap loads and Bending Fatigue in Diving Bell Handling Systems.
Offshore Technology Conference (OTC 4089), 1981.
- [18] Liu, F.C.
Fly Away Deep Ocean Salvage System (Fadoss) - a Compensated Lift System.
In *Current Practices and New Technology in Ocean Engineering.* New York, N.Y.,
February, 1986.
- [19] Main, I.G.
Vibrations and Waves in Physics.
Cambridge University Press, Cambridge, Great Britain, 1984.
- [20] Migliore, H. and McReynolds, E.
Cable Analysis Using Orthogonal Collocation.
the Journal of the Waterway, ASCE 107(WW2):113-118, May, 1981.
- [21] Migliore, H. and McReynolds, E.
Ocean Cable Dynamics Using an Orthogonal Collocation Solution.
AIAA Journal, AIAA 82-4185 20(8):1084-1091, August, 1982.
- [22] Orszag, S. A.
Spectral Methods for Problems in Complex Geometrics.
In S.V. Parter (editor), *Proceedings of an Advanced Seminar on Numerical Methods
for Partial Differential Equations.* 1979.
- [23] Shin, H.
Numerical Solution of the cable Dynamic Equations Using the Linearized
Equivalent Damping Force.
Master's thesis, Engineer Thesis : MIT, 1985.
- [24] Triantafyllou, M. S., Blik, A. and Shin, H.
Dynamic Analysis as a Tool for Open-Sea Mooring-System Design.
Transactions, The Society of Naval Architecture and Marine Engineering (12),
November, 1985.

- [25] Triantafyllou M. S., Bliet A., and Shin H.
Static and Fatigue Analysis of Multi-leg Moored Systems.
Technical Report MITSG 86-21, Sea Grant College Program, April, 1987.
- [26] Triantafyllou M. S.
Private Communications.
1987.
Triantafyllou's numerical results are used.
- [27] Weinberger, H.F.
Partial Differential Equations.
Blaisdell Publishing Company, Waltham, Massachusetts, 1965.